University of Zurich[UZH]

Covid-19 grounding - Monitoring air pollution at Zurich Airport during the pandemic using trees as bio-indicators

GEO 511 Master's Thesis

Author
Jana Gemperle
15-729-536

Supervised by
Prof. Dr. Paolo Cherubini (paolo.cherubini@wsl.ch)
Paula Ballikaya

Faculty representative
Prof. Dr. Markus Egli

29.04.2022
Department of Geography, University of Zurich

UNIVERSITY OF ZURICH

Covid-19 grounding - Monitoring air pollution at Zurich Airport during the pandemic using trees as bio-indicators

MASTER THESIS
April 29, 2022

Author:
Jana GEMPERLE

Supervisor:
Prof. Dr. Paolo CHERUBINI

Co-Supervisor:
Paula BALLIKAYA

University Representative:
Prof. Dr. Markus EGLI

Abstract

When the world stayed at home at the time of the Covid-19 pandemic in 2020, it also suddenly became quiet around Zurich/Kloten Airport. The turbines stopped and aircraft remained on the ground. The movement restrictions had the effect that air traffic was reduced by 91%. In fact, you could call it a "Covid-19 grounding". In this thesis, the effects of the pandemic lockdown and the associated reduction in traffic-related emissions on air quality are studied using Norway spruce trees (*Picea abies* (L.) H.Karst) as bio-indicators at Zurich Airport. For this purpose, three sites were investigated, two of which were located at exposed locations to air (runway site) and road (carparking site) traffic and one control site further away from traffic-related emission sources. Using the radiocarbon method, spruce needles from four generations (pre-pandemic: 2018-2019 and pandemic: 2020-2021) were analyzed and a decreasing dilution effect (^{14}C enrichment) was detected in the lockdown needle generations (2020) at sites near traffic-related emission sources. This effect comes from reduced combustion of fossil fuels and release of ^{14}C free CO_2. The mean decreases in -F^{14}C in needles from 2020 was 30% at the carparking site, like the decrease in local road traffic, and 52% at the runway site, which was thus additionally affected by the reduction of air traffic. In contrast, nitrogen isotope analysis at none of the three sites showed a significant change in the δ^{15}N nor δ^{13}C ratio in the 2020 needle generation compared to previous years. The method appeared less suitable than the radiocarbon method for examining short-term reductions in air pollutants. Similarly, the mean tree-ring chronologies at the sites did not correlate with the mean annual NO_2 concentrations measured at Zurich Airport, but rather with local climate factors such as precipitation and temperature. The results of the stable isotope and tree-ring analysis showed that the signals caused by pollution or climate are difficult to distinguish. The same applies to changes in measured concentrations of air pollutants during the pandemic, which are strongly dependent on meteorological conditions that influence the distribution and dilution of pollutants in the air. Determining which changes in air quality are actually caused by emissions and which are due to weather conditions is therefore one of the greatest challenges to date.

Acknowledgements

First of all, I would like to thank my supervisor Prof. Dr. Paolo Cherubini for the opportunity to write my Master's thesis at the Research Institute for Forest, Snow and Landscape (WSL) and for his constant support and valuable advice. A special thanks goes to Prof. Dr. Markus Egli for his precious feedback and advice. I would also like to express appreciation to Paula Ballikaya for her energetic support and advice, her steadfast patience and encouraging words. Moreover, a big thanks for all cut branches in dizzying heights goes to the gardeners of WSL: Gabor Reiss, Claudio Cattaneo and Peter Suter. Your climbing skills are unique! For the support in the WSL laboratory I would like to thank Dr. Matthias Saurer who enabled the nitrogen isotope analysis, as well as Loic Schneider and Anne Verstege for their assistance. Furthermore, a special thanks goes to the Laboratory of Ion Beam Physics at the ETH, Dr. Lukas Wacker for the exceptional opportunity of radiocarbon dating, as well as Melanie Alter and Giulia Guidobaldi for their assistance. For the many valuable contacts I would like to thank the city of Kloten, especially Marc Osterwalder, Head of Habitat, Dr. Daniel Martinelli, Head of Environment and Energy and Melitta Cadosch, Head of construction police. Working at the Kloten construction office, I was able to experience that the construction of an airport is never finished. At this point also many thanks for the trust and support to the local foresters Thomas Hubli (community Rümlang), Thomas Kuhn (city of Bülach), Michel Kern (community Winkel) and the Cantonal Conservation Officer Adrienne Frei: without you the project would not have been possible! For the information and data provided, I would like to thank Flughafen Zürich AG (FZAG), in particular Emanuel Fleuti, Head of Environment, Meteo Swiss, and Jörg Sintermann, Head of Air Quality, Climate and NIS, as well as Roy Eugster, Deputy Head of Monitoring at WWEA (AWEL): Office for Waste, Water, Energy and Air, Canton of Zurich. A personal and heartfelt thank you to all of you who supported me during my master thesis. Without you I would not have seen the forest for the trees: Pascal Weber, Michele Bösiger, Prof. Dr. John Marshall, Ursina Boos, Nicola Paltenghi, Davide Bernasconi, Kurt Weber, Philipp Rüegg, Wenqi Song and Enkh-Uchral Batkhuyag.

Contents

List of Figures

List of Tables

List of Abbreviations

ETH	**E**idgenössische **T**echnische **H**ochschule
WSL	Eidgenössische Forschungsanstalt für **W**ald, **S**chnee und **L**andschaft
NABEL	**Na**tionale **Be**obachtungsnetz für **L**uftfremdstoffe
Empa	**E**idgenössische **M**aterial**p**rüfungs- und Forschungs**a**nstalt
FZAG	**F**lughafen **Z**ürich **AG**
BAFU	**B**undes**a**mt für **U**mwelt
OAPC	**O**rdinance on **A**ir **P**ollution **C**ontrol
NAO	**N**oise **A**batement **O**rdinance
WHO	**W**orld **H**ealth **O**rganization
BAG	**B**undes**a**mt für **G**esundheit
ESA	**E**uropean **S**pace **A**gency
NZZ	**N**eue **Z**ürcher **Z**eitung
DALY	**D**isability **A**djusted **L**ife **Y**ears
CO_2	**C**arbon di**o**xide
CH_4	Methane
SO_2	**S**ulfur di**o**xide
N_r	**N**itrogen **r**eactive
N_2	**N**itrogen
^{15}N	**N**itrogen- **15** isotope (stable)
^{14}N	**N**itrogen- **14** isotope (stable)
NO_2	**N**itrogen di**o**xide
NO_x	**N**itrogen **o**x**i**de
VOC	**V**olatil **O**rganic **C**arbon
^{14}C	**C**arbon- **14** isotope or radiocarbon
^{13}C	**C**arbon- **13** isotope (stable)
^{12}C	**C**arbon- **12** isotope (stable)
$F^{14}C$	Fraction Modern **C**arbon- **14** isotope or radiocarbon
TRWPs	**T**ire and **R**oad **W**ear **P**article**s**
TRAPs	**T**raffic-**R**elated **A**ir **P**ollution**s**
UFP	**U**ltra **F**ine **P**article
PM	**P**articulate **M**atter
NP	**N**ano **P**article

ABA	**A**cid **B**ase **A**cid
RWI	**R**ing **W**ith **I**ndex
GLK	**G**leichl**ä**ufig**k**eit
TSAP	**T**ree **S**eries **A**nalysis and **P**resentation
MICADAS	**Mi**ni **Ca**rbon **Da**ting **S**ystem
SAPALDIA	**S**wiss cohort study on **A**ir **P**ollution **A**nd **L**ung and Heart **D**iseases **I**n **A**dults
ATANMOS	**A**irport **T**rack **A**nd **N**oise **MO**nitoring **S**ystem
AMS	**A**ccelerator **M**ass **S**pectrometry
IRMS	**I**sotope **R**atio **M**ass **S**pectrometer
IADF	**I**ntra **A**nnual **D**ensity **F**luctuations
LA-ICPMS	**L**aser **A**blation **I**nductively **C**oupled **P**lasma **M**ass **S**pectrometry
TD-PTR-MS	**T**emporal **D**esorption-**P**roton **T**ransfer **R**eaction-**M**ass **S**pectrometry

1 Introduction

> "Airports stand for mobility, flows, lack of history, commerce. In fact, they are connected to their environment in many ways, as they are complex structures in which technology and nature, science, economy and society, past and future unite."
>
> (Güttler et al., 2018)

1.1 Zurich Airport - concrete jungle and nature oasis

Squealing tires, roaring turbines and a slightly dizzying scent of kerosene fills the air. The weather situation in Kloten has changed noticeably. The city with its more than 20'000 inhabitants is not far from Switzerland's largest airport, which has already received the "World Travel Award" as the best airport in Europe for the 18th time - Zurich Airport.

In 1946, the majority of Zurich citizens voted for the construction of an intercontinental airport on the former military ground between the sparsely populated villages Kloten, Rümlang and Oberglatt (Bauer, 2008). The marsh area was anything but an optimal location for the construction of an airport. Due to the environmental conditions, the construction of the runways was very costly and demanded complex civil engineering work (Bauer, 2008). However, the explanation for the choice is understandable: one did not want to lose a cultural landscape and the location and the prevailing wind conditions of the area were very advantageous (Güttler et al., 2018). The effort required the drainage of the "unproductive" marsh land and the canalization of the surrounding streams (Güttler et al., 2018; Bauer, 2008). Nature had to give way, the marsh land with its carrs and fens became the asphalted western Runway 10/28 on which the first aircraft landed on June 14th, 1948.

At that time, little attention was paid to the high biodiversity of marsh lands. The situation was different with the forest areas. The surrounding communities defended every square meter of forest and opposed the shifting of the further planed Blind Runway 16/34 by 500 m further to the east. In the end, Zurich Airport was nevertheless given a clearing permit for aviation reasons (Güttler et al., 2018). A few months later, Blind Runway 16/34 was built and opened on November 17th 1948, giving Zurich Airport the most modern runway system in the world (see Figure 1.1a). With the new pure runway system, two generously proportioned runways with high load-bearing capacity were already sufficient for landing of large aircraft (>50 tons), regardless of wind direction. The construction of

(A) 1950 (Friedli, 1950) (B) 1977 (Swissair Photo AG, 1977)

FIGURE 1.1: Aerial photograph Airport Zurich-Kloten view from the south towards Oberglatt

Zurich Airport opened a gateway to the world, and as demand for air mobility increased, the airport and its surrounding villages continued to expand (Güttler et al., 2018).

With the increasing demand for air mobility and jet aircraft taking over the sky, Zurich airport decided in the late 1960s to extend the already existing runways and build another runway to the north, today's V Runway 14/32 (Güttler et al., 2018; Bauer, 2008). At the same time, the idea of environmental protection also gained importance. Conservationists under the direction of professor and plant ecologist Frank Klötzli pointed out to the government council the high ecological value of the area where the new runway was planned (Güttler et al., 2018). A compromise was found, resulting in the world's first marsh replanting of this kind to make way for the new runway. During the replanting, a special excavator dug up the plants with their entire root system and relocated them to a new site with similar conditions (Güttler et al., 2018; FZAG, 2020b). Finally, the V Runway 14/32 was opened on April 1st 1976 and, together with the existing runways, formed the typical three-runway system that can still be found today (Bauer, 2008).

1.2 Aircraft emissions and human health

1.2.1 The louder the turbines, the louder the opponents

When jet aircraft arrived in the 1960s and jumbo jets in the 1970s, the debate about aircraft noise also became louder (Bauer, 2008). Unlike propeller planes, jets with their turbines reached a whole new noise level. For the first time, the blue sky of euphoria over air mobility became cloudy. While wind and weather conditions were the main concerns in the 1950s, it was now the unpleasant local inhabitants who complained about the ever-increasing aircraft noise (Güttler et al., 2018). Consequently, aircraft noise has been measured at Zurich Airport since 1966. Today, it is a modern system consisting of 14 measuring stations in the airport's

catchment area: the ATANOMS (Airport Track And Noise Monitoring System), which has been in operation since 2008 (FZAG, 2019). The data are published monthly in the noise bulletin with thresholds set by NAO (Noise Abatement Ordinance) and presented in a noise exposure map. These data are also used to create noise charge models, which are intended to motivate airlines to fly to Zurich Airport with aircraft types that are as low-noise as possible (FZAG, 2019). Nevertheless, over the past decade, every year, Zurich Airport has received 2'000-3'000 complaints from affected inhabitants regarding noise pollution (FZAG, 2019; FZAG, 2020a).

1.2.2 Air pollution- burning fossil fuels

Natural greenhouse effect ensures a pleasant average temperature of 15°C, making life on planet Earth possible. However, this balance of naturally occurring greenhouse gases in the atmosphere such as carbon dioxide (CO_2), methane (CH_4) and nitrogen dioxide (NO_2) has been lately disturbed by anthropogenic influences. Since the industrial revolution, atmospheric CO_2 levels have been rising due to anthropogenic activities such as deforestation, artificial fires, land use changes and the burning of fossil fuels (Schönwiese, 2013). Using ice cores from the polar regions and direct atmospheric measurements (since 1958 on Mauna Loa, Hawaii) it is possible to quantify the changes in greenhouse gas concentrations in the atmosphere over the last centuries (Etheridge et al., 1996; Keeling, 1991). Atmospheric CO_2 concentration exceeded 400 ppm in 2015, reaching 144% of pre-industrial levels and today's atmospheric CO_2 concentration is 418 ppm (as of January 27th 2022) (Keeling et al., 2001; WMO, 2017). This global annual increase of about 2 ppm is primarily due to emissions from fossil fuel combustion and cement production with 95% of these emissions released in the northern hemisphere (WMO, 2017; Levin and Hesshaimer, 2000). The annual increase would also be much greater if natural sinks such as the oceans and the terrestrial biosphere would not remove around 50% of human emissions from the atmosphere again and thus buffer the measured actual signal (WMO, 2017; Levin and Hesshaimer, 2000).

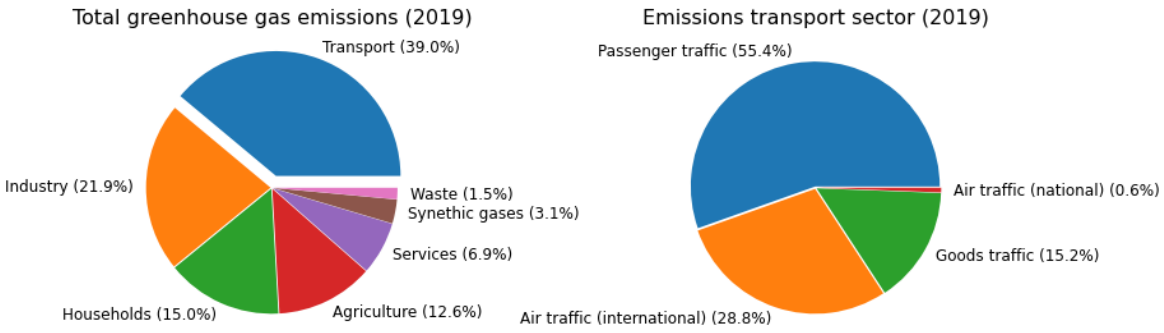

FIGURE 1.2: Greenhouse gas emissions in Switzerland in 2019 (national aviation included). Total emissions (left), emissions from transport sector (right) (data: BAFU, 2021b).

Burning fossil fuels releases large amounts of CO_2, which increases the greenhouse effect and warms the earth's surface. Indirectly, anthropogenic CO_2 emissions influence the environment and - through various interactions - thus also human health. However, the combustion of fossil fuels such as kerosene also releases air pollutants like: nitrogen oxides (NO_x), sulfur dioxide (SO_2), carbon monoxide (CO), hydrocarbons and diverse particulate matter (BAZL, 2020). In Switzerland, 39% of greenhouse gas emissions in 2019 are attributable to transport, with the remainder coming from industry, agriculture and households for generation of heat, light and electricity (BAFU, 2021b, see Figure 1.2). Including international aviation this amount to a total of 19.92 million tons of CO_2 that were emitted by transport throughout Switzerland in 2019, 55.2% of which was emitted by private cars, 28.8% by international air traffic, 15.2% by good traffic and 0.6% by national aviation (BAFU, 2021b). Overall, this means that a share of 11.49% of CO_2 emissions comes from aviation. Whereas, worldwide air traffic contributes about 2-2.5% to global anthropogenic fossil CO_2 emissions (BAZL, 2020).

1.2.3 Particulate matter - "plastic is in the air!"

Besides gaseous pollutants, very fine solid and liquid particles, so-called particulate matter (PM) or aerosols, are produced during the combustion of fossil fuels and during mechanical processes. PM is a complex mixture of liquid and solid particles of organic and inorganic substances that are small enough to be transported by the air (WHO, 2016). Their composition can be very diverse from heavy metals to secondary inorganic components such as nitrate, sulphate and ammonium (Hueglin et al., 2012). The pollutant sources that make up PM can also be of natural origin, for example wind-blown desert dust, sea spray aerosols or tissues from plants like pollen (Zhongming et al., 2012). Furthermore, a distinction is made between primary and secondary particles, the latter being formed by chemical and physical reactions in the atmosphere with other pollutants such as ammonia, volatile organic compounds (VOCs), NO_x and SO_2 (BAFU, 2021c). They are categorized into three sizes: PM_{10} (diameter <10 μm), $PM_{2.5}$ (diameter <2.5 μm) and ultrafine particles (UFP diameter <0.1 μm) (Zhongming et al., 2012; OSTLUFT, 2021). Whereas, traffic but especially air traffic is one of the major sources for UFP (Fleuti, 2020; OSTLUFT, 2021). The dispersion of PM and UFP of different sizes, composition and origins are strongly dependent on local meteorological weather conditions (e.g. precipitation, wind direction/speed, etc.) as well as time of day (Allen et al., 2019; Fleuti, 2020; OSTLUFT, 2021; Materić et al., 2021). A good example is the widely transported Saharan dust in the atmosphere, which turns the snow in the Swiss Alps distinctly yellow at the same time every year.

While Saharan dust is clearly visible as a layer in the snow cover, it looks somewhat different when referring to nanoplastic particles. "In the Alps it's snowing plastic" is a very recent article by EMPA of January 25th 2022 (Waldmann, 2022), which makes it clear that plastic pollution is by far no longer just a problem in the oceans, but also in the air. In

FIGURE 1.3: Landing aircraft at Zurich Airport with tire abrasion dust plume

various studies, airborne micro- and nanoparticles have been detected at distant locations far from anthropogenic influences (Allen et al., 2019; Bergmann et al., 2019; Materić et al., 2021). A large source of air pollution from plastics are tire and road wear particles (TRWPs) generated by abrasion during acceleration but especially during braking on the road (Kole et al., 2017; Baensch-Baltruschat et al., 2020). This becomes particularly apparent on the example of a landing aircraft: when landing, strong forces act on the wheels as they are first strongly accelerated, heated and then braked, whereupon an exhaust plume is created (see Figure 1.3). The estimated rubber loss per landing using the example of a Boeing 747 can be up to 1kg (Bennett et al., 2011).

1.2.4 Human health

Zurich Airport emits several pollutants that affect human health. Noise is also a pollutant in form of a frequency that has various health, economic and spatial/social impacts on society. Aircraft noise affects a rather small catchment area compared to road traffic noise, but the affected inhabitants are exposed to significantly higher sound levels (BAFU, 2018). Emission values are exceeded especially in the approach and departure corridors of Zurich Airport. Continuous noise increases the risk of health problems, especially at night as our organism is particularly sensitive to noise. Noise levels of 40-50 dB already considerably reduce the quality of sleep which can lead to reduction in cognitive performance (BAFU, 2018). Physiologically, the body is on alert under noise and releases stress hormones, which in the long term can promote cardio-metabolic disorder such as diabetes type 2 and hypertension, increasing risks of heart attacks and strokes (BAFU, 2018; Franssen et al., 2004; Münzel et al.,

2017). According to Ecoplan, 2019, a total of 69,300 DALYs ("disability adjusted life years" (WHO, 2018); 1 DALY = one year of life lost in perfect health) are lost in Switzerland due to traffic noise-related health effects, 10% of which are attributable to aircraft noise.

Gaseous and solid air pollution have even more far-reaching consequences both spatially and in terms of the number of people affected. Since the 1952 smog episode in London, it has been clear that air pollution has a negative impact on human health. The World Health Organization (WHO) estimated the number of premature deaths worldwide from air pollution at 4.2 million per year in 2016. In Switzerland, around 2300 to 3000 people die prematurely every year as a result of air pollution (BAFU, 2014). Inhalation of the pollutants can irritate the respiratory tract and cause acute and chronic respiratory, cardiovascular diseases and strokes (BAFU, 2014). The smaller the particles are, the deeper they can penetrate the lungs, enter the bloodstream, and reach other organs (Ohlwein et al., 2019; WHO, 2016; BAFU, 2014; BAFU, 2020). One of the main contributors to air pollution is traffic. However, whether traffic-related air pollution (TRAPs) can also affect the brain and lead to cognitive dysfunction and later dementia development is still controversial (Cipriani et al., 2018). The good news is that people's health recovers quickly with improved air quality, according to a cohort study SAPALDIA (Swiss Cohort Study on Air Pollution and Lung and Heart Diseases in Adults) (BAFU, 2020).

For this reason, measures were already taken in the 1980s and greater efforts have been made in recent years to improve air quality in Switzerland. Since 1985, air quality has improved significantly due to technical advances in the filtering of exhaust gases and particulate matter (BAFU, 2014; BAFU, 2021c; BFS, 2021). Nevertheless, the emission thresholds are still exceeded at heavily polluted sites and at certain times of the year (BAFU, 2021c; BFS, 2021). Unlike for gaseous pollutants and PM, no threshold values for UFP are defined in the Ordinance on Air Pollution Control (OAPC; for further information: fedlex.admin.ch - The publication platform for federal law). In the future, it will be necessary to study the sources of air pollution, as well as its consequences for humans and the environment, in order to take urgently needed action.

1.3 Covid-19 pandemic - effects on transportation and air quality

"Mysterious outbreak of lung disease in central China - some voices fear a new outbreak of Sars lung disease" (NZZ, 2019). The headline in the NZZ at the end of 2019 sounded alarming but still so far away. At that time, no one could even imagine the scope of this newly discovered disease Sars-CoV-2. Following the news, the first case of the new Sars variant was confirmed in Switzerland in February 2020 (BAG, 2020b). The assessment of the risk posed by the virus to the Swiss population was initially considered moderate. Three weeks later, the Federal Council announced the exceptional situation and a nationwide lockdown (BAG, 2020a). The viral disease was soon no longer an epidemic, but a pandemic.

1.3.1 "Stay at home!"- how the world pauses

As of March 17th, 2020, economic and public life came to a standstill. The measures and restrictions taken to reduce contagion were most noticeable in traffic. At the beginning of the lockdown, the greatest decrease was recorded in public transport at 65% and in private transport at 42%, while business traffic hardly decreased at 13% (Moser, 2020). Overall, the volume of road traffic has been reduced by 20% and in some places up to 50% depending also on the day of the week, thus on average 35% (Sintermann, 2020; Moser, 2020). Looking specifically at the Zurich Airport area, road traffic decreased by an average of about 39.3%, while air traffic came to an almost complete halt with a 91% decrease in aircraft movements (Fleuti, 2020) (see Figure 1.4). Compared to public transport and air traffic, road traffic recovered quickly after the end of the closure on May 11 th, 2020, which could be due to the fear of contagion in public transport and thus increased use of individual road transport (Moser, 2020; Buck and Weinstein, 2020). Similar or even more strict pandemic-related movement restrictions were applied in all countries around the world.

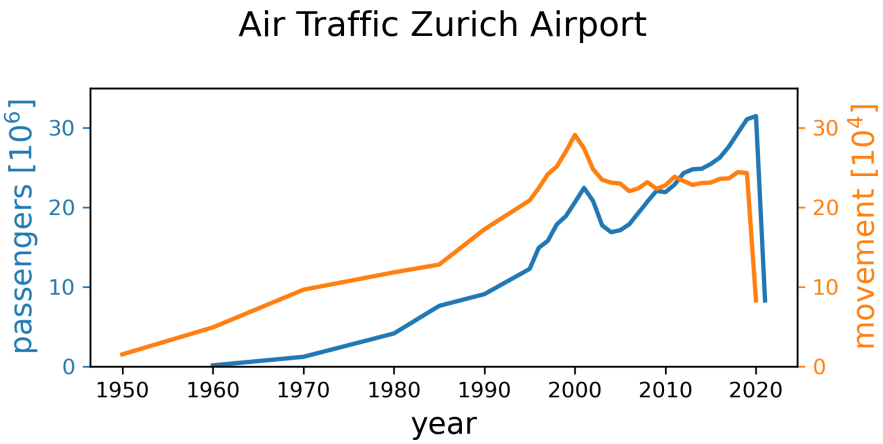

FIGURE 1.4: Air traffic at Zurich Airport (data: BFS and BAZL, 2021). In blue number of passengers [10^6] and in orange number of flight movements [10^4].

The reduced mobility worldwide due to the restrictions caused by the Sars-CoV-2 virus had a temporary but very significant impact on air quality. One study estimated that daily global CO_2 emissions decreased by 17% in April 2020 compared to mean daily emissions of 2019 (Le Quéré et al., 2020), while another study found a global overall decrease of 8.8% during the first half of 2020 compared to 2019 (Liu et al., 2020). The change can be seen especially in decline of daily global emissions in the month of April, as the emissions recovered quickly due to the relaxation of the measures (Liu et al., 2020).

Furthermore, European satellite imagery (Copernicus Sentinel-5P) observed a 45-50% drop in nitrogen dioxide (NO_2), a harmful indirect greenhouse gas, over metropolitan areas such as Paris and Milan (ESA, 2020). Bayesian spatio-temporal models (BST) determined a 29.5% decrease in the average surface concentration of NO_2 over Europe due to pandemic

related restrictions, considering also other factors (e.g. weather conditions) that could influence the measured concentration (Beloconi et al., 2021).

The decrease in NO_2 but also CO_2 was particularly significant in countries with strict lockdown conditions and travel restrictions (Cooper et al., 2022; Liu et al., 2020). Reduction in air pollutants due to travel restrictions as part of the Covid-19 pandemic measures have temporarily partly improved air quality. This was especially evident in metropolitan areas and densely populated countries such as China, India, and Nigeria, where advanced technologies for air pollution control are often lacking (Karkour and Itsubo, 2020; Han and Hong, 2020; Berman and Ebisu, 2020).

Air quality also changed in Switzerland, although to a smaller extent than in other parts of Europe. This could be related to the fact that the Swiss population had to follow less strict measures to combat the Covid-19 pandemic and because of the fact that major efforts have already been made by policymakers to reduce air pollution in recent years (Stuart K. et al., 2020; BAFU, 2021c). Nevertheless, air monitoring networks (NABEL and OSTLUFT) on busy roads show a significant decrease of NO_2 concentrations in Switzerland during the pandemic lockdown (BAFU, 2021c; Sintermann, 2020; Stuart K. et al., 2020). At Zurich Airport, this NO_2 reduction is reflected very impressively due to the strong decrease in air and surrounding road traffic (see Figure 1.5 and 2.4; FZAG, 2020a; Fleuti, 2020).

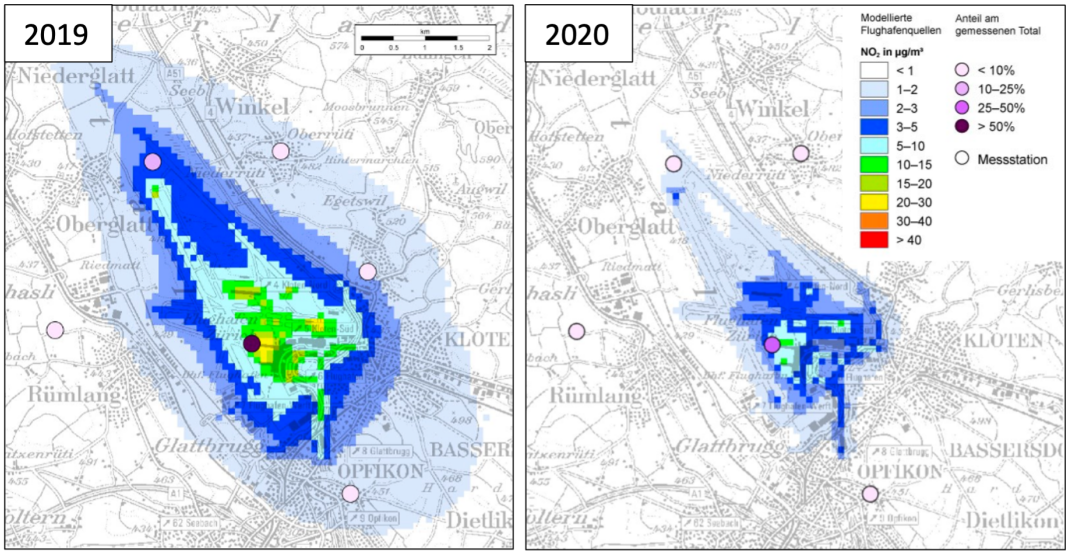

FIGURE 1.5: NO_2 $[\mu g/m^3]$ concentration at Zurich Airport, 2019 (left) and 2020 (right). Source: FZAG, 2019; FZAG, 2020a: Influence of the airport on local air quality.

It is reasonable to assume that the reduction in traffic-related noise and pollutants has also led to a reduction in associated health problems. Recently published studies also show a possible association between long-term exposure to air pollution especially fine $<PM_{2.5}$ and severe Sars-CoV-2 courses with a higher probability of mortality (Pozzer et al., 2020; Münzel et al., 2021; Wu et al., 2020; Travaglio et al., 2021). This interaction is not surprising and shows how people's activities change the environment in which they live, which in turn can affect their health. Therefore, future efforts to monitor air quality on a continuous, long-term, and detailed basis are all the more essential in order to be able to take concrete measures to improve air quality.

1.4 Trees as bio-indicators for air pollution and climate

It is known that trees can have a positive impact on air quality and climate, especially in urban areas (Leung et al., 2011; Nowak et al., 2018). For instance, tree canopies and transpiration can influence local temperatures, radiation/energy balance, and thus the local microclimate (Nowak et al., 2018). However, they can also have negative impacts on air quality and climate by releasing natural particulate matter in form of pollen and biogenic VOCs, whereby the latter play an important role in the formation of ozone and secondary particulate matter (Ballikaya et al., 2022; Eisenman et al., 2019; Grote et al., 2016; Samson et al., 2017). Their canopy can even reduce ventilation and thus dilution of air pollutants in the atmosphere; this aerodynamic effect can lead to lower air quality locally, especially in poorly ventilated streets (Vos et al., 2013; Samson et al., 2017). Plants can therefore clean the air of pollutants, be amplifiers and polluters themselves, but also be so-called pollutant carriers.

Trees are capable of trapping and absorbing gaseous air pollutants and particulate matter (Ballikaya et al., 2022; Samson et al., 2017; Nowak et al., 2018). Generally, air pollutants are deposited wet or dry on the bark, branches, and leaves of the tree, but gaseous pollutants can also be taken up directly through the stomata of the leaves (Samson et al., 2017; Schwab et al., 2016; Eichert et al., 2008). Stomatal regulation aims to maximize photosynthesis and minimize damage from water deficiency, but it also opens the way for air pollutants that could be harmful to the tree at high concentrations and with prolonged exposure (Samson et al., 2017). In this way, some particles can be absorbed by the tree through foliar uptake, while other intercepted particles in turn remain on surfaces and are later resuspended by precipitation, wind or leaf fall into the atmosphere or pedosphere, where they can be taken up by roots (Nowak et al., 2018).

1.4.1 Tree-ring archive - the logbook of the trees

The air pollutants absorbed via leaves, roots and bark can be deposited in the wood (Lepp, 1975; Cocozza et al., 2021; Ballikaya et al., 2022). With the help of dendrochemistry, it has been possible since the 1970s to analyze the chemical composition of the annual rings (Cocozza et al., 2021; Binda et al., 2021). Together with dendrochronology, the age of the tree can be determined and conclusions can be drawn about the influencing environmental factors under which the tree grew in a certain year, such as climatic conditions, and air quality (Battipaglia et al., 2010; Ballikaya et al., 2022). In this way, historical pollution events and climate trends can be captured both spatially and temporally in the form of records in tree rings (Binda et al., 2021; Ballikaya et al., 2022).

Many studies have used a variety of different biomarkers such as trace elements (Mg, Mn, S, Zn, etc.), stable isotope ratios (δ^{15}N, δ^{13}C, δ^{18}O, δ^{2}H) and radiocarbon (^{14}C) to quantify air pollution in tree rings coming from fossil fuel combustion and other anthropogenic activities (Cocozza et al., 2021; Leonelli et al., 2012; Battipaglia et al., 2010; Savard et al., 2009; Rakowski et al., 2008; Saurer et al., 2004). There are several analytical methods commonly used for the analysis of trace elements and stable isotopes in tree rings: Laser ablation - inductively coupled plasma mass spectrometry (LA-ICPMS), X-rays, fluorescence, and isotope ratio mass spectrometry (IRMS) (Binda et al., 2021). In this way, dendrochronology and -chemistry opens a wide range of analytical possibilities in environmental monitoring, especially since perennial plants are abundant and widespread compared to other environmental archives (Binda et al., 2021).

FIGURE 1.6: Trees as bio-indicators: tree-rings and leaves archives.

1.4.2 Foliage records - the whisper of the trees

Compared to root uptake, particle uptake via leaves has been less explored. Recent studies showed that deposition and uptake of particle concentrations via leaves is not negligible compared to the root pathway (Cocozza et al., 2019; Luo et al., 2019; Sun et al., 2021). In an experiment with different tree species and treatment with silver (Ag) nanoparticles (NP), Cocozza et al., 2019 it was shown that the treatment of leaves (spraying of leaves) resulted in higher Ag concentrations in the trunk than treatment of roots (watering), and that this was highly species-specific. Another study demonstrated that maize seedlings foliage exposed to polysterene nanoplastics with different surface charges can take up plastic particles through the stomata and transport them within the plant to the roots (Sun et al., 2021). In this regard, particle absorption depends not only on the external characteristics and metabolism of the plant species, but also on particle properties such as size, chemical composition, water solubility, surface coating, and electrical charge, etc. (Schwab et al., 2016). Therefore, nanoparticle-size uptake of pollutants via stomata is possible and so far, the only proven pathway of leaf uptake (Ballikaya et al., 2022; Eichert et al., 2008; Lv et al., 2019). Other pathways of particle uptake via leaves through cuticle, trichomes, hydathodes, lenticels, and wounds are known but have been insufficiently investigated (Schwab et al., 2016).

Various studies have therefore also examined leaves as an archive for air pollutants with the same biomarkers commonly used in dendrochemical analyses (Ammann et al., 1999; Siegwolf et al., 2001; Alessio et al., 2002; Saurer et al., 2004; Kalugina et al., 2017; Sensuła et al., 2017). Compared to the tree rings, the leaves are directly exposed to the emission sources and may show a clear pollution signal if an uptake occurs. This could be advantageous since the possible loss or blurring of the biomarker signal due to internal translocation of compounds between tree rings is one of the main challenges in dendrochemistry. However, a disadvantage is that the leaves are shed annually for deciduous trees and are also replaced after a few years for conifers. This makes the archive time-limited and less suitable for long-term air pollution or climate records. Although leaves have been used as bio-indicators of air pollution and climate in many environmental monitoring studies, no one has yet attempted to reconstruct air quality using different generations of leaves at annual resolution.

1.5 Research question and hypothesis

The exceptional situation in spring 2020 due to the Covid-19 pandemic and the resulting decrease in road and air traffic has drastically changed air quality locally as well as globally. This unprecedented situation provides a unique opportunity to study air quality in places with highly modified traffic flows and thereby gain new insights into anthropogenic air pollution. Long-lived plants such as trees with clearly visible annual ring structures can be used as bio-indicators to reconstruct both past environmental conditions under which the tree was growing and air pollution events (Ballikaya et al., 2022). Therefore, trees are particularly suitable for environmental monitoring. Thereby trees take up nutrients and potential pollutants not only through their roots but also through their leaves. Evergreen conifers retain their foliage for several years compared to deciduous trees and are therefore of special interest for the study of leaves as a potential archive for air quality. For this reason, and due to their aerodynamic properties, conifers tend to remove more air pollutants and they are able to capture large amounts of PM with their small needles (high leaf area index) and complex shoot structures (Freer-Smith et al., 2005; Samson et al., 2017). The ability of other tree components to adequately capture both spatial and temporal changes in past air pollution events and trends is assessed in this research. Spruces are frequently studied in dendro-scientific analyses due to their distinct tree rings, high adaptability and wide distribution. In addition, the branches and thus the needles can be clearly assigned to a specific year based on the morphology of the tree, which makes the tree species a good leaf-archive for past environmental conditions. The following research question arises:

Research Question Can changes in air quality related to the reduction of air traffic during the Covid-19 pandemic be detected in the needles and tree-ring width of Norway spruce trees (*Picea abies* (L.) H.Karst) near the Airport Zurich/Kloten?

Answering this specific question, some sub-questions need to be answered first:

- How did air quality change during the pandemic?
- How much of this change can be attributed to the reduction in road or air traffic?
- To what extent does the biosphere reflect changes in the air quality and climate?
- Can the underlying cause of the detected signal be attributed to climate or air pollution?

Hypothesis Spruce needles and tree-ring width reliably reflect local changes in air pollution; the pandemic lockdown in spring 2020 with reduced air traffic and the associated improvement in air quality is clearly detectable.

The objective of this study is to quantify atmospheric pollutants over the last four to six years through chemical analyses of Norway spruce needles, with a focus on the Covid-19 pandemic exceptional situation in spring 2020. In addition, the growth of Norway spruces under changing environmental conditions, such as air quality and climate, is studied using tree rings. The difficulty lies in assigning the measured mixed signal in the atmosphere as well as in the biosphere to the individual emission sources. Hence, several sites with emission sources in different proximity are investigated. The focus of many studies is on the dendrochemical analysis of tree rings; less studies use leaves as an archive for air pollution. The extent to which leaves can absorb and transport pollutants from the air and how this can have an effect on tree growth is poorly understood and part of ongoing research. Therefore, two chemical analyses are carried out on the basis of Norway spruce needles: 1) nitrogen isotope analysis (WSL, Isotope Laboratory, Dr. Matthias Saurer) measuring stable nitrogen and carbon isotopes, and 2) the radiocarbon method (ETH, Laboratory for Ion Beam Physics, Dr. Lukas Wacker). In addition, increment cores will be taken from the same trees, evaluated using dendrochronology, and compared with air pollutant and meteorological measurements from local monitoring stations. The goal is to quantify changes in Norway spruce needles of direct (CO_2) and indirect (NO_x) greenhouse gases produced by the combustion of fossil fuels (pre-pandemic, lockdown, and post-pandemic conditions), emitted by aircrafts of Zurich Airport and to assess the effect on tree-ring growth.

2 Material and Methods

2.1 Study site

The study site covers an area of 9.53 km^2 and is located in the Swiss midlands in the canton of Zurich between Kloten, Rümlang, Oberglatt, Niederglatt and Bülach at 426 meters above sea level. The moraine landscape was once formed by the Linth glacier, which left behind a shallow lake after the last cold period 180'000 years ago (FZAG, 2020b). This shallow lake slowly developed into a marsh which was partly drained for the construction of Zurich International Airport in 1946 (FZAG, 2020b; Güttler et al., 2018). Some areas of Zurich Airport and its surroundings are still characterized by these marshes, including 43 hectares of objects of national importance that are under strict protection (FZAG, 2020b). Together with swamp and mixed forests the wetland maintains its exceptionally high biodiversity. The airport area is advantageously flat and mainly characterized by westerly winds and breezes (north-east winds) (see Figure 2.2, MeteoSwiss, 2022). The local climate is humid with an average annual temperature of 9.8°C and an average annual rainfall of 995mm (see Figure 2.1, MeteoSwiss, 2022).

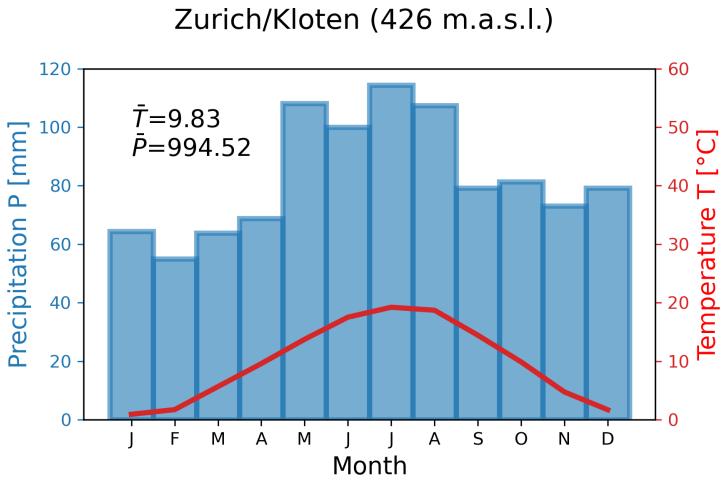

FIGURE 2.1: Climate diagram Zurich/Kloten, calculated with annual precipitation and temperature data from the period 1991-2020 (data: MeteoSwiss, 2022). In blue the average precipitation sums per month [mm] and in red the average monthly temperature [°C]. $\bar{T}$ = 9.83°C average annual temperature. $\bar{P}$ = 994.52mm average annual precipitation sum.

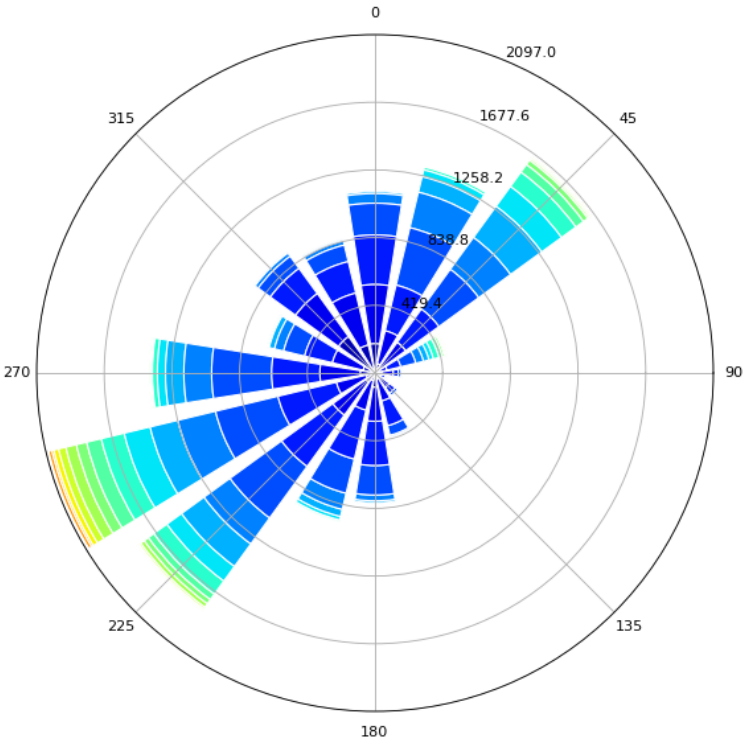

FIGURE 2.2: Wind diagram Zurich/ Kloten, calculated with daily wind speed and direction data from the period 1981-2021 (data: MeteoSwiss, 2022). Wind direction in angular measure [0°-360], 0° = north. Wind speed [m/s] from blue to orange at intervals of 0.5m/s, wind speed max. = 10.5m/s. The radial compartments correspond to the number of occurrences [days] of a particular wind speed and direction, main wind direction: W, SW and NE.

In order to assess the air pollutants coming from aircraft movements at Zurich Airport suitable locations were chosen close to the emission source. Since attempts to obtain permission for sampling on the airport area itself failed, sites were chosen in the immediate vicinity. When choosing the location, it was important to be as close as possible to the airport's docks, runways or flight paths and thus to the source of emissions. The wind direction was also considered in the further planning. Based on the approach concept of the different runways (rule of thumb: aircraft land against the prevailing wind direction) and the frequent westerly winds, locations in the east of the airport were preferred. Moreover, the choice of location in the east of the airport was limited due to the A51 motorway. To avoid a strong mixed emission signal from road and air traffic, the distance to the motorway was kept as large as possible. Given this challenge, another site to the west of the airport was selected for comparison.

Norway spruces (*Picea abies* (L.) H.Karst) were chosen as the tree species for the study. The evergreen conifers are very suitable for tree-ring analysis and form new twigs with needles every year, which are the main object of investigation in this thesis. This limited the choice of sites a little more, especially in the east of the airport, where mainly deciduous trees predominated. Furthermore, the forests under consideration had different ownership structures. They belonged to private individuals, corporations, municipalities, the canton of Zurich or the federal government. Therefore, permission first had to be obtained from the responsible authorities for sampling at the respective site.

Site 1 - Carparking (430 m a.s.l.): The first site was located north-east of Zurich Airport at the end of Runway 14/32 (see Figure 2.5). The A51 motorway was located about 550 m away and the flight path was about 400 m away. In the immediate vicinity there was a road with low traffic and a car park with a viewpoint. The forest "Äglenriet" belongs to the federal government and is used by the military. The area itself lies within the municipality of Winkel (forester: Michel Kern). Norway spruces (*Picea abies* (L.) H.Karst) were sampled within a radius of 10 m from the chosen location, where the selected canopies were especially exposed to the flight path and Runway 14/32 (SW orientation).

Site 2 - Runway (420 m a.s.l): Another site was chosen in the western part of the airport at the middle of Runway 16/34 (see Figure 2.5) in the forest "Gstöck" of the municipality of Rümlang (forester: Thomas Hubli). The trees of interest were located in a marsh, called "Langensegen", which still is under nature conservation. Therefore, permission to enter and take samples had to be obtained from the Canton of Zurich (Supervision: Dipl. Forsting. ETH, Adrienne Frei). The nature conservation area "Langensegen" was difficult to access due to the wet and unpredictable terrain. The area impressively showed what it must have looked like here before Zurich Airport was built (see Figure 2.3a and 2.3b). The nearest busy road was approximately 1 km west from the site and the average distance to the runways was about 300 m. Norway spruces were sampled within a radius of 150 m, that were again exposed to the flight path and runway (NE orientation).

Site 3 - Touchdown oaks (423 m a.s.l.): In the eastern part of the airport along the Himmelbach (see Figure 2.5) only deciduous trees were found such as willows, oaks, maples, birches and beeches. Given the proximity to the touch down point of Runway 14/32, some European oaks (*Quercus robur* L.) were also sampled. However, these were not compared with the tree species of the other sites. The oaks were sampled within a radius of 550 m with a distance of 350-200 m to the runway and flight path (SW orientation). The A51 motorway was again located about 500 m from the site.

Site 4 - Control (440 m a.s.l.): The control site was chosen approximately 1.7 km further north from the carparking site and 4.4 km from the runway site (see Figure 2.5). Efforts

were made to ensure that the site was as far away from the motorway as the carparking site. This site was the last to be sampled and was used for comparison with the other sites closer to Zurich Airport. The "Höragen" forest belongs to the municipality of Bülach (forester: Thomas Kuhn). The selected Norway spruces were located on a slight hill and were sampled within a radius of 15 m. Smaller clearings existed since 2019 due to bark beetle infestation.

(A) marsh in summer 2021 (B) dragonfly in summer 2021

FIGURE 2.3: Nature conservation area Langensegen - runway site, Zurich Airport

2.2 Monitoring stations

In order to be able to compare the measurement results with atmospheric air pollutants and climatic factors, data were requested from the operators of measuring stations in the immediate vicinity of the airport. Thus, a Meteo-Swiss station at Zurich Airport area provided the necessary meteorological parameters to describe the climatic conditions at the various locations and to perform further climate analyses (approx. station's distance to runway and control site: 2 km-2.7 km) (see Figure 2.5). For this purpose, the meteorological parameters: temperature and precipitation of the Meteo-Swiss station were processed (data source: MeteoSwiss, 2022). In each case, an average value was calculated for the growing season of one year. The growing season was defined as the time span from the beginning of earlywood (April) to the end of latewood formation (October). In addition, two measuring stations were selected to measure air pollutants in the vicinity of Zurich Airport. The stations selected were Zurich Airport, Terminal A, operated by FZAG (approx. station's distance to runway and control site: 1.7 km-5.8 km; data source: FZAG, 2022), and the Balsberg station, Opfikon, operated by OSTLUFT, the air quality monitoring service of the cantons of eastern Switzerland and the Principality of Liechtenstein (approx. station's distance to runway and control site: 3.6 km-7.8 km; data source: OSTLUFT, 2022) (see Figure 2.5 and 2.4). Although other monitoring stations were available that were closer to the study sites, these two stations were selected because they were less affected by measurement interruptions and provide complete data sets at least up to 2008.

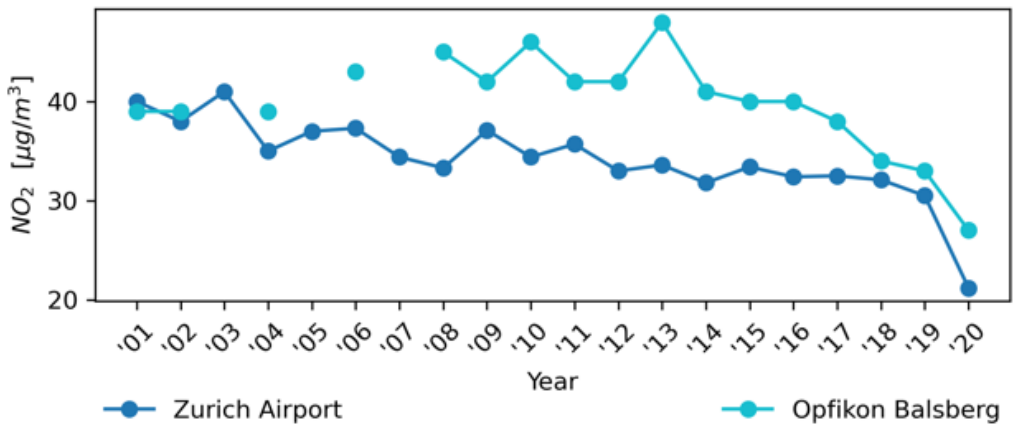

FIGURE 2.4: Atmospheric annual mean NO_2 [$\mu g/m^3$] concentration at Zurich Airport from 2001 to 2020 at different measuring stations. Dark blue: Zurich Airport Terminal A (data: FZAG, 2022) and light blue: Opfikon, Balsberg (data: OSTLUFT, 2022)

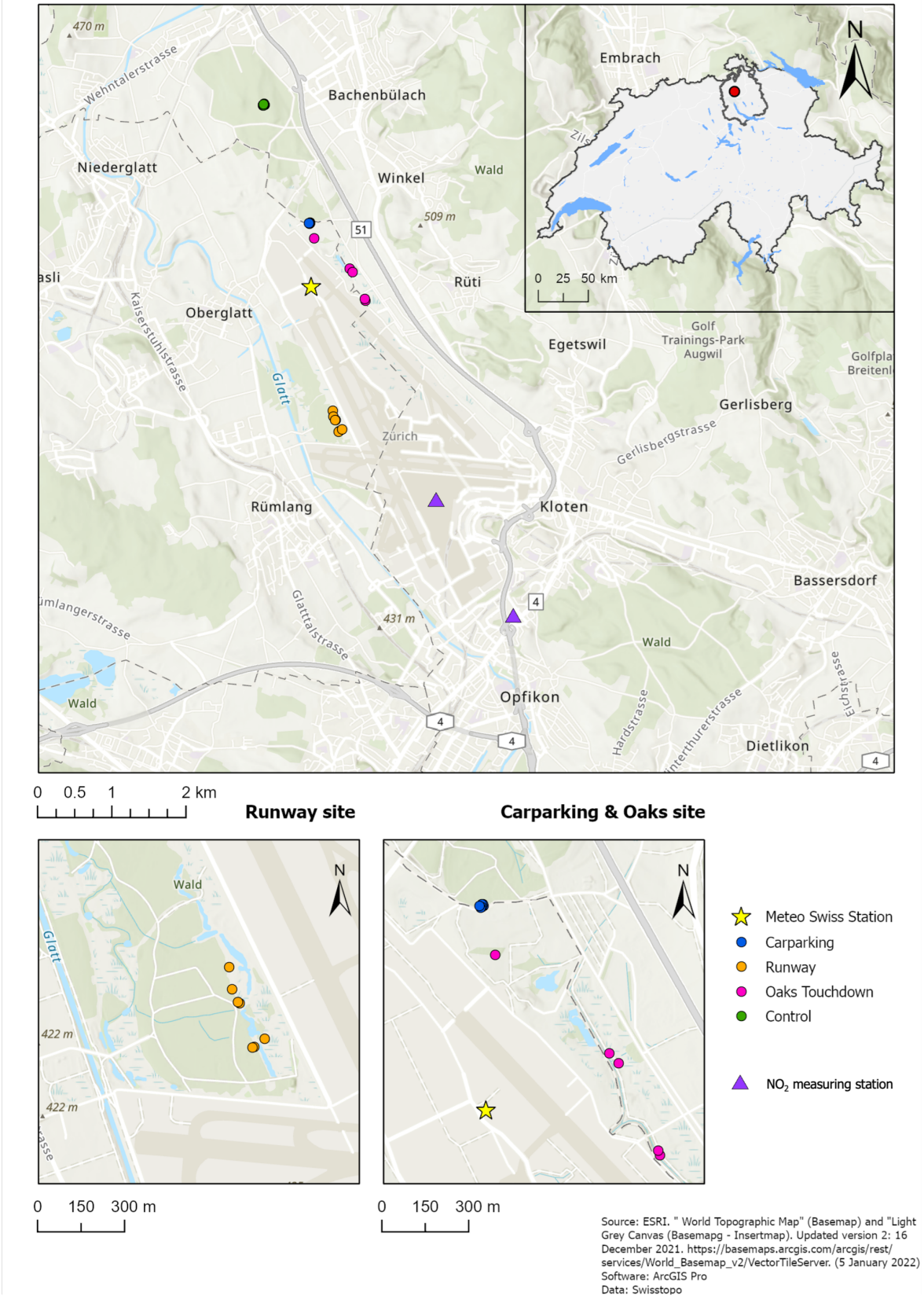

FIGURE 2.5: Map Airport Zurich/Kloten (Switzerland) - Sites Carparking (blue), Runway (orange), Oaks Touchdown (pink), Control (green), meteorological measuring station (yellow) and NO_2 measuring stations: Zurich Airport Terminal A (FZAG) and Balsberg, Opfikon (OSTLUFT) (violet).

2.3 Sampling

The sampling of the different sites was carried out in several stages due to the pending permits, the size of the area and the mobility at the sites. Therefore, sampling took place from May through September 2021. Specifically, six exposed Norway spruce or European oak trees were selected and sampled. Since the selection of trees with the above-mentioned constraints (distance from the emission source, orientation, species, and accessibility) was relatively small, healthy trees were selected whose crowns were free-standing and well exposed to the runway.

Two tree cores were extracted from two sides of each chosen tree on breast height (1.3 m above ground) using an increment corer (5 mm diameter) (see Figure 2.6a). All parts of the corer were disinfected after each tree sampling to prevent contamination of the samples and the transfer of fungal infections between the trees. The remaining holes were marked with a number for the respective tree and a letter for the extracted core. The same designation was given to the increment cores after they were wrapped into paper straws. In addition, the coordinates of the trees were noted. The coordinates and the marking of the trees were extremely important in order to be able to find the sampled trees again at a later date for the second sampling, when the branches were cut off.

(A) Extracting tree cores with increment corer

(B) Cutting branches at dizzying height (Claudio Cattaneo and Peter Suter from WSL)

FIGURE 2.6: Sampling at the carparking site, Zurich Airport

With the help of the employees of the experimental garden at Birmensdorf, WSL (Gabor Reiss, Claudia Cattaneo, and Peter Suter), the Norway spruces at the carparking, runway and control sites were sampled a second time. Using a ladder construction and climbing equipment, three main branches per spruce were cut off at dizzying heights (see Figure 2.6b). The branches were selected based on their height above ground and their orientation to the emission source. Afterwards, the branches were packed in plastic bags, labelled and frozen at -5°C in the freezer of the WSL for further analysis. The bags were kept slightly open to avoid condensation, to keep the spruce needles fresh and to prevent the formation of fungi.

2.4 Preparation

The increment cores were taken out of the paper straw and air-dried on supports. They were covered with paper to avoid possible contamination. In order to prepare the increment cores for tree-ring width analysis, the cores were cut perpendicular to the longitudinal axis of the wood cells using a Core-Microtome from the WSL wood anatomy laboratory (see Figure 2.7). The clean cut with the Core-Microtome keeps the cell walls smooth and free of swarf so that the annual rings and thus the difference between late and early wood is better visible (Gärtner and Nievergelt, 2010). Another advantage of this technique is that the cells are not filled with swarf as in the case of sanding, which is an important aspect for isotope and chemical analysis of individual tree rings (Gärtner and Nievergelt, 2010). However, especially the increment cores of European oak, but also Norway spruce were very difficult to cut when dried, so the cores had to be treated with water to be able to cut the wood properly and avoid breakage. For some chemical analyses, the preparation of the increment cores is essential to avoid potential contamination of the samples. In this case, the treatment of the cores with water was not an issue.

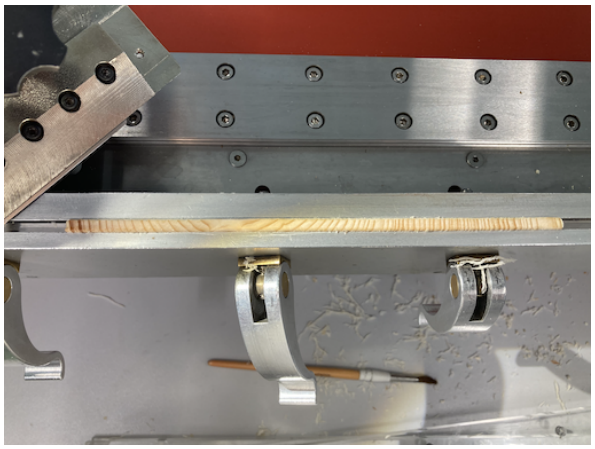

FIGURE 2.7: Cutting tree cores with Core-Microtome at Anatomy and Isotope Laboratory, WSL

The branches of the Norway spruces were first separated by the age of the twigs (see Figure 2.9a). The counting was done from the leader twig of the current year along the main branch. In this case the branches were cut in 2021 and the new needles are clearly recognizable by their light green color (see Figure 2.9b). Using the junctions and nodes it was possible to count back to the year of 2016. This technique required a lot of experience

because nature does not follow a perfect symmetry. The older the twigs, the higher the error rate. So-called sleeping buds can persist for years and sprout somewhere at a later date, this disrupts the order and the counting gets difficult (Aas et al., 2017). In case of doubt, the tree rings of the twig could be counted under the microscope (see Figure 2.9c). However, as this was very time-consuming, counting along the main branch was the fastest and safest option (see Figure 2.8). After dividing the twigs by year, the needles were carefully separated from the twig and placed in labelled envelopes. The bare twig was also placed with the respective needles to keep the option for further analyses open. Finally, there were 18 samples per tree (3 branches x spruce needles 2016-2021) which were dried in the oven by 60°C for 48h in open envelopes.

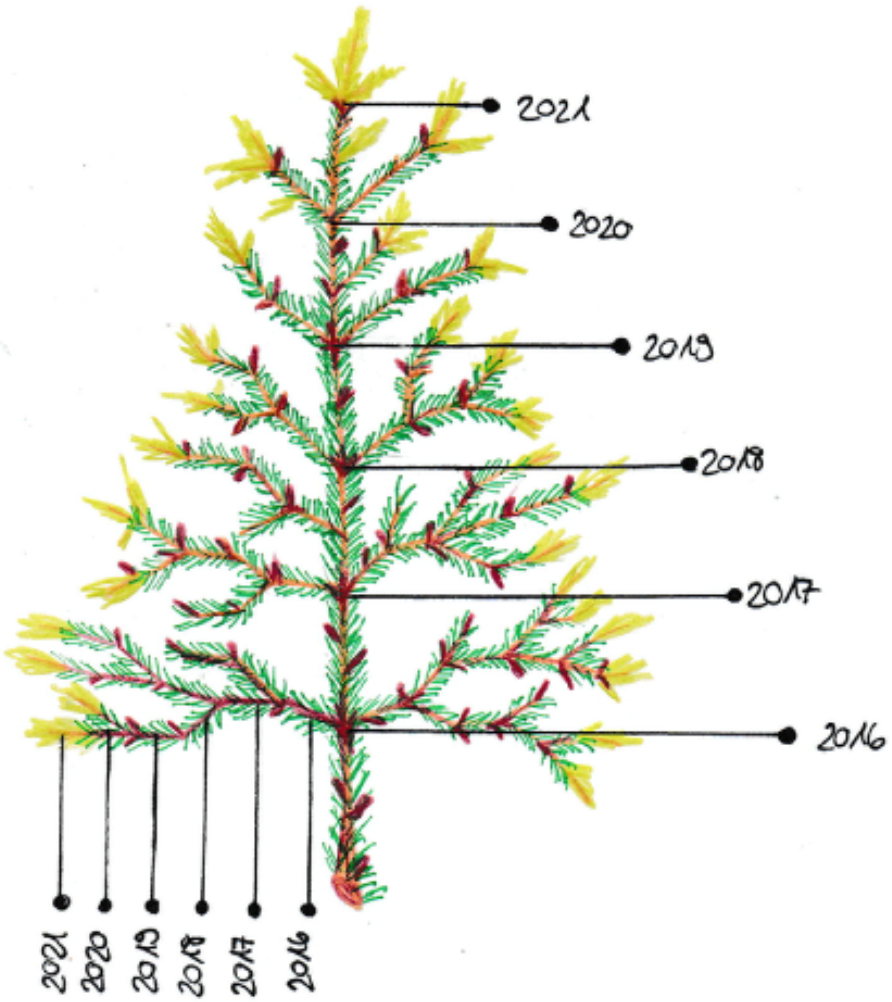

FIGURE 2.8: Norway spruce main branch - how to count

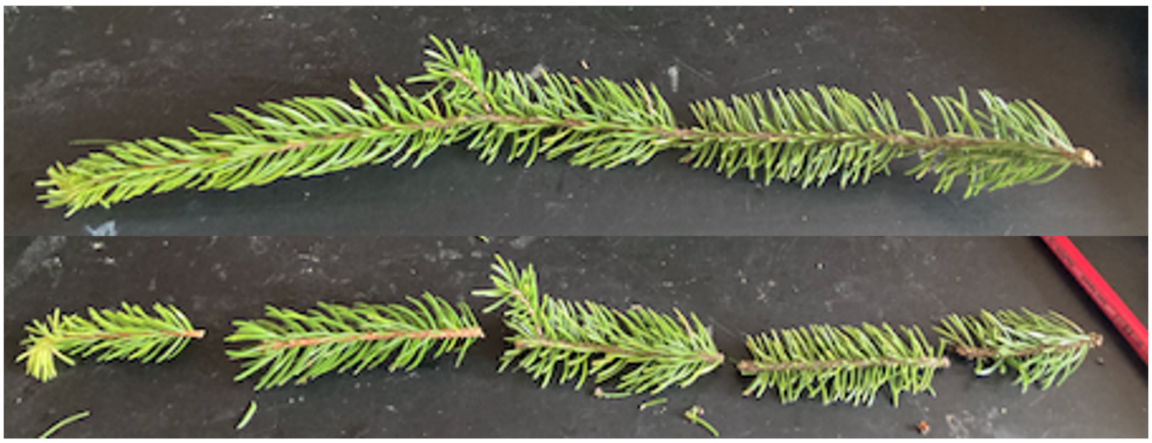

(A) Complete Norway spruce twig (top) and separated by years (bottom)

(B) New needles in light green from 2021

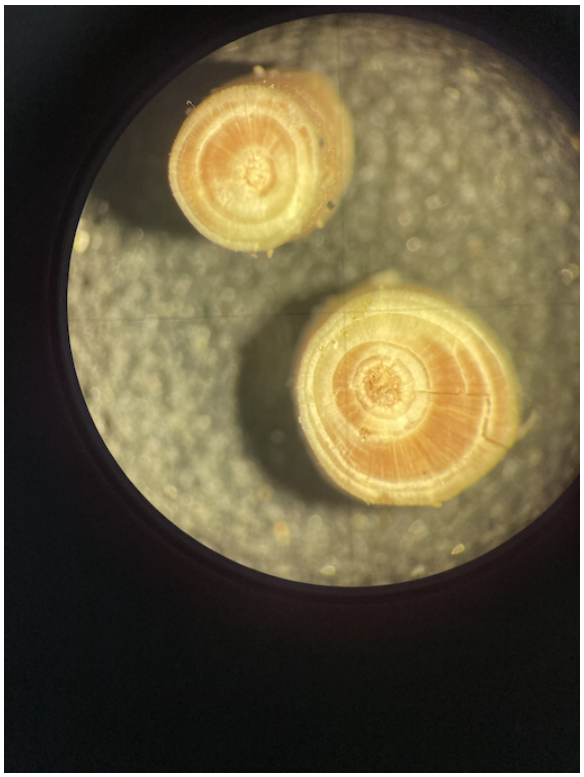

(C) Counting tree rings in twigs under the microscope

FIGURE 2.9: Separating Norway spruce needles by years

2.5 Tree-ring analysis

In a further procedure, one of the two cores of a tree was sanded and, if necessary, treated with chalk to facilitate visual measurement of tree-ring width under the microscope. Sanded cores are not appropriate for chemical analyses of annual rings, since the fine dust produced in the process is distributed over the entire cross-section and thus contaminates other rings. To preserve the possibility of a dendrochemical analysis, the second core was only cut. Finally, the cores were then clamped in a holder and examined under the microscope.

2.5.1 Ring width measurement

Trees can respond to changes in environmental conditions (e.g., temperature increase/ decrease and water availability), which can be reflected in the annual rings by the variation in ring width and growth anomalies (Schweingruber, 1988; Schweingruber, 1993). Therefore, the tree rings were measured under the stereomicroscope with the LINTAB measuring device and the Time Series Analysis and Presentation software for dendrochronology (TSAP-Win from RINNTECH, Heidelberg, Germany) in the WSL (Birmensdorf) tree-ring laboratory to an accuracy of 0.01 mm. The result was a curve showing the tree-ring width change over time. An annual ring always consists of early and late wood, whereas the development of annual rings is related to the secondary thickening caused by the cambium (living cells) between the xylem (wood) and the phloem (inner bark) (see Figure 2.10; Schweingruber, 2007). In spring, the tree begins to form early wood with large cells and thin walls, which are optimal for the necessary water transport. In late summer, the tree starts to form late wood, the cells are rather small and have thick walls, this gives the tree the necessary stability for the winter (Schweingruber, 1983; Schweingruber, 2007). Counting was done from the ring boundary, the sharp transition from early to late wood, which was clearly visible in color, from bark to pith. There were several difficulties in measuring the width of the tree rings: some cores were broken due to natural weaknesses or due to

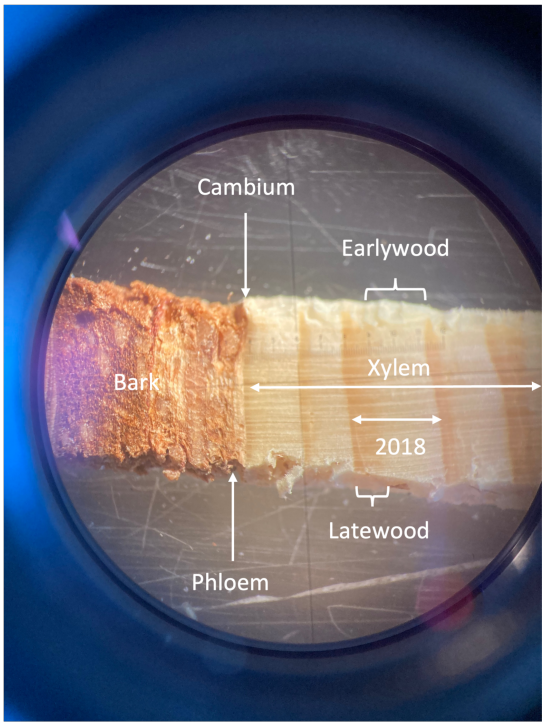

FIGURE 2.10: Anatomy of a tree core view under microscope - consisting of phloem, cambium and xylem (an annual tree ring: early and late wood)

preparation with the Core-Microtome, so that rings may have been lost. In addition, so-called missing and false rings can interfere with the counting process and thus later with cross-dating (Schweingruber, 1980; Schweingruber, 1988; De Micco et al., 2016; Novak et al., 2016). In the midlands, false rings caused by intra-annual density fluctuations (IADF) are a particular problem. These IADF can occur in latewood, but also in earlywood due to the tree's response to changing environmental conditions (Schweingruber, 1980; Schweingruber, 1988; De Micco et al., 2016). In most cases, it was helpful to look at the second core and compare the cores from each site to identify missing or false rings through cross-dating.

2.5.2 Cross-dating

Multiple trees at a particular site can be cross-dated or, if available, compared with an existing chronology to reliably determine the age of the trees and to detect growth anomalies. This method has been used for over 80 years to compare tree-ring patterns and synchronize ring series (Douglass, 1941). These ring series from living, but also from fossil trees can be put together like puzzle pieces to form a main chronology, which in return can provide information about past environmental conditions or serve as a reference (Schweingruber, 1988). Therefore, the tree-ring growth series of this study were visually and statistically cross-dated. The accuracy and reliability of the cross-dated tree-ring series can be checked by calculating the so-called Gleichläufigkeit (GLK). The GLK measures the similarity of the curve segments of two tree-ring series and is expressed as a percentage (Schweingruber, 1988). Together with the GLK, the used program TSAP-Win (RINNTECH, Heidelberg, Germany) indicates the statistical significance (Student's t-test determining the degree of correlation between the curves). The mean values per location were subsequently computed by only considering significant samples with high correlation. Thus, from a GLK of 63%, the tree-ring series of the same tree were first averaged, and then the mean chronology curve between the trees of a site was formed. The chronology was finally detrended using a cubic smoothing spline (command: detrend(rwl = df, method ="Spline") and default options in the R package DPLR to remove the growth trend coming from the increasing age of the tree (Bunn, 2008). In this way, chronologies can be compared with external factors, such as temperature and air pollution data, which can influence the growth of the tree.

2.6 Radiocarbon method

2.6.1 Approach

During its life, an organism is in constant exchange with the carbon cycle. Natural carbon consists of three isotopes - the two stable isotopes ^{12}C and ^{13}C and the radioactive ^{14}C (abundance: ^{12}C > ^{13}C > ^{14}C). The isotope ^{14}C is formed from a nitrogen atom under cosmic radiation in the stratosphere (Bronk Ramsey, 2008). The radiocarbon enters the biosphere through atmospheric mixing and photosynthesis in form of CO_2 (Bronk Ramsey, 2008). Since plants prefer to take up light carbon isotopes, a mass-fractionation effect occurs (Stenström et al., 2011). If the organism dies, it no longer participates in the exchange process with the carbon cycle and the ^{14}C atoms decay according to Godwin (1962) with a half-life of $t_{1/2}$= 5730 years ($\pm$ 30) (Bronk Ramsey, 2008). To correct for the isotope fractionation effect, the ^{14}C is measured with respect to the stable carbon isotopes, compared with a standard material (δ^{13}C) and normalized (Stenström et al., 2011; Reimer et al., 2004). Together with these findings and conventional radiocarbon dating, it is possible to determine the age of organic material (Libby et al., 1949).

The **production rate** of radiocarbon and thus the ratio of stable and unstable carbon isotopes in the atmosphere is subject to fluctuations, caused in part by natural but also anthropogenic factors. Natural fluctuations of the Earth's magnetic field or cyclical changes in solar activity and occurring sunspots (de-Vries effect) influence the production of radiocarbon (Bronk Ramsey, 2008; Vries, 1958 cited in Grootes and Plicht, 2021; Stuiver, 1961). **Exchange processes** between large carbon reservoirs such as the ocean (upwelling) and permafrost (thawing) can also influence the carbon isotope ratio of the atmosphere (Levin and Hesshaimer, 2000). Moreover, since the industrial revolution, greenhouse gases in the atmosphere have increased due to **anthropogenic influences** like land use changes, deforestation or burning of fossil fuels (Levin and Hesshaimer, 2000). The release of carbon dioxide ^{14}C-free (also called "dead" carbon) through the burning of fossil fuels (coal and oil) decrease the ^{14}C/^{12}C ratio of atmospheric CO_2; this phenomenon is called Suess effect (Levin and Hesshaimer, 2000; Suess, 1955). Testing nuclear weapons in the 1950s and 1960s almost doubled the radiocarbon content of the atmosphere (nuclear weapon effect) and thus increased the ^{14}C/^{12}C ratio (Levin and Hesshaimer, 2000; Bronk Ramsey, 2008; Grootes and Plicht, 2021). This effect was so strong that it overshadowed the ^{14}C Suess effect (Levin and Hesshaimer, 2000). For this reason, the ^{14}C concentration in the atmosphere is still falling today and will do until the pre-bomb concentration is reached (Bronk Ramsey, 2008).

Atmospheric $^{14}CO_2$ has been measured quasi-continously since 1959 at three European mountain sites: Vermunt, Austria (1800 m.a.s.l.), Jungfraujoch, Switzerland (3450 m.a.s.l.) and Schauinsland in the Black Forest, Germany (1205 m.a.s.l.) (Levin and Kromer, 2004). The measurements from the Jungfraujoch station represent atmospheric conditions as they would be in the mid-latitudes of northern hemisphere without a dilution effect by ^{14}C free

CO_2 coming from fossil fuels (Levin and Kromer, 2004). Nevertheless, seasonal fluctuations in ^{14}C can be explained by the stable atmospheric stratification in winter and a stronger vertical mixing in summer, with which emissions also reach higher altitudes (Levin and Kromer, 2004). This measured background ^{14}C free CO_2 level over Europe can be used as a reference for estimating the local influence of fossil fuel CO_2.

The first discovery of the Suess effect was made by measuring radiocarbon concentration of annual tree rings (Suess, 1955). Trees incorporate carbon isotopes from the atmosphere into their cell structure in the form of cellulose (polysaccharides) through photosynthesis. (Bronk Ramsey, 2008). With the construction of the cells, they thus archive the carbon isotope composition of the atmosphere at a specific place and time. With the completion of a tree ring, the cells no longer actively participate in carbon exchange and the ^{14}C atoms decay (Bronk Ramsey, 2008; Hajdas et al., 2021). The leaves (needles) of Norway spruce also contain cellulose in their cell walls. Compared to the annual rings, the time span of the carbon archive of the needles is much shorter. In the midland, up to seven generations of needles can coexist before the needles become too old and are shed. To investigate the research question of this study, the carbon isotope ratio of four needle generations was measured.

Sample preparation

The radiocarbon dating was carried out at the Laboratory of Ion Beam Physics, ETH-Zurich, under the direction of Dr. Lukas Wacker. As the ^{14}C analysis is very time-consuming and costly, three to four trees were selected at each site, from which the Norway spruce needles of 2018-2021 were analyzed. It was assumed that 2020 needles, exposed to lower emissions coming from air traffic and thus dilution effect during the lockdown, would differ significantly in their isotope ratio from those of previous years 2018 and 2019 (pre-Covid 19 pandemic and "business as usual"). The year 2021 post-lockdown (special situation) was measured to examine the after-effects. In addition, different blanks (kauri, brown coal and phthalic anhydride (chemical blank)) were prepared to determine background signal and cross-contamination from the measurement process and pre's (pre-conditions, sample material) to "clean" the system after every measurement (Wacker et al., 2010b; Sookdeo et al., 2020-08). References (wood) and standards (oxalic acid: (OxI and OxII) with known ^{14}C concentration were used for calibration and control (Sookdeo et al., 2020-08).

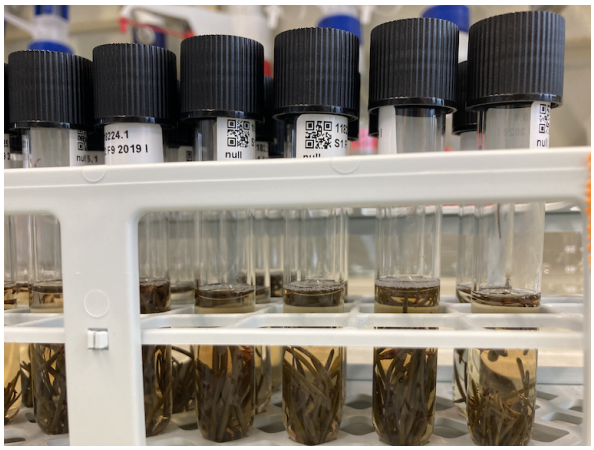

FIGURE 2.11: Acid-base-acid bleaching of Norway spruce (*Picea abies* (L.) H.Karst) needles at the Laboratory of Ion Beam Physics, ETH-Zurich

The samples as well as the references and blanks were then cleaned with an acid-base bleach (see Figure 2.11). The so-called ABA (acid-base-acid) procedure is used to remove hydrolysable carbons and other mobile components on the outermost layer of the needles that could influence the isotopic ratio measure (Němec et al., 2010; Gaudinski et al., 2005). For this purpose, the vials with the samples were carefully covered with a hydrochloric acid solution (0.5 mol/L HCl). Then the samples were heated in the oven at 60°C for one hour. Afterwards, the acid was carefully poured away and the needles were cleaned in 3-4 wash cycles with ultrapure water. Next, the needles had to be treated with a sodium hydroxide solution (0.1 mol/L NaOH) and heated again for one hour at 60°C in the oven. Again, the alkaline solution was removed and 3-4 washes with ultrapure water followed. After that the same procedure was carried out again with hydrochloric acid (0.5 mol/L HCl). The remaining liquid was removed from the vials after the last washing and the samples were then frozen and dried overnight using a freeze-dryer.

In the next step the samples were prepared for graphitization. The spruce needles were chopped/milled, weighed into aluminum capsules and round folded (3-4mg). The same was done with the blanks, references and standards (oxalic acid: OxI and OxII). The capsules were placed in an Automated Graphitization Equipment (AGE-3, Ionplus), burnt and graphitized (see Figure 2.12a). By burning the samples with the help of oxygen (O_2) and helium (He) in the elemental analyzer, CO_2 is produced and absorbed in a column filled with zeolite material (Sookdeo et al., 2020-08; Wacker et al., 2010b). The zeolite column is heated and the CO_2 enters the reactors by gas expansion, where hydrogen (H_2) is added and graphitization takes place (Wacker et al., 2010b). The combustion process went wrong a few times and some samples had to be prepared a second or even third time. Not like other organic material, the spruce needles burn poorly and the temperature as well as the duration of the combustion had to be adjusted. The graphite resulting from the combustion (ca. 1mg) was pressed into aluminum cathodes which were placed into a magazine (see Figure 2.12b). Finally, the sample were measured on a MICADAS (MIni CArbon DAting System), a small radiocarbon AMS (accelerator mass spectrometry) system, also found in the Laboratory of Ion Beam Physics, ETH-Zurich (see Figure 2.12c) (Synal et al., 2007; Wacker et al., 2010a).

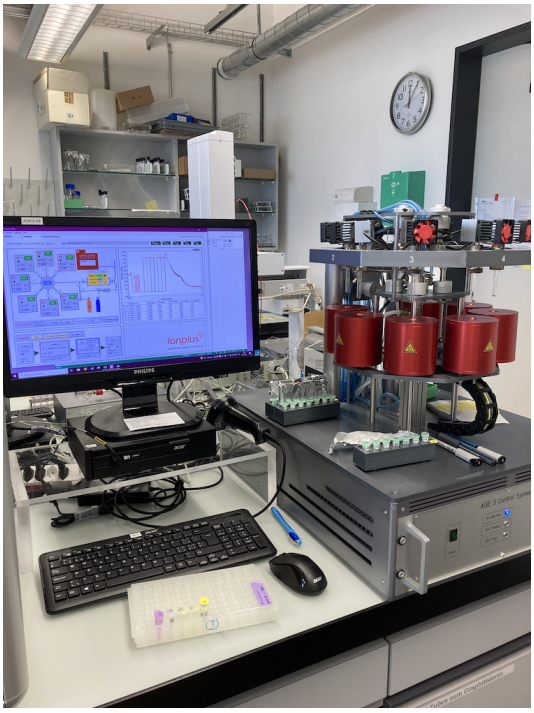

(A) Automated Graphitization Equipment

(B) Pressing graphite into aluminum cathodes

(C) Mini carbon dating system (MICADAS)

FIGURE 2.12: Sample preparation for radiocarbon dating at the Laboratory of Ion Beam Physics, ETH-Zurich

2.7 Stable isotopes

Stable nitrogen and carbon isotope analyses were performed on spruce needles to determine changes in air traffic emissions during the Covid-19 pandemic and their contribution to air pollution over the past six years.

2.7.1 Nitrogen isotopes

Approach

The main component of the Earth's atmosphere is elemental nitrogen (N_2) with a share of around 78%, making it the largest nitrogen pool in the global nitrogen cycle. In addition to elemental nitrogen, reactive nitrogen (N_r) occurs in a wide variety of forms such as nitrogen oxides, ammonia, ammonium, nitric acid and nitrates. As the name suggests, some of these N_r especially NO_x play an important role for many biogeochemical processes, for instance in the Earth's radiation balance, in the chemistry of the ozone layer in the stratosphere and in the formation of secondary PM (Fowler et al., 2013). Natural sources of N_r are biological nitrogen fixation (BNF) and NO_x produced by lightning (Fowler et al., 2013). Human activities such as the burning of fossil fuels in transportation and industry, electricity production, biomass combustion, and the synthetic production of ammonia (Haber-Bosch process) for agriculture to increase yields lead to elevated N_r concentrations in the atmosphere, soil, and water. This additional anthropogenic N_r source amplifies air pollution and climate change and leads to acidification and eutrophication of aquatic and terrestrial ecosystems, which can result in biodiversity losses (Savard et al., 2021; Fowler et al., 2013). This anthropogenic N_r source has doubled globally since the beginning of industrialization and significantly changed and accelerated the biogeochemical nitrogen cycle (Geng et al., 2014; Fowler et al., 2013).

The additional nitrogen input from anthropogenic activities in forests often leads to a nutrient imbalance which can have ambiguous effects on trees: toxic and beneficial (Siegwolf et al., 2001). At N-limited ecosystems the nitrogen input can have a fertilizing effect and even promote carbon sequestration and biomass production (Norby, 1998; Brunner and Brodbeck, 2001; Galloway et al., 2008). However, it can also disturb the relationship root/shoot ratio, since when nitrogen availability is high, a lot of carbon is invested in the foliage, which in turn can have negative consequences in the long term (Siegwolf et al., 2001). The soil-plant system is very sensitive when the soil is fertilized with one nutrient (e.g. nitrogen); suddenly another nutrient (e.g. phosphorus) can become the limiting factor for plant growth (Vitousek et al., 2010). Therefore, how trees respond to nitrogen fertilization depends strongly on the prevailing conditions of their ecosystem such as nutrient availability, soil properties (e.g. pH, soil temperature), symbioses with mycorrhizas, change in soil microbe communities etc., but also on the type and duration of nitrogen emission

input (Brunner and Brodbeck, 2001; Bukata and Kyser, 2007; Guerrieri et al., 2009; Vitousek et al., 2010; Savard et al., 2021).

Changes in the nitrogen cycle can be studied using nitrogen isotope analysis. The varying nitrogen isotope concentration of the less abundant stable isotope ^{15}N is expressed as a ratio ^{15}N/^{14}N, using an international reference standard atmospheric N_2 (Mariotti, 1983; Saurer et al., 2004). Various studies have shown that the ratio of stable nitrogen isotopes (δ^{15}N) of polluted urban and industrial areas, and roads differed significantly from remote unpolluted places and that this variation was reflected in the vegetation involved in the nitrogen cycle (Freyer, 1991; Ammann et al., 1999; Siegwolf et al., 2001; Saurer et al., 2004; Bukata and Kyser, 2007; Savard et al., 2009). Trees are suitable for the analysis of nitrogen isotopes in tree rings and thus record changes in the nitrogen cycle due to their longevity and geographical distribution (Bukata and Kyser, 2007). As examined in several studies, tree rings and foliage δ^{15}N can provide information on past releases of anthropogenic N_r (Ammann et al., 1999; Siegwolf et al., 2001; Saurer et al., 2004; Bukata and Kyser, 2007; Savard et al., 2009; Leonelli et al., 2012).

However, there are some limitations to the use of nitrogen isotope analysis for distinguishing different emission sources. The isotopic ratio depends not only on changes in N_r emissions, but also on regional climatic conditions (changes in precipitation and temperature) and local soil conditions, and is thus subject to seasonal and geographic fluctuations (Bukata and Kyser, 2007). Furthermore, the two pathways of nitrogen uptake via the leaves and the roots make it difficult to assign the measured signal to a specific uptake pathway and to differentiate between nitrogen background (soil) and emission (exhausts) sources (Bukata and Kyser, 2007; Saurer et al., 2004; Siegwolf et al., 2001; Savard, 2010). Moreover, lateral transport (mobility) of nitrogen in the stem from heartwood to sapwood, during cell death, can also blur the time-related signal (Saurer et al., 2004; Bukata and Kyser, 2007; Savard, 2010). These plant-internal nitrogen transports could also be an issue for the needles and should not be neglected.

2.7.2 Carbon isotopes

Approach

The carbon in the organic matter of plants comes from atmospheric CO_2 taken up during photosynthesis. The stable carbon isotope ratio of plant material such as tree rings or leaves is influenced by the isotopic composition of the source and further by fractionation effects during the uptake of CO_2, which mainly occur during the diffusion of CO_2 through stomatal openings and biochemical reactions (Siegwolf et al., 2001). These processes are in turn influenced by climate (water availability and irradiance), so that drier conditions lead to stomatal closure of (C3) plants, which results in increased ^{13}C levels (Leonelli et al., 2012). Therefore, stable carbon isotope analysis is often used in studies about carbon uptake limitations and water use efficiency in trees (Panek and Waring, 1997; Leffler and Evans, 1999).

In contrast, CO_2 emissions from combustion processes result in a relatively low ^{13}C values (δ^{13}C CO_2 of atmospheric origin is about -8 ‰ CO_2; δ^{13}C CO_2 of fossil fuels is about -25 ‰), at high exposure to such emission sources one could expect also a more negative ^{13}C signal of the plant material (Alessio et al., 2002). However, several studies demonstrated increased δ^{13}C in tree rings by affecting carbon discrimination upon exposure to elevated atmospheric pollutants such as NO_2 (Niemelä et al., 1997; Rennenberg and Gessler, 1999; Siegwolf et al., 2001; Guerrieri et al., 2009Battipaglia et al., 2010). This shows that the physiological response of the tree leaves to exposure to air pollutants can vary, with stomatal conductance either decreasing or increasing depending on whether the substance is toxic or beneficial (Siegwolf et al., 2001). These findings show that the stable carbon isotope signal in tree rings and leaves is a good proxy for studying the physiological responses of trees to external factors.

Sample preparation

The nitrogen isotope analysis was carried out at WSL under the direction of Dr. Matthias Saurer and laboratory support from Loic Schneider. For the carparking and runway sites, dried needles from three different branches per tree from the years 2016 to 2021 were analyzed. Thus, there were 18 samples per tree, 54 from one site and 108 for both sites. Due to the limited number of analysis possible, the needles from the branches of one tree were pooled into one sample per year for the control site. Hence, 18 additional samples were analyzed for the control site (total: 126 samples). The dried Norway spruce needles were milled with a centrifugal mill (ZM 200, Retsch, Germany) to a fine powder (<0.05 mm), which was filled into plastic centrifuge tubes (see Figure 2.13a). This milling process was very time-consuming, as the mill had to be dismantled into individual parts after each run, properly cleaned with water and dried, to avoid contamination. The spruce needle powder was also very sticky (see Figure 2.13b), which made the cleaning process even more challenging.

A total of 180 samples were milled. In the next step, 1 mg ($\pm$ 0.1 mg) of spruce needle powder from the milling was weighed in tin capsules using a highly precise analytical balance (see Figure 2.13c). The round folded capsules were sorted into a labeled magazine and the weight recorded in a log. The prepared samples were then measured in the WSL Isotope Laboratory using a high-performance elemental analyzer (IsoEarth from Secron, Crewe UK) and an isotope ratio mass spectrometer (IRMS, IsoEarth from Secron, Crewe, UK). For this purpose, the tin capsule with the sample was burnt in the elemental analyzer under oxygen, producing gases such as CO_2, N_2, NO_x, and H_2O. The nitrogen oxides (NO_x) were reduced to N_2 with the help of copper and the water vapor was removed. The remaining CO_2 and N_2 were separated by gas-chromatography and fed into the IRMS, where δ^{15}N and δ^{13}C [‰] was measured as well as the total N- and C-concentration [%]. The isotope values were expressed in the δ-notation (in per mill) as a relative deviation from the international standard.

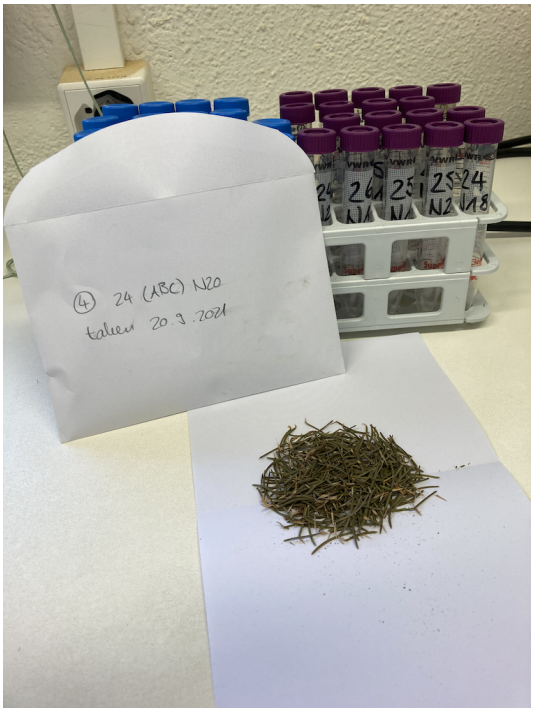

(A) Sample preparation for milling process

(B) Sticky spruce needle powder in mill

(C) Weighing spruce needle powder in tin capsules

FIGURE 2.13: Sample preparation for nitrogen isotope analysis at the Anatomy and Isotope Laboratory, WSL

3 Results

The effects of traffic-related emissions from Zurich Airport and its surroundings were investigated using three different analyses. Stable and radioactive isotope analyses of the elements carbon and nitrogen were performed on Norway spruce needles to determine the effects of fossil fuels combustion pre-pandemic (business as usual) and during the lockdown (traffic reduction). In the last section, tree-ring analysis was performed on the sampled trees to provide information on influencing factors on tree-ring growth such as climate conditions and air pollution in the study area.

3.1 $F^{14}C$ - Radiocarbon results

The results of the measured samples of radiocarbon analysis by MICADAS at ETH Zürich were reported as Fraction Modern $F^{14}C$ (Reimer et al., 2004; Stenström et al., 2011). The fractionation effect has already been corrected with the ratio of stable carbon isotopes $\delta^{13}C$ and normalized to a standard value (see Section 2.5.2). The results were first compared with the $F^{14}C$ dataset of Levin and Kromer (2004) (see Figure 3.1). Data came from measurements at stations in remote mountain regions in Germany (Schauinsland), Austria (Vermunt) and Switzerland (Jungfraujoch), which were subsequently processed at the Heidelberg Radiocarbon Laboratory in Germany (Levin and Kromer, 2004). This dataset is available to the public and shows atmospheric conditions with negligible dilution effect coming from fossil fuel combustion (^{14}C free CO_2). It should be noted here that minimal anthropogenic influence through vertical exchange processes in the atmosphere cannot be completely excluded even at these remote sites (Levin and Kromer, 2004). Nevertheless, the atmospheric $F^{14}C$ background dataset is a good reference for the analysis of anthropogenic air pollution in the study area.

Since the dataset only extends to 2019, the data were extrapolated to obtain comparative values for the 2020 and 2021 samples ($r^2 = 0.996$). For this purpose, the atmospheric measurements of the summer months (growing season) were extrapolated using a nonlinear fit of a function that behaves like $1/x$ (see orange curve in 3.1). It should be noted that the extrapolation is an estimate and may differ from the actual measurements. The $F^{14}C$ values and thus the $^{14}C/^{12}C$ ratio of all measured spruce needles were lower than the extrapolated data from the atmospheric background measurements (see Table 3.1). The depletion of ^{14}C in the spruce needles with respect to the ^{14}C background of the "undisturbed" atmosphere, gives an indication about the influence of a fossil source ^{14}C dilution effect. The

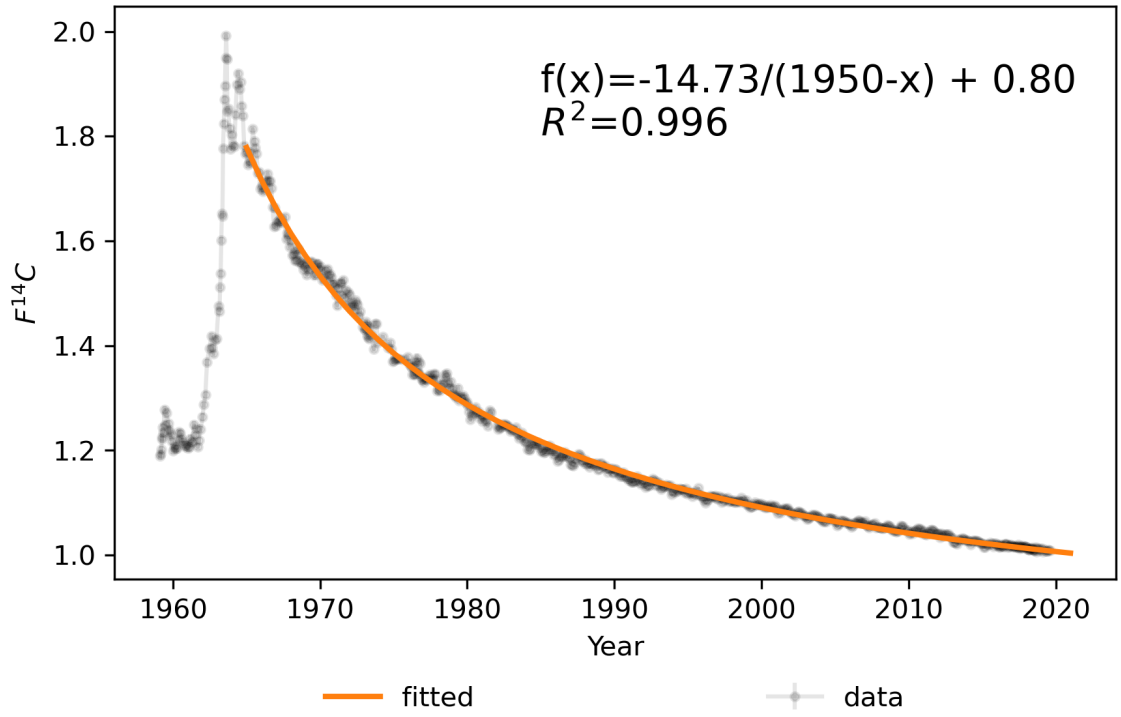

FIGURE 3.1: ^{14}C activity in atmospheric CO_2 for the northern hemisphere, expressed in units of Fraction Modern F^{14}C post-bomb levels. In orange extrapolated reference curve $1/x$ (data: Levin and Kromer, 2004).

diluted signal in spruce needles can be attributed to the uptake of ^{14}C free CO_2 from the atmosphere, which may come from burning of fossil fuels. It could also be observed that the sites are affected differently by this local ^{14}C dilution effect. With the exception of one tree, the measured F^{14}C signal in the spruce needles from the control site appeared to be closest to the atmospheric background dataset. The control site was less depleted in ^{14}C compared to the other sites studied (carparking and runway site), possibly because it was farther from local emission sources of ^{14}C free CO_2. Therefore, to determine local air and road traffic pollution, the sites were analyzed in comparison to the control site. For this purpose, a weighted mean$_j$[F^{14}C] for site j using the variance var$_i$[F^{14}C] and the mean$_i$[F^{14}C] of the measurements of the trees $i = 1, \ldots, N$ per year was calculated using

$$\text{weighted mean}_j[\mathrm{F}^{14}\mathrm{C}] = \sum_{i=1}^{N} w_i \,\text{mean}_i[\mathrm{F}^{14}\mathrm{C}]\,, \quad \text{where} \quad w_i = \frac{\text{var}_i[\mathrm{F}^{14}\mathrm{C}]^{-1}}{\sum_{i=1}^{N} \text{var}_i[\mathrm{F}^{14}\mathrm{C}]^{-1}}\,. \tag{3.1}$$

Tree no. 24 was considered an outlier in the analysis due to its location (clearing with possible change in air circulation) and range of values, and was excluded from further statistical analysis. In order to measure the variation between the exposed sites to traffic-related

TABLE 3.1: Table showing mean $F^{14}C$ values for measured spruce needles for 2018, 2019, 2020, and 2021 for the different sites (control, runway, and carparking) and extrapolated background atmospheric $F^{14}C$, using data from Levin and Kromer, 2004

Year	Background	Control	Runway	Carparking
2018	1.0127	1.0073	1.0018	1.0016
2019	1.0096	1.0051	0.9980	0.9980
2020	1.0065	1.0026	0.9999	0.9973
2021	1.0036	1.0030	0.9995	0.9983

emissions and the control site, the differences $\Delta F^{14}C_j$ for $j = \{carparking, runway\}$ of the carparking and runway sites to the calculated mean value of the control site (weighted $\text{mean}_{control}[F^{14}C]$) were calculated

$$\Delta F^{14}C[j] = \frac{\text{weighted mean}_j[F^{14}C] - \text{weighted mean}_{control}[F^{14}C]}{\text{weighted mean}_{control}[F^{14}C]}. \tag{3.2}$$

Error propagation with an assumed systematic uncertainty of 0.1% was used to compute the variance of the differences. From the differences of the sites to the control site, the differences of the differences of the years were additionally calculated (see Figure 3.2).

In the calculated differences between the sites and years, three important things became clear: 1) there was a distinct difference between the two sites, carparking and runway, with the carparking site being more depleted in ^{14}C than the runway site and thus possibly being more affected by the dilution effect. However, the difference between the two sites was not significant, except for the youngest needle generation in 2021, 2) both sites showed a sudden drop in ^{14}C depletion from 2019 to 2020 and the dilution effect appeared to be less pronounced in 2020 than in the previous year 2019, and 3) this sudden decrease from 2019 to 2020 was more evident at the runway site than at the carparking site. The standard deviations were relatively large given the young age of the samples studied. Nevertheless, the difference between 2019 and 2020 at the carparking site and runway site were significant with $p<0.02$ and $p<0.001$, respectively. Expressed as a percentage and in terms of standard deviation, a significant reduction of $-F^{14}C$ of about 30%, was found at the carparking site and of 52% at the runway site. A slight, non-significant increase in the dilution effect ($-F^{14}C$) was observed in 2018 to 2019 and 2020 to 2021 at both sites.

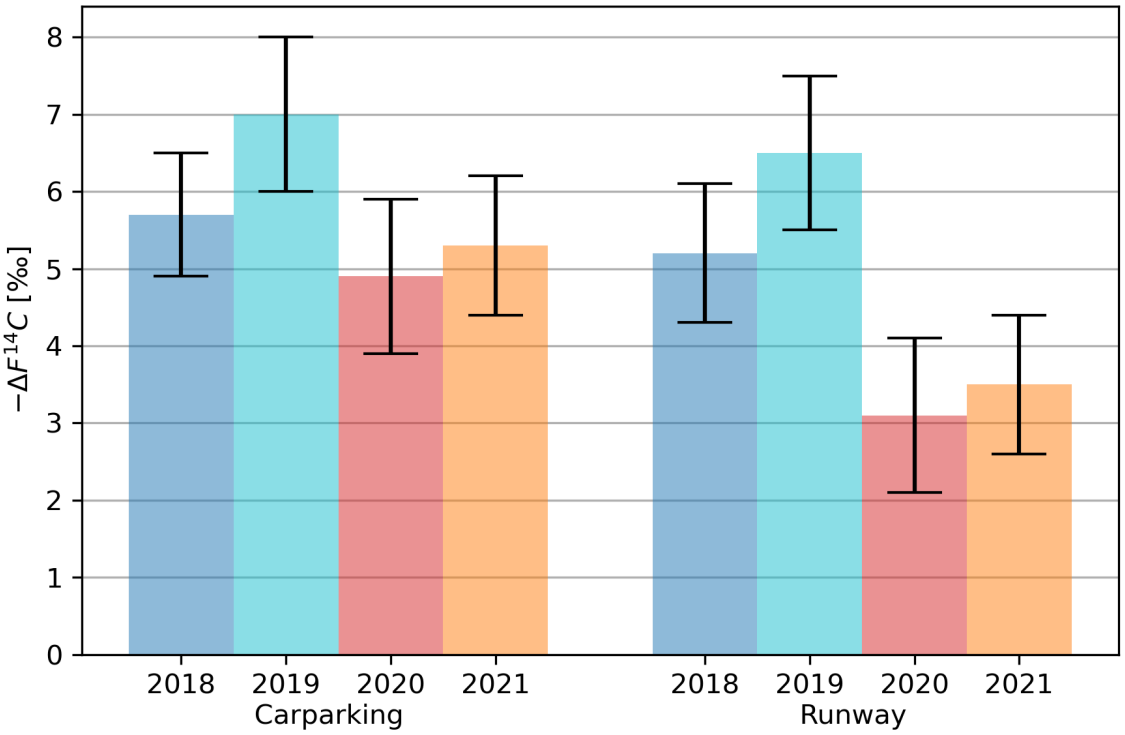

FIGURE 3.2: Relative difference of mean $F^{14}C$ from measured spruce needles of the sites (carparking and runway) from the weighted mean $F^{14}C$ of the control site with standard deviations ($\pm$ SD, inc. systematic error 0.1%) given as $-\Delta F^{14}C$. In blue before pandemic (2018 and 2019) and in red during and after pandemic-related lockdown (2020 and 2021).

3.2 Stable nitrogen and carbon isotope ratio results

The results of the nitrogen isotope analysis of the measured samples include four different attributes: carbon $\delta^{13}C$ [‰], C concentration [%], nitrogen $\delta^{15}N$ [‰], and N concentration [%] (detailed graphics see appendix A). Three different trees were measured at each site and three different branches of each were additionally measured for the carparking and runway sites (replicates: A, B, and C). The differences $\Delta X[j]$ for the sites $j = \{carparking, runway\}$ and quantities $X = \{\delta^{15}N, \delta^{13}C\}$ was examined by computing the relative difference

$$\Delta X[j] = \frac{\text{mean}_j[X] - \text{mean}_{control}[X]}{\text{mean}_{control}[X]}\,. \tag{3.3}$$

Error propagation was used to compute the variance of the differences.

3.2.1 Stable Nitrogen

In the results of the nitrogen concentration, great variability between the trees and, in some cases, the branches of the same needle generation were observed at the runway site with a mean of 0.85 $\pm$ 0.12% (see Figure 3.3). At the carparking site, however, this dispersion of the data was less pronounced. While at the carparking site the youngest needles from 2021 had the highest nitrogen content, this pattern was less evident at the other two sites. However, N concentrations appeared to decrease with increasing needle age at all three sites, with the exception of the needle generation 2019 at the control site.

Similar to the N concentrations, the δ^{15} N results for all three sites showed high variability between trees as well as within a tree (between branches). This could indicate the importance of plant-internal translocation and fractionation processes as well as micro-site environmental conditions for determining the needle δ^{15} N. While at the control site average δ^{15} N values increased annually, for the carparking and runway sites this trend was not as evident (see Figure 3.3). Nevertheless, at all three sites, the youngest spruce needles had the highest nitrogen isotope ratio compared to the older generations of needles, which may be a plant physiological characteristic along with the high N concentrations. Compared to the evaluation of N concentrations, the difference in δ^{15} N between sites was much more evident. The control site was most depleted in δ^{15} N with a mean of -5.15 $\pm$ 0.19‰ and thus significantly different from the other two sites with higher nitrogen ratios. It seemed like the carparking site still had slightly higher δ^{15} N values than the runway site, but this was not significant except for the most recent 2021 needle generation (see Figure 3.3 and 3.4).

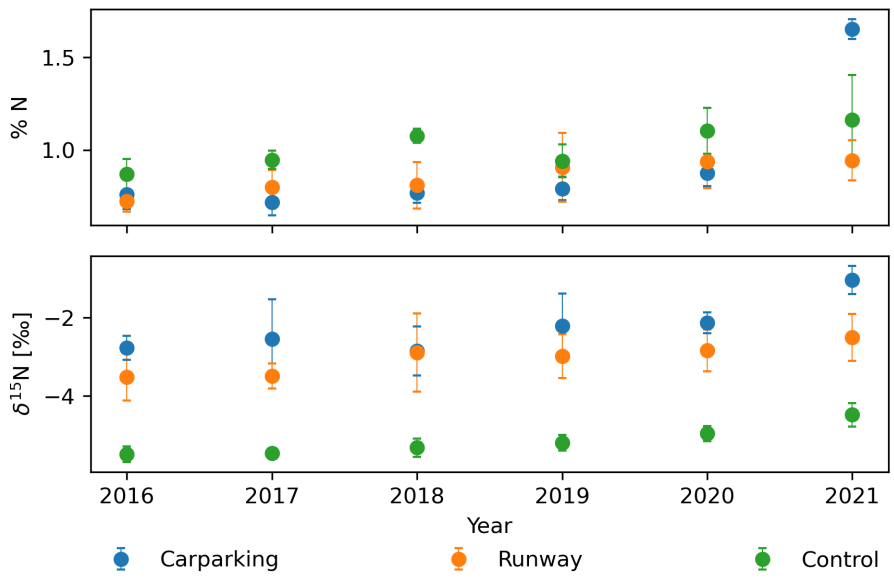

FIGURE 3.3: Mean N concentration [%] and δ^{15} N [‰] with standard deviation ($\pm$ SD) for the spruce needle generations 2016-2021 of the sites carparking (blue), runway (orange) and control (green).

The Figure 3.4 shows the differences in the δ^{15} N values of both the carparking and runway sites compared to the control site. However, in contrast to the F^{14} C results, there was no significant difference in the δ^{15} N values between the pre-pandemic year (2019) and the lockdown year (2020), neither for the carparking nor the runway site (p>0.2). The difference between the most recent needle generation (2021) and the previous year (2020) was only significant at the carparking site with p<0.001. In addition to the plant physiological aspects mentioned above, the time of sample collection might also be a relevant factor.

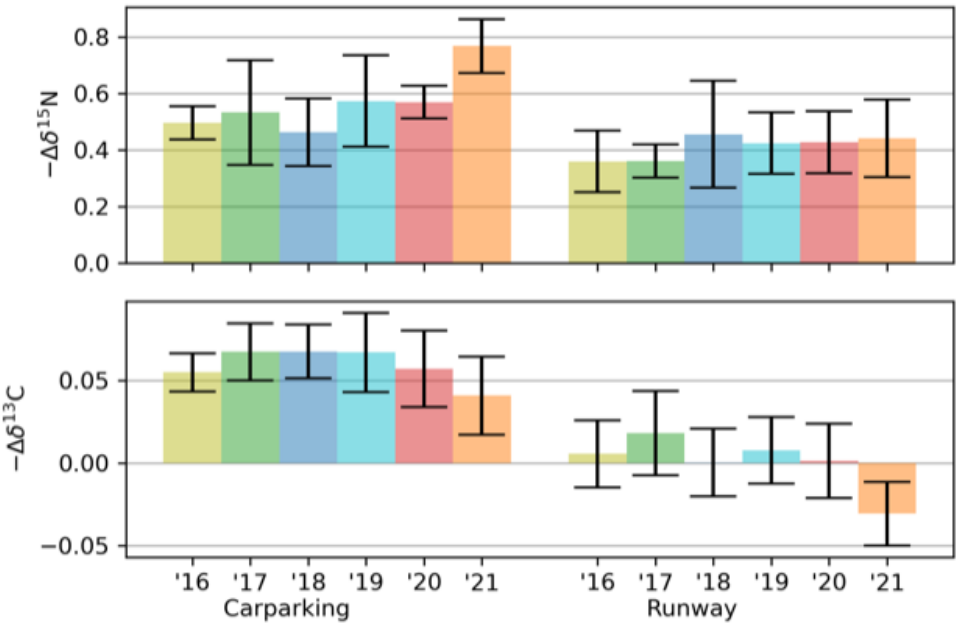

FIGURE 3.4: Relative difference of mean δ^{15} N and δ^{13} C from measured spruce needles (2016-2021) of the sites carparking and runway to mean δ^{15} N and δ^{13} C of the control site with standard deviation ($\pm$ SD).

Based on the similar pattern in the N concentration and δ^{15} N results, a correlation analysis was performed. Assuming a mixing of two sources, mainly background N (soil) and emission N (traffic exhausts), a negative relationship between measured ^{15} N and 1/N can be expected (Saurer et al., 2004). Following this approach, the nitrogen ratio δ^{15} N was plotted against the reciprocal of N concentration (see Figure 3.5). A linear trend could be observed for the carparking and control sites, while the samples from the runway site appeared to be uncorrelated. Linear regression of the data yielded R^2 coefficients of 0.35, 0.01, and 0.43 for the carparking, runway, and control site, respectively. This indicates that the two-source model is mainly applicable for the carparking and control sites, while more sources may be involved for the runway site.

The y-axis intercept of the linear regression can be interpreted as an approximation for the average $\delta^{15}N$ from local NO_x emissions (Saurer et al., 2004). Due to the fact that NO is poorly water soluble and toxic, the minor uptake of NO by tree needles can be neglected

and the reconstructed signal can be attributed to local NO_2 emissions (Saurer et al., 2004). The axis intercepts were -0.16 for the carparking site, -2.67 for the runway site, and -3.23 for the control site, i.e., more negative for the control site, as would have been expected if ^{15}N of pollutant emissions were relatively enriched, as some studies have found (Ammann et al., 1999; Saurer et al., 2004; Savard et al., 2009).

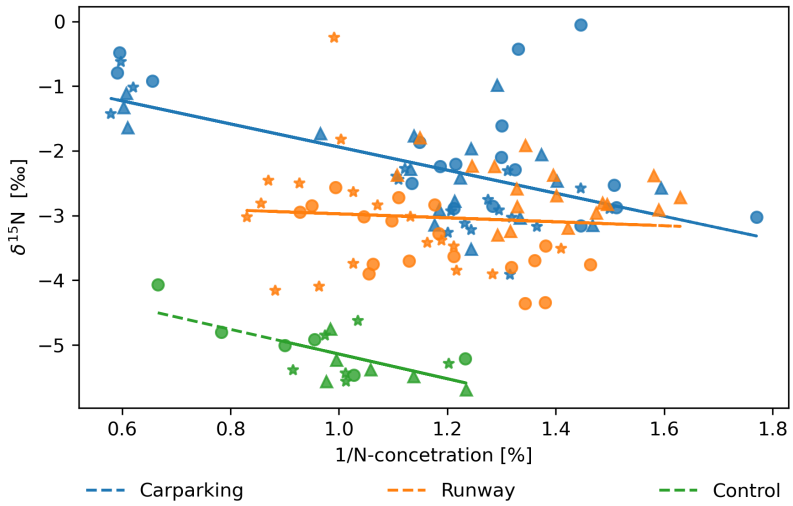

FIGURE 3.5: Relationship between reciprocal N concentration [%] and δ^{15}N [‰] of spruce needles. A linear fit on the data is shown as a line for each site (blue: carparking, orange: runway and green: control site). The markers are used to distinguish samples from different trees at the site. R^2 values of 0.35 (carparking), 0.01 (runway), and 0.43 (control) and y-intercept values of -0.16 (carparking), -2.67 (runway), and -3.23 (control).

In further correlation analyses, the relationship of the measured δ^{15} N values of spruce needles from all three sites with the atmospheric NO_2 data of the respective years of Zurich Airport was investigated using Pearson product moment correlation (Pearson's r) and cross-correlation. The annual mean atmospheric NO_2 values at the two stations (Zurich Airport Terminal A and Opfikon, Balsberg) per se showed a decrease in NO_2 in the lockdown year 2020 compared to previous years (see Figure 2.4; data source: FZAG and OSTLUFT). This decrease was obviously not reflected in the δ^{15} N values of the measured spruce needles as expected. The Pearson's r correlation analysis showed no significant correlation between the measured spruce needles from the carparking and runway sites to the measured NO_2 levels at Zurich Airport Terminal A (see Figure 3.6). Unexpectedly, the control site showed a significant negative correlation of -0.88 with a p-value of 0.02 to the annual mean NO_2 values. However, given the amount of data used for the statistics, this negative linear dependence could also have occurred by chance and the emerging trend could have other unknown causes. The cross-correlation as a measure of similarity showed an agreement of the time series of the two variables and no major shifts. This additionally showed that the samples were assigned to the correct year during processing.

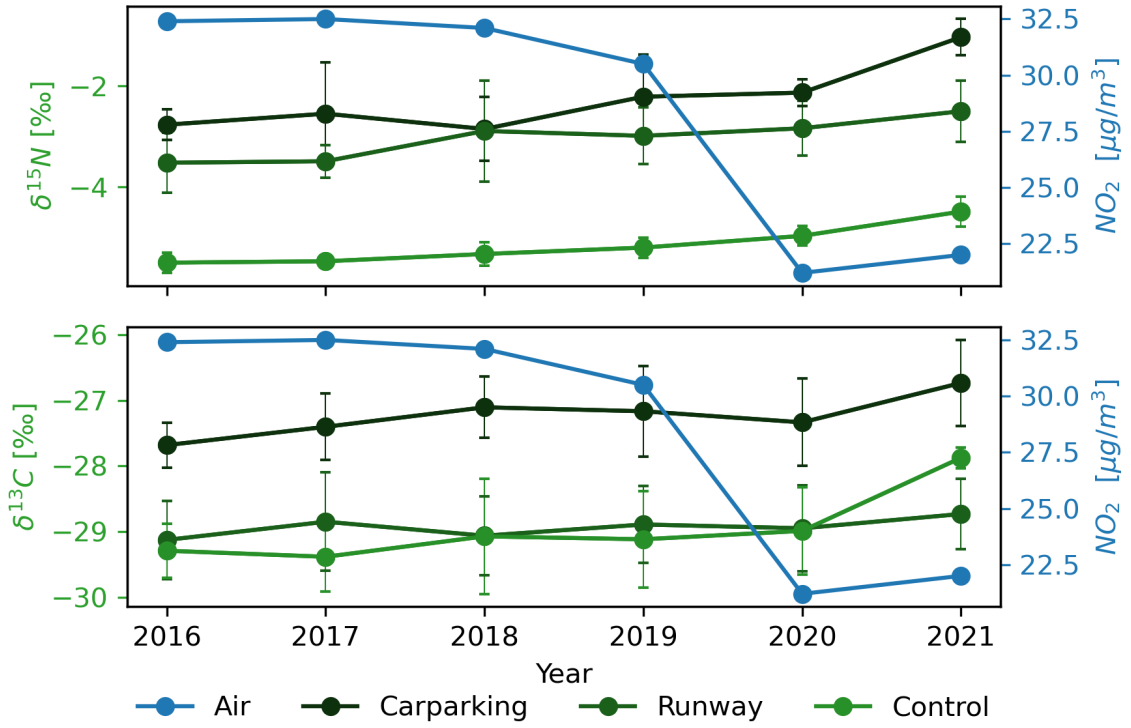

FIGURE 3.6: Correlation of mean δ^{15} N [‰] with standard deviation ($\pm$ SD) for the spruce needle generations 2016-2021 (green) of the sites carparking, runway, and control and annual mean atmospheric NO_2 [$\mu g/m^3$] concentration (blue) from the station Zurich Airport Terminal A (data: FZAG, 2022).

3.2.2 Stable Carbon

Carbon concentration and the stable ratio δ^{13} C were measured simultaneously with the nitrogen parameters. The C concentration of the needles varied between 43% and 46% at all three sites (see Figure 3.7). However, only at the carparking site did the C concentration decrease with decreasing age of the needles. The other sites showed no clear age trend. The δ^{13} C values presented a similar picture (see Figure 3.7). The carparking site differed significantly from the other two sites with a higher ratio of δ^{13} C of -27.24 $\pm$ 0.55‰. In contrast, the runway site and the control site were well below -28‰ and were barely distinguishable from each other, except for the recent 2021 needle generation. This may be due to several reasons. Here, the radiocarbon method was more sensitive because the relative difference between background and burning ^{14} C-CO_2 was much larger than for ^{13} C.

The significant difference in δ^{13} C values between the control site and the carparking site is even more evident in Figure 3.4. This is not the case for the runway site expect for the needle generation 2021 with clearly more negative δ^{13} C values compared to the control site. Furthermore, no significant difference could be seen between the needle generations for either the carparking site nor the runway site. To investigate a possible interaction between

NO_2 and δ^{13} C as found in the study of Siegwolf et al., (2001), a correlation analysis was performed between NO_2 measurements from Zurich Airport Terminal A and δ^{13} C values from the needles (see Figure 3.6). There was no dependence found between the two measured variables at any of the three sites.

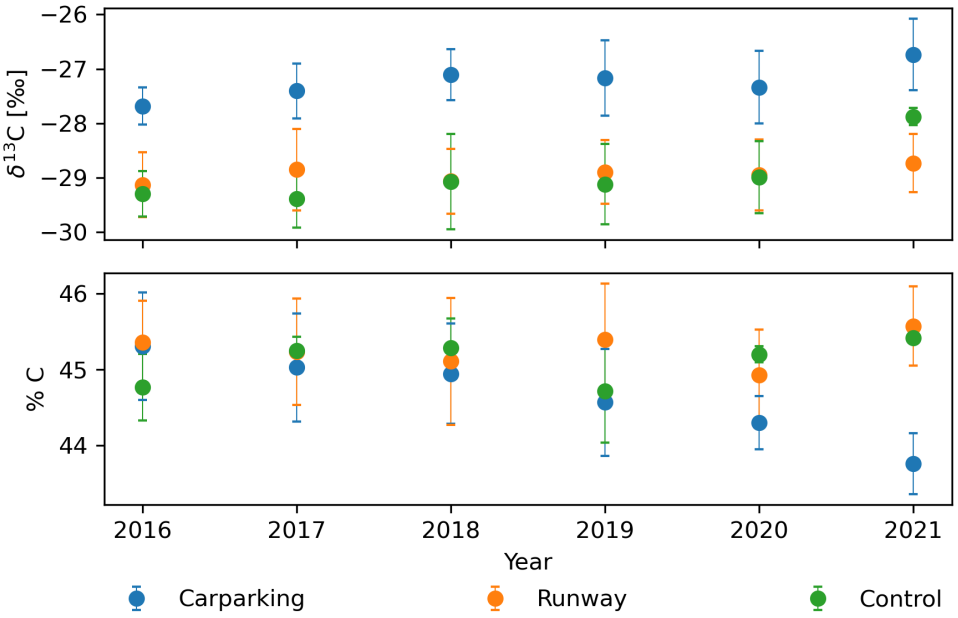

FIGURE 3.7: Mean C concentration [%] and δ^{13} C [‰] with standard deviation (± SD) for the spruce needle generations 2016-2021 of the sites carparking (blue), runway (orange) and control (green).

3.3 Tree-ring analysis

As described in section 2.5.2, tree-ring widths were measured and averaged on the basis of GLK and GSL (see Table 3.2). The mean chronologies of the carparking, runway and control sites were detrended using a cubic spline fit implemented in the R framework DPLR. The trees used for this purpose were on average 67 years old, with the trees at the control site being the oldest at 74 years old (see Table 3.3). The oldest trees were located at the control site, which was not affected by the road and runway constructions compared to the other sites. The carparking site showed a general decline in tree-ring width up to 1986 (see Figure 3.8). This trend was less observed at the other two sites. In contrast, synchronous growth declines in tree-ring widths were evident at all three sites over the past two decades in 1998, 2003, 2015, and 2018. However, the variability in tree-ring width between the sites increased with increasing age of the trees.

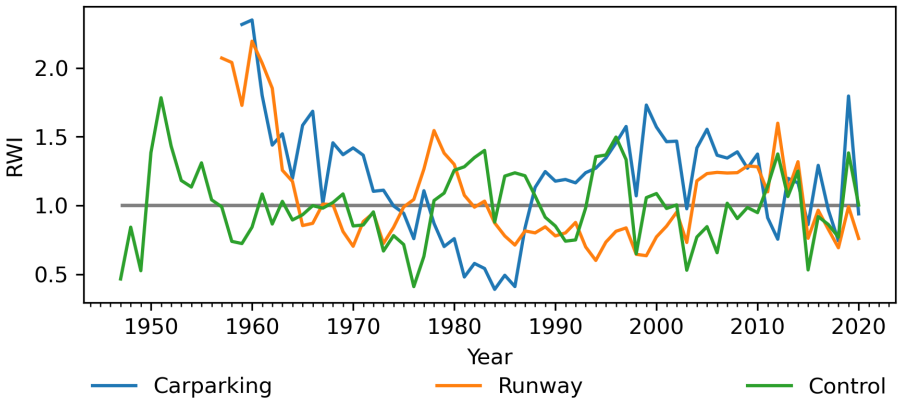

FIGURE 3.8: Detrended mean chronology of Norway spruce tree-ring width series (RWI = ring width index) per site in blue: carparking, orange: runway and green: control, performed with R software package "dplR" using "Spline" (Bunn, 2008). Excluded tree-ring width series: S103 and S210 with a non-significant GLK (see Table 3.2).

TABLE 3.2: Table showing statistics of cross-dating comparing sample (mean time series of two cores per tree (tree numbers: 01-28)) to the mean chronology of the sites (carparking (S1), runway (S2), and control (S4)). GLK, percent agreement of sample to mean site chronology (Gleichläufigkeit); GSL, statistical significance of the GLK: *** p<0.001, ** = p<0.01, * = p<0.05. Excluded tree-ring width series: S103 and S210 with a non-significant GLK.

Sample	GLK	GSL
S101	65	*
S102	66	*
S103	60	
S104	71	***
S105	97	***
S106	63	*
S207	70	***
S208	62	*
S209	80	***
S210	60	
S211	81	***
S212	63	*
S213	64	*
S423	80	***
S424	83	***
S425	75	***
S426	72	***
S427	69	**
S428	65	**

TABLE 3.3: Table showing statistics of detrending in R with software package "dplR" (Bunn, 2008).

Number of dated series	3
Number of measurements	222
Average series length	67
Series length	74
Span	1947-2020
Years with absent rings listed by series:	
Series Mean S2	1947-1956
Series Mean S1	1947-1958
Total absent rings	22 (9.91%)
Mean (Std dev) series intercorrelation	0.297 (0.048)
Mean (Std dev) AR1	0.775 (0.076)

When plotting the air pollution and tree-ring growth (see Figure 3.9), no correlation could be observed. The performed cross-correlation and Pearson's r correlation analysis confirmed this picture (see Appendix C). Similar to the δ^{15} N values of spruce needles, there was no correlation found between tree-ring widths and the mean NO_2 concentration for the respective year. Furthermore, there was no significant correlation for either the raw data nor the detrended tree-ring widths. Given the short time series of NO_2 measurements at Zurich Airport, the observed trend change in 1986 at the carparking site could not be explained conclusively. Therefore, tree-ring widths of spruces had not been shown to be a sensitive measure of changes in atmospheric NO_2 concentrations on an annual resolution. However, a relationship between tree-ring growth and air pollutants could not be excluded due to the lack of available data.

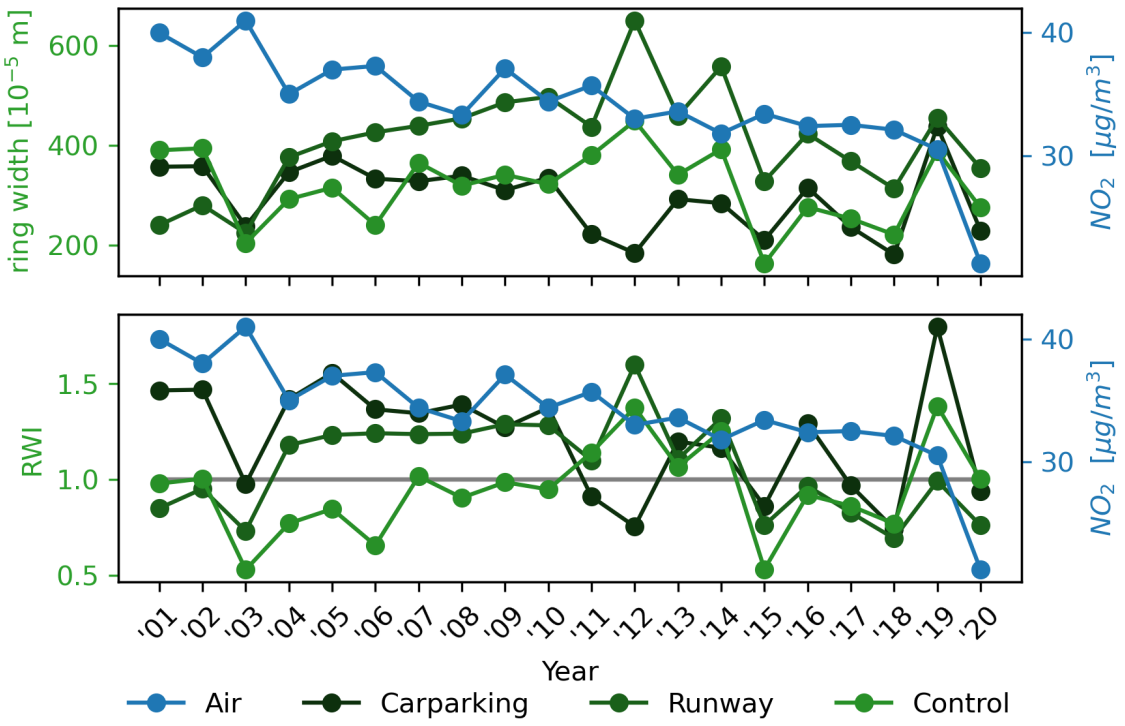

FIGURE 3.9: Correlation of mean tree-ring width [$10^{-}5$ m] raw data (top), mean tree-ring width index (RWI) (bottom), of the sites carparking, runway, and control and annual mean atmospheric NO_2 [$\mu g/m^3$] concentration (blue) from the station Zurich Airport Terminal A (data: FZAG, 2022).

Instead, when considering the striking decline in tree-ring growth at all three sites in 1998, 2003, 2015, 2018, and 2020 (see Figure 3.8), it became apparent that the reduction in tree-ring width is rather related to a large-scale climatic factor. A look at the data from a local weather station shows that these years were particularly warm and/or dry. Therefore, the tree-ring width measurements were additionally examined in correlation analyses with local meteorological data.

Pearson's r correlation analysis between tree-ring width (raw data) and mean temperature during the growing season revealed a significant negative correlation of -0.66 with a p-value well below 0.05 for the control site (see Figure 3.10). A significant negative correlation of -0.58 was also found for the carparking site. In contrast, there was no significant correlation with temperature for the runway site. The same analysis was performed with the detrended data (RWI), leading to similar or slightly different results (control: -0.47, carparking: -0.58, and runway: no significance).

Furthermore, the correlation analysis between tree-ring widths (raw data and detrended RWI) and mean growing season precipitation showed a significant positive correlation of 0.58 with a p-value of 0.003 only at the carparking site (see Figure 3.11). No linear dependence was found at the other two sites. This showed that the trees at the control site but especially the ones from the carparking site reacted strongly to climatic factors such as high temperatures and water deficit. At the runway site, however, other factors seemed to have an influence on the tree-ring width. Nevertheless, the droughts of the pointer years (1998, 2003, 2015, 2018, and, 2020) could also be seen at this site.

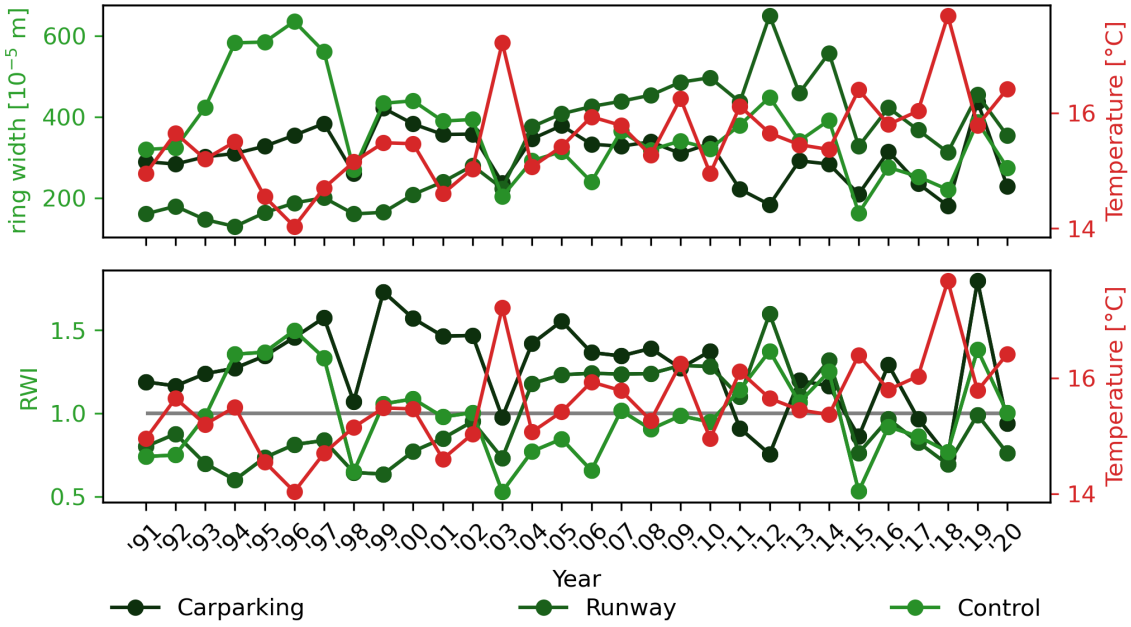

FIGURE 3.10: Mean tree-ring width [$10^{-}5$ m] raw data (top), mean tree-ring width index (RWI) (bottom) of the sites carparking, runway, and control and the mean temperature [°C] (red) during the growing season [April-October] at Zurich Airport (data: MeteoSwiss, 2022).

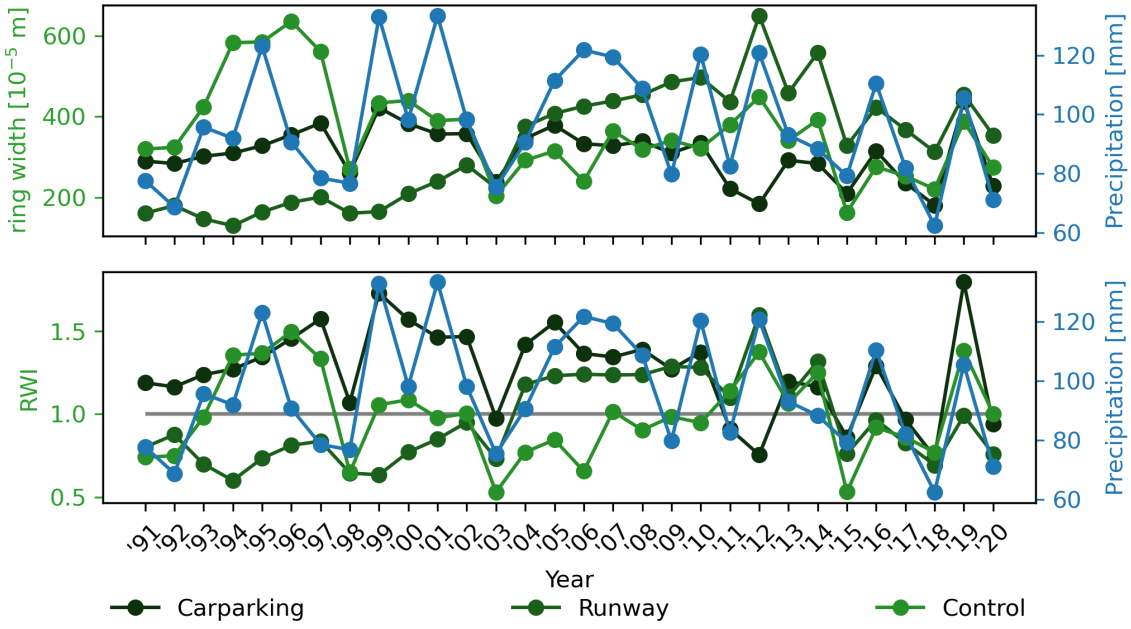

FIGURE 3.11: Mean tree-ring width [$10^{-}5$ m] raw data (top), mean tree-ring width index (RWI) (bottom) of the sites carparking, runway, and control and the mean precipitation [mm] (blue) during the growing season [April-October] at Zurich Airport (data: MeteoSwiss, 2022).

4 Discussion

The combustion of fossil fuels such as kerosene releases various direct and indirect greenhouse gases (BAZL, 2020). In Switzerland, about 39% of these greenhouse gases come from the transport sector (as of 2019), in total 19.92 million tons of CO_2 per year (including international air traffic). More than 2/3 of the traffic-related emissions come from road traffic (55.4% individual traffic and 15.2% from goods traffic) and 1/3 from air traffic (international 28.8% and national 0.6%). Furthermore, road traffic is responsible for 40% of the total NO_x emissions, whereas air traffic contributes with a share of 11.5% and 15% of Switzerland's total CO_2 respective NO_x emissions (BAFU, 2021a; Sintermann, 2020). Due to the Covid-19 pandemic lockdown in March 2020, there was a drastic decrease in traffic flows in the transport sector all over the world and also in Switzerland. Air traffic was the most affected, with a 91% decrease in aircraft movements at Zurich Airport (Fleuti, 2020; FZAG, 2020a). Road traffic decreased by 35% in the canton of Zurich and by an average of 39.3% in the area of Zurich/Kloten Airport, with public and private transport being most affected (Fleuti, 2020; Sintermann, 2020; Moser, 2020).

This short-term reduction in anthropogenic activities in the transportation sector in spring of 2020 resulted in lower environmental impacts, which was particularly reflected in air quality. Numerous studies evaluating atmospheric measurements from monitoring systems and modeling had shown that this decrease in emissions had led to a reduction in atmospheric concentrations of pollutants worldwide by restricting mobility (Le Quéré et al., 2020; Karkour and Itsubo, 2020; Han and Hong, 2020; Berman and Ebisu, 2020; ESA, 2020; Beloconi et al., 2021; Cooper et al., 2022). This extraordinary situation provided a unique opportunity to study and better understand the relationship between traffic-related emissions and air pollutant concentrations using trees as bio-indicators in a "lockdown experiment" outside the laboratory.

In this thesis, the influence of traffic-related emissions and their changes over time before (pre-pandemic) and during the outbreak of the Covid-19 pandemic (lockdown) were studied in Norway spruces from the immediate vicinity of Zurich Airport. Due to the pandemic-related reduced road and air traffic flows, air quality changed significantly globally as well as in the area under investigation. Using radiocarbon method and stable isotope analysis, it was examined whether this short-term strong change in the amount of anthropogenic influence was reflected in carbon and nitrogen isotopic composition of Norway spruce needles and whether this had an effect on tree-ring growth.

4.1 Radiocarbon method

The relationship between traffic-related "dead carbon" (^{14}C free CO_2) from fossil fuel combustion and radiocarbon concentrations in tree rings and leaves of different tree species has already been studied: e.g. in tree rings of pine trees (*Pinus sylvestris*, *Pinus densiflora*, and *Pinus radiata*) in urban areas: Kraków (Poland), Nagoya (Japan), and Arequipa (southern Peru) (Rakowski et al., 2008), in leaves of *Quercus ilex* (L.) and *Pinus pinea* (L.) along a pollution gradient in Rome (Villa Ada) compared to rural areas (Alessio et al., 2002), and combined in tree rings and leaves of *Pinus pinea* (L.) in the urban area of Caserta (southern Italy) (Battipaglia et al., 2010). In all three studies, the dilution effect of radiocarbon in the atmosphere was examined using organic material from trees. However, none of these studies attempted to establish a chronology of the average state of the atmosphere based on different leaf generations (annual resolution) from the investigated evergreen trees.

In this study, a clear signal of increased uptake of "dead" carbon was found at all three sites under investigation. F^{14}C measurements from the "polluted" sites carparking and runway were significantly lower than the measurements from background ^{14}C of the "clean" atmosphere and the F^{14}C values from the chosen local control site. This shows that the Norway spruce needles had absorbed ^{14}C free CO_2 from fossil fuel combustion. Consistent with the findings of previous studies(Rakowski et al., 2008; Alessio et al., 2002; Battipaglia et al., 2010), the ^{14}C concentration increased and thus the dilution effect decreased with increasing distance to the emission source. As expected, the highest F^{14}C values were measured at the control site, which come close to the F^{14}C background values of "clean" air, indicating a low anthropogenic influence. In contrast, the carparking and runway sites, which were closer to traffic-related emissions, showed a significant additional impact of ^{14}C free CO_2 (depletion) compared to the weighted mean F^{14}C values of the control site.

At the time of the lockdown in 2020, the needles from the carparking and runway sites showed a significant increase in F^{14}C (lower depletion) compared to the control site, reflecting a less pronounced dilution effect, which could come from the reduction of surrounding air and road traffic (see Figure 3.2). At the carparking site, the mean -F^{14}C difference for the 2020 needle generation decreased significantly by 30% and at the runway site by 52% compared to the previous year. Considering the data evaluation from the traffic monitoring stations (difference in traffic counts between 1.-7. April 2019 and 1.-7. April 2020) around Zurich Airport as well as the reduction of aircraft movements, there was a total traffic reduction of 39.3% during the lockdown on the entire airport area (Fleuti, 2020). In Figure 4.1 it can be seen that the traffic reduction varies spatially with the highest decrease in air traffic (91%) and road traffic towards the airport (61%).

Near the carparking site, a road traffic reduction of 29% was recorded at that time, which is exceptionally close to the measured reduction of -F^{14}C at 30%. Assuming a linear dependency between traffic volume and the measured F^{14}C signal in Norway spruce needles, this

could indicate that the carparking site was mainly influenced by the surrounding road traffic. However, the influence of reduced air traffic at this site could not be excluded. There were no roads in the immediate vicinity of the runway site and thus no traffic counts. Here, one would expect the reduced air traffic to have a greater impact on the $F^{14}C$ signal due to its proximity to the airport runway. In fact, the higher measured decrease in mean -$F^{14}C$ from 2020 compared to the previous year suggests that the signal cannot be attributed to the decrease in road traffic alone. Rather, it could be a mixed signal of mainly air but also road traffic. The mean -$F^{14}C$ of the 2021 needle generation at the runway site still showed, a significant difference from 2019, quite in contrast to the carparking site. Since road traffic increased faster than air traffic after the lockdown, this result also fits well with the assumption that the found reduction in mean -$F^{14}C$ was due to the change in emissions from air and road traffic respectively.

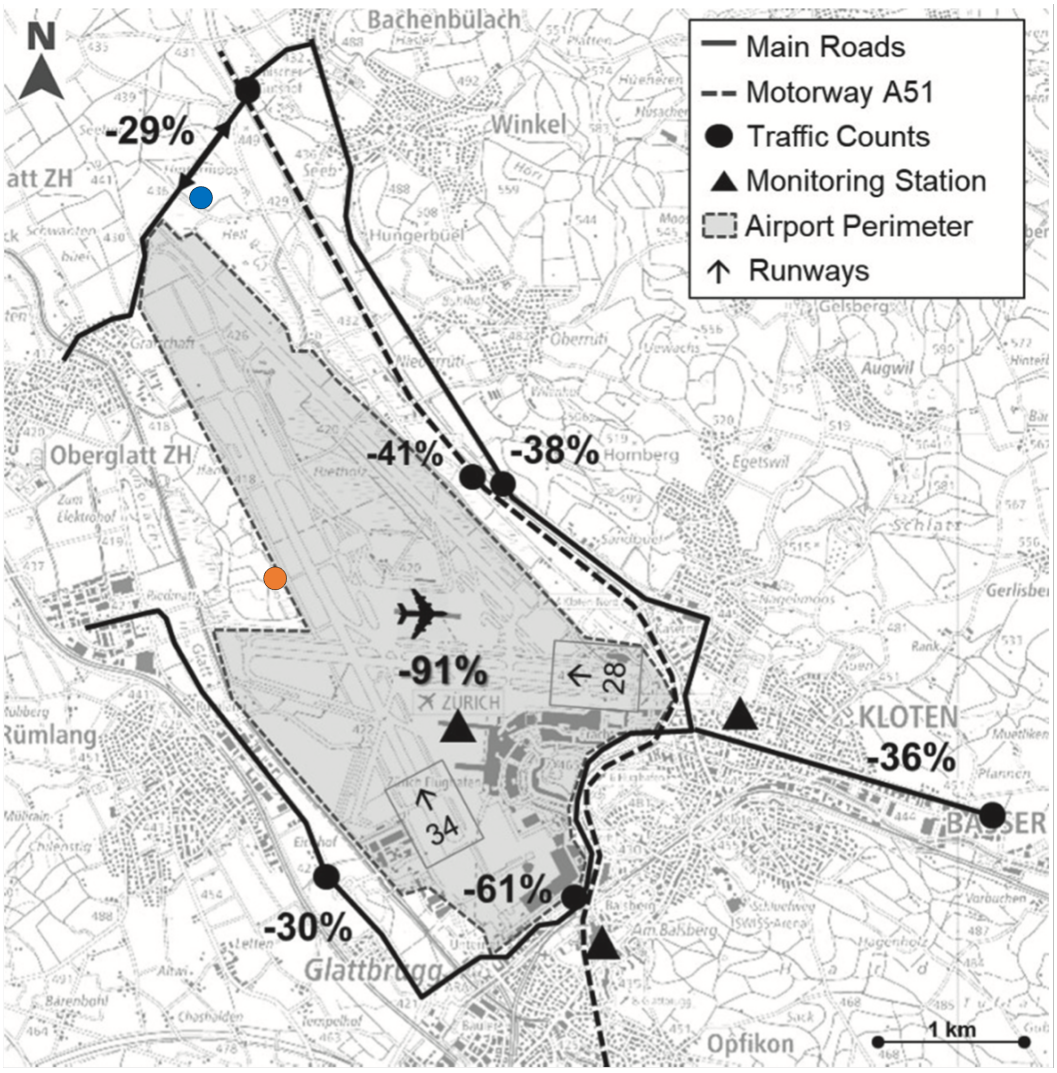

FIGURE 4.1: Traffic decreases at and around Zurich Airport (source: Fleuti, 2020). Own supplements: runway site (orange) and carparking site (blue).

4.1.1 Limitations

Using the background ^{14}C measurements of the "clean" atmosphere in remote mountain regions, natural variations in ^{14}C production and the seasonal mixing effect can be separated from anthropogenic induced variations in ^{14}C concentration. These background measurements were needed to estimate the local anthropogenic influences at the control site. Since the continuous atmospheric background measurements were published only until 2019, the growing season measurements of previous year were extrapolated with the function $1/x$. Therefore, it is uncertain whether the real measured values correspond to the extrapolated values. It would be interesting to see if the change in emissions due to the lockdown in 2020 had an impact on the atmospheric background ^{14}C measurements. This could clarify the uncertainty regarding a minimal anthropogenic influence even at these remote sites.

However, the control site showed a slight but distinct anthropogenic influence with lower $F^{14}C$ values compared to the atmospheric background measurements. By forming the difference to the "polluted" sites, part of the anthropogenic signal was lost; nevertheless the difference between the pre-pandemic needle generations and the lockdown at the two "polluted" sites was clearly visible. Another difficulty was to assign the change in anthropogenic influence measured by ^{14}C in spruce needles to a single emission source. For example, ^{14}C free CO_2 is also produced by domestic heating, and this influence is stronger or weaker depending on the season (Levin and Hesshaimer, 2000; Alessio et al., 2002). A linear relationship between traffic reduction and the measured radiocarbon signal was therefore only possible under the assumption that other emission sources remained constant during the lockdown. However, it was highly unlikely that during the lockdown with the federal government's *"stay at home"* message and the average monthly temperatures of 2020 at this location, all households in the vicinity of Zurich Airport turned off their heaters.

The measured cellulose in spruce needles is mainly formed in spring (April), when the buds start to grow and the new shoots are formed. Thus, for cellulose, mainly the ^{14}C in the air at this time was used, which was depleted of ^{14}C free CO_2 due to the lockdown that occured at the same time. Nevertheless, buds are already prepared for the next year in the previous year and have very likely also assimilated CO_2 from the previous year (Aas et al., 2017). This carbon from the previous year must have been relatively low because the majority of cellulose was produced in the spring when the tree invested in the new needles. Based on the values, this also seemed to be the case. As an additional control, radiocarbon could be measured in the annual rings of the trees.

Consistent with the results of previous environmental monitoring studies, the radiocarbon method is a sensitive tool for reconstructing past atmospheric radiocarbon concentrations and quantifying the influence of CO_2 of anthropogenic origin using bio-indicators such as tree rings and leaves (Rakowski et al., 2008; Alessio et al., 2002; Battipaglia et al., 2010). In this thesis, the ^{14}C isotope records in spruce needles reflected the average local atmospheric concentrations of the respective years, and thus it was possible to draw conclusions

about changes in traffic-related emissions based on these records. The measured samples were very young, the deviations were in the per mill range and yet a significant difference between the lockdown year 2020 and the previous years could be measured, which demonstrated the precision and sensitivity of the radiocarbon method.

4.2 Stable Isotopes

Previous studies have already made use of stable isotope ratios (δ^2 H, δ^{13} C, δ^{18} O, and δ^{15} N) measured in tree rings and leaves of various tree species not only for climate reconstructions, but also to study changes in air quality and soil chemistry due to anthropogenic pollutant emissions (Ammann et al., 1999; Siegwolf et al., 2001; Saurer et al., 2004; Bukata and Kyser, 2007; Guerrieri et al., 2009; Savard et al., 2009; Battipaglia et al., 2010; Leonelli et al., 2012). Some of these studies focused on measuring δ^{15} N (often in combination with other stable isotopes: multi-approach studies) to investigate environmental changes due to anthropogenic traffic-related N emissions in form of NO_x (NO + NO_2) in diffusely polluted urban/industrial and highway areas.

4.2.1 δ^{15} N an indicator of pollution

Spatial changes of δ^{15} N ratio

In this study, although measurements were not made along a pollution gradient, the control site was located farther away from traffic emission sources and thus should have been less exposed to traffic-related pollution compared to the carparking and runway sites. In fact, a significant difference was found between the measured spruce needles of the control site (overall mean -5.15‰ $\pm$ 0.19‰) and the carparking and runway sites, which were less depleted in δ^{15} N (see Figure 3.3 and 3.4). Furthermore, the two-member mixing model (see also Saurer et al., 2004), which was mainly applicable for the control site and the carparking site, showed that the reconstructed local NO_2 emission signal coming from car exhausts for the control site (-3.23) was considerably lower than for the carparking site (-0.16) (see Figure 3.5). While Ammann et al. (1999) and Saurer et al. (2004) found positive δ^{15} N values for sites close to the pollution source, Guerriere et al. (2009) determined only negative values even for the site very close to the emission source (5 m). However, looking at the relative values and thus the spatial trend, the results of these previous studies agreed with the measurements of this study, where a significant increase of δ^{15} N was found at sites closer to emission sources compared to more distant and less exposed sites. Together with the findings of Ammann et al. (1999), Saurer et al. (2004), and Guerrieri et al. (2009) one could conclude that the more distant control site was less influenced by traffic-related emissions compared to the other sites and this could be shown in more depleted mean δ^{15} N ratios measured in Norway spruce needles.

Ammann et al. (1999) collected NO_x samples at a Swiss highway in Solothurn (built in 1965) and obtained a δ^{15}N mean of +5.7‰ ± 2.8‰ for NO_2 and +3.1‰ ± 5.4‰ for NO. The δ^{15}N ratios of Norway spruce (needles and roots) and soil were measured at 5, 130, and 980 m from the highway. The measured δ^{15}N values of the needles decreased with increasing distance from the highway. Further studies confirmed such a decrease in the δ^{15}N ratio with increasing distance from the emission source. Saurer et al. (2004) continued the study of Ammann et al. (1999) and also performed nitrogen isotope analyses on tree rings of Norway spruce along a pollution gradient (distances: 20, 150, 1000 m) from the same highway in Switzerland. In the tree rings, the δ^{15}N ratio also decreased with increasing distance from the highway with δ^{15}N values increasing up to +7.9‰ after 1965 at the closest site (20 m) to the highway. Compared to the needles (+1.3‰ ± 0.4‰ to -4.4‰ ± 0.4‰), this spatially dependent trend was two times more pronounced than in the tree rings at two of the three sites.

Guerriere et al. (2009), who measured several stable isotopes in tree rings and leaves of deciduous trees (*Quercus cerris*) and conifers (*Picea abies*) as well as in soil samples in two areas (Southern Italy and Gotthard, Switzerland) at different distances from emission sources (oil refinery and highway) also found decreasing δ^{15}N values in leaves with increasing distance from the emission source (-2.63‰ ± 0.81‰ to -5.34‰ ± 0.32‰) at the highway site in Switzerland.

Temporal changes of δ^{15}N ratio

Similar to the studies by Battipaglia et al. (2010) and Leonelli et al. (2012), no significant temporal difference in measured δ^{15}N ratio was found in trees under changing air pollutant concentrations in this study. The 2020 needle generation (pandemic lockdown) showed no significant change in δ^{15}N values compared to the previous needle year generations (2016-2019 pre-pandemic: business as usual) (see Figure 3.4). The only temporal pattern detected was a slight decreasing δ^{15}N trend with increasing needle age, which was also found by Ammann et al. (1999) and Gebauer et al. (1993). This trend might be from younger needles having a more active metabolism than older needles and thus assimilate a lot of nitrogen (Gebauer and Dietrich, 1993).

Battipaglia et al., (2010) studied tree rings (needles and soil) of *Pinus pinea* (L.) in front of a railroad crossing on a polluted road in the city of Caserta (southern Italy) using stable (δ^{13}C and δ^{15}N) and radioactive isotopes (see Section 4.1). The road was opened in 1980 and traffic volumes increased since that time, as well as atmospheric NO_x concentrations (measured by monitoring stations in the area during 1995-2004). Tree-ring δ^{15}N values varied widely among trees and over time, with some increase in this variability after 1980, but overall no clear pattern (increase or decrease after 1980) in tree-ring δ^{15}N values was observed.

In a later study, Leonelli et al. (2012) analyzed the change of different isotopic ratios (δ^{13}C, δ^{18}O, and δ^{15}N) in tree rings of *Larix decidua* (Mill.) at three sites with different

distances to the highway and the tunnel of Mt. Blanc in the western Alps (Italy). The tunnel was opened in 1965 and closed for three years in the period 1999-2002 for reconstruction work. No change in nitrogen isotope signal in tree rings were found at any of the three sites, neither for the time of the opening of the tunnel in 1965 nor for the closure of the tunnel between 1999 and 2022. They concluded that trees are more likely to respond to long-term pollution events and trends than to short-term lack of pollution.

4.2.2 δ^{13}C ratio an indicator of environmental stress

In the results of this study, significantly higher mean δ^{13}C of -27.24 $\pm$ 0.55‰ was measured for the carparking site than for the other two sites (see Figure 3.7). Using the findings from previous studies and comparing the sites, it could be concluded that the carparking site was exposed to greater environmental stress than the control site and runway site, if it is assumed that the climate at all three sites was the same because of their proximity to each other, the difference between the sites could be explained as followed: 1) the carparking site was more affected by drought due to its soil or geomorphological characteristics, e.g. less soil water capacity or faster runoff of precipitation, leading to more frequent stomatal closers and higher δ^{13}C ratios (Panek and Waring, 1997; Leffler and Evans, 1999; Battipaglia et al., 2010; Leonelli et al., 2012), or 2) in view of the results from other studies which mostly found increased δ^{13}C values at exposed sites to pollution sources (Siegwolf et al., 2001;Alessio et al., 2002; Guerrieri et al., 2009) and including the findings from the radiocarbon method, the carparking site was exposed to higher air pollutants reacting with stomatal closer and increased δ^{13}C values. However, it cannot be conclusively determined whether reason 1) or 2) was responsible for increased δ^{13}C ratios. Furthermore, similar to the δ^{15}N results, no significant difference was found in the mean δ^{13}C values between pre-pandemic needle generations and the 2020 lockdown needles from the carparking and runway sites compared to the control site.

Moreover, the data analysis of different monitoring stations in the area of Zurich Airport showed an exemplary decrease in NO_x as well as NO_2 concentrations in 2020 compared to previous years. However, no correlation was found between the annual mean atmospheric NO_2 and the measured mean δ^{15}N or δ^{13}C values of the three sites in the respective needle generation. This result supports the statement of Leonelli et al. (2012) that a short-term decrease or absence of pollution at a given site is less likely to be recorded by trees and consequently a change in isotopic composition cannot be detected.

Some of the presented studies measured in addition to the δ^{15}N ratio or radiocarbon, also δ^{13}C in leaves (Siegwolf et al., 2001; Guerrieri et al., 2009; Alessio et al., 2002) and tree rings (Guerrieri et al., 2009; Battipaglia et al., 2010; Leonelli et al., 2012):

Siegwolf et al. (2001) was one of the first to demonstrate increased δ^{13}C ratios in leaves of hybrid poplars (*populous x euramenicana*) which were exposed to elevated NO_2 concentrations in an experiment. According to Siegwolf, increased δ^{13}C levels are a response to

anthropogenic N input and are strongly linked to stomatal conductance and photosynthetic rate. Also, in the studies of Alessio et al. (2002) and Guerrieri et al. (2009) higher mean δ^{13}C values were found in oaks (*quercus ilex* (L.) respective *quercus cerris*) the closer they grew to the emission source. However, neither study found this effect in conifer needles, suggesting that the response to increased anthropogenic N input of a tree depends on species-specific differences.

The situation was different in tree rings of conifers. Guerrieri et al. (2009) found increased δ^{13}C values in tree rings of Norway spruces (*Pinus pinea*) growing closest to the highway. After the tunnel opening (1980), δ^{13}C values at all three sites close to the highway became more negative even though traffic volume increased. Similar, Leonelli et al. (2012) detected an increase in δ^{13}C in tree rings of larches (*Larix decidua* (Mill.)) growing at the closest site to the highway in 1999, when the tunnel at Mt. Blanc closed for three years. In contrast, Battipaglia et al. (2010) detected again an increase in δ^{13}C and simultaneous decrease in tree-ring width of *Pinus pinea* (L.) starting in 1980, when the investigated road in the urban area of Caserta (southern Italy) was completed and traffic gradually increased. However, it is important to note here that after 1980, a significant correlation was also found between measured δ^{13}C in tree rings and precipitation in the study of Battipaglia et al. (2010) at the area of Caserta. This climatic correlation between precipitation (and temperature) and δ^{13}C was also found by Leonelli et al. (2012) in tree rings of larches in the western Alps, especially in the summer months. Increased δ^{13}C values can therefore also be an indication of drought events in a certain area and provide information about water availability.

Scientists agree that for these reasons it is difficult to interpret the δ^{13}C signal and attribute the observed change to either a pollution event or a climate trend (Alessio et al., 2002; Guerrieri et al., 2009; Leonelli et al., 2012; Battipaglia et al., 2010). Nevertheless, Battipaglia et al. (2010) described increased δ^{13}C values measured in trees as good indicators of environmental stress, regardless of whether the stress was caused by pollution, climate, or both.

4.2.3 Tree-ring growth

The mean tree-ring chronology of the carparking site showed a possible relationship with traffic-related air pollution. Tree-ring growth of Norway spruces at this site decreased until 1986, after which a trend inversion occurred, which was in agreement with the measures taken to improve air quality in Switzerland. In the late 1980s, different measures were taken to reduce air pollution, such as the introduction of stricter emission standards in the energy sector, but especially in road transport through the use of three-way catalysts, which significantly reduced air pollutants (BAFU, 2014). Due to the proximity to the highway, it was likely that trees at the carparking site were impacted by road traffic and could have responded to the higher standards in the energy sector and the associated improvement in air quality. Nevertheless, no correlation between annual tree-ring growth and mean atmospheric NO_2 concentrations was found at any of the three sites (see Figure 3.9). As previously recognized by Saurer et al. (2004), the absence of a growth response in the tree to increased anthropogenic N input from traffic-related NO_2 emissions does not mean that no N fertilization effect occurred, but only that other factors may influence and mask the signal.

A number of studies investigated whether traffic-related pollution and associated anthropogen N input also had an effect on tree-ring growth. Most studies found no change in secondary growth of trees due to higher pollution rates (Saurer et al., 2004; Guerrieri et al., 2009; Leonelli et al., 2012). However, the study of Battipaglia et al. (2010) found a slight decrease in tree-ring width of *Pinus pinea* (L.) after the opening of a main road in Caserta in 1980 ($r=0.32$, $p<0.05$). Similarly, Guerrieri et al. (2009) detected a striking but short-lasting decrease in tree-ring width of Norway spruces (*Pinus pinea*) at the closest site to the highway after the opening of the St.Gotthard tunnel in Ticino in 1980.

In this study, a significant negative correlation was found between tree-ring growth and mean temperature, and a positive correlation with mean precipitation for the carparking site (see Figure 3.11 and 3.10). This supports the assumption, based on the increased δ^{13} C ratios, that Norway spruces at the carparking site responded strongly to water deficiency and were influenced by climatic conditions for their secondary growth. A significant negative correlation between temperature and tree-ring growth was also found for spruces at the control site. Instead, no correlation was found between climate data and growth of annual rings at the runway site. Since this site was located in a wetland, it most likely did not suffer from drought. Nevertheless, at this site as well, the heat years were clearly evident in the decline of tree-ring growth.

4.2.4 Limitations

One of the main challenges of stable isotope analysis is that climatic conditions indirectly influence the measured stable isotope ratio in the trees. In particular, the δ^{13} C ratio changes under dry conditions when leaf stomata close to minimize transpiration and associated water loss from the tree. Furthermore, meteorological parameters could change the nitrogen cycle in the soil and thus the measured δ^{15} N signal in the tree (Bukata and Kyser, 2007; Battipaglia et al., 2010). This implies not only temporal changes in the isotope ratio due to climatic influences, but also spatial changes depending on the different water regimes at the sites that most likely influence the response of trees to external stress such as droughts. The geology and soil characteristics of the sites, therefore, also play an important role in water availability. Since it was beyond the scope of this thesis, neither hydrological nor soil examinations were conducted at the different sites of Zurich Airport, therefore no further conclusions can be drawn.

On the basis of the two-member mixing model conducted in this study, it became clear that the measured nitrogen signal from spruce needles, at least at the carparking site and control site, were composed of two sources: nitrogen uptake by roots from the soil and foliar uptake of NO_2 emissions from the air. One possible explanation why the two-source principle was not applicable to the runway site is that there was actually a third source. For example, NO_2 from aircraft exhaust could have a different δ^{15} N than NO_2 from car exhaust, so the mixing of the two sources would result in a blurred signal. Moreover, Saurer et al. (2004) and Ammann et al. (2001) estimated the contribution of NO_2 uptake to the nitrogen content in needles to be 10-25%, a similar result was reached by Siegwolf et al. (1999). In this context, most of the nitrogen in leaves would originally come from the soil, which has a slow N turnover compared to the atmosphere, considering the different subprocesses of the nitrogen cycle in the soil (mineralization, nitrification, and denitrification). This could explain why the reduction in transport-related N emissions due to the Covid-19 pandemic lockdown in 2020 was not evident in spruce needles based on the change in the δ^{15} N ratio. Thus, returning to the statement of Leonelli et al. (2012), it makes sense that a short-term absence or reduction in pollution cannot be detected in the δ^{15} N ratio of tree rings or, as in this case, in needles of conifers.

Another attempt to explain why the δ^{15} N signal of the needles did not change for 2020 compared to previous years is an internal N cycling. Similar to tree rings relocating nitrogen between heartwood and sapwood, different needle generations might do the same. This recycling and translocation of nitrogen from older generations of needles directly to younger needles or indirectly through mineralization of needle litter in the soil was already detected by Ammann et al. (2001). Thus, the trend of decreasing nitrogen concentration and ratio δ^{15} N with increasing age of needles observed in this study might not only be a physiological effect, as determined by Gebauer et al. (1993), but also indicative of internal N cycling. Following Ammann et al. (2001), it can be summarized that the measured δ^{15} N values in

needles could be influenced by the following mechanisms: 1) uptake and assimilation of ammonium and nitrate and mineralized needle litter (old needles) by the roots from the soil 2) redistribution of nitrogen from the older needles or the stem, and 3) uptake of atmospheric N emissions via needles gas exchange. Therefore, the interpretation of a temporal change in the isotope signal was difficult because it could be blurred by these various mechanisms.

Another explanation why no change in stable isotope ratios could be detected in 2020 is simply the distance to the emission source and the strong dilution of the plumes (Vogel et al., 2000). For aviation, there is also the fact that 1) for safety reasons, there are no trees in close proximity and the trees studied are relatively far away with 300 m, (Saurer et al. (2004) claimed that already after 150 m the pollutant signal fades) and 2) the aircraft gain altitude rapidly within a very short time; Fleuti (2020) argued that only the emissions below 300 m above ground actually contribute to the measured ground level pollutant concentration. A look at the NO_2 concentration map (extrapolation between monitoring stations) of Zurich Airport from the years 2019 and 2020 shows that the largest changes were indeed mainly in the terminal area where aircraft are idling. Nevertheless, the runway site was clearly within the area of influence of air traffic, especially of runway 16/34, and could well have recorded a change in the reduction of pollutants in 2020.

Considering the numerous limitations discussed, stable isotope analysis appears to be a less sensitive tool for short-term temporal changes in anthropogenic emissions from fossil fuel combustion than the radiocarbon method. Nevertheless, the analysis can provide important insights into long-term temporal changes in anthropogenic emissions, the influence of climatic conditions, and spatial changes related to distance from specific emission sources.

4.3 Emission or weather?

As discussed for the radiocarbon results, a linear dependence can be assumed between reductions in traffic volumes and changes in measured atmospheric pollutant concentrations, assuming that other emission sources have remained stable. However, the changes in emissions are not always reflected 1:1 in the actual measured concentration in the atmosphere (Sintermann, 2020). In fact, the monitoring station Zurich Airport, Terminal A showed a mean annual reduction in NO_2 concentration of 30.5% and a decrease of 44% in mean day levels during the lockdown compared to the previous year 2019 (Fleuti, 2020). Thus, the measured atmospheric signal at Zurich Airport cannot be explained by air traffic reduction (91%) alone and, according to Fleuti (2020), is not linearly dependent on flight operations. Despite the fact that also the reduction in local road traffic might influence the measured NO_2 concentration at Terminal A, meteorological conditions such as wind direction/velocity and precipitation influence the transport and dilution of pollutants in the atmosphere. Various studies found a relationship between air pollutant concentrations and weather conditions (FZAG, 2020a; Sintermann, 2020; BAFU, 2021c; ESA, 2020; Fleuti, 2020; Stuart K. et al., 2020; Beloconi et al., 2021). This means that air quality can fluctuate due to weather conditions even though emission rates remain constant, which in turn makes it difficult to determine the impact of the emission change coming from the Covid-19 lockdown on air quality using just air pollutant data. Indeed, shortly after the lockdown, the weather changed to a strong and stable breeze with higher temperatures (Sintermann, 2020).

In general, higher NO_2 concentrations were measured at Zurich Airport when there was no wind than, for example, when there were westerly winds, which indicates that there was a dilution effect of pollutants in the atmosphere (Fleuti, 2020). Apart from this, certain wind directions also bring air pollutants from more distant locations, which is particularly evident in the PM_{10} measurements at Zurich Airport. Depending on the wind direction, concentrations during the lockdown even reached unexpectedly higher daily mean PM_{10} concentrations than the previous year, even though air traffic had almost come to a standstill. Fleuti (2020) argued that Saharan dust events occurred at the time of the lockdown, making it difficult to interpret the impact of the lockdown effect on PM concentrations. Therefore, for a comprehensive picture, a before-and-after comparison of changed air pollutant concentrations is not sufficient to quantify the impact of the lockdown on air quality. Statistical evaluations, modeling approaches and weather corrections are advisable to better capture relationships between emissions, dispersion and dilution effects, and air pollutant concentrations (Sintermann, 2020; Stuart K. et al., 2020; Beloconi et al., 2021).

In addressing the questions posed in this thesis, it can be summarized that air quality at Zurich Airport improved during the pandemic lockdown in 2020 with respect to NO_x, VOCs, and UFP, but not to PM_{10} concentrations. How much of this change was actually due to the pandemic lockdown and the associated reduction in air and road traffic could

not be clearly quantified due to the influence of meteorological conditions. However, several studies have demonstrated that, when weather factors were considered, reduced traffic was a major contributor to lower measured atmospheric NO_x and CO_2 concentrations in the lockdown year 2020 (Sintermann, 2020; Stuart K. et al., 2020; Beloconi et al., 2021). At Zurich Airport, the decrease in UFPs and VOCs during the lockdown was mainly associated with reduced air traffic (Fleuti, 2020). Nevertheless, the decrease in NO_2 concentration cannot be explained only by the reduction in air traffic - other emission sources such as road traffic and meteorological conditions play an important role. Although CO_2 concentrations were not measured at Zurich Airport, radiocarbon measurements in Norway spruce needles showed that during the lockdown, traffic-related ^{14}C free CO_2 emissions and associated atmospheric concentrations decreased. Spruce needles are thereby a good bio-indicator of changes in ^{14}C concentration in the atmosphere, reflecting changes in air quality by up to seven years. Whereby the analysis of tree rings could cover even a larger time range. In contrast, the results of nitrogen isotope analysis showed no short-term changes in δ^{15}N and δ^{13}C ratios in spruce needles of the 2020 lockdown year compared to pre-pandemic years. The analysis appeared to be less suitable for capturing short-term pollutant reductions as an annual record. In addition, it was difficult to interpret the isotopic ratios and attribute an influence of climate or pollutant factors to the measured signals. Similarly, tree-ring growth in spruce was found to be related to site-specific and climatic conditions (temperature and precipitation) rather than changes in air quality (NO_2). Nevertheless, nitrogen isotope analysis, together with other stable isotopes (multi isotopic approach), can provide many important insights into spatial questions as well as long-term trends related to air pollution and climate impacts. In summary, the hypothesis: **"Spruce needles and tree-ring width reliably reflect local changes in air pollution; the pandemic lockdown in spring 2020 with reduced air traffic and the associated improvement in air quality is clearly detectable"** can only be confirmed on the basis of the radiocarbon results. However, the measured signal at the runway site, which most likely represents air traffic, should be interpreted with caution, as it could not be clearly attributed to air or road traffic and is rather a mixed signal.

4.4 Outlook

The results of the nitrogen isotope analysis showed partly high variability within and between the trees of the different sites. The statistical power could have been increased by a higher number of samples and by removing outliers. However, the latter is always difficult to justify and would have gone beyond the scope of the thesis. In addition, it would have been useful to extend the nitrogen isotope analysis to soil samples to better understand the N source in the soil background and thus the signal in the spruce needles. In this way, it would also have been possible to exclude site-related influences on the measured isotope ratio. Furthermore, it would be interesting to measure the δ^{15} N ratio of NO_x samples from the exhaust plume of aircraft. Various studies have already determined positive as well as negative values from NO_x samples of car exhaust (Ammann et al., 1999; Heaton, 1990). It would be plausible that significantly different δ^{15} N-NO_x values are measured for aircraft due to the combustion of kerosene at much higher temperatures. This result would also lead to a better understanding and interpretation of the measured δ^{15} N signal in the needles.

In this thesis, no suitable method was found to examine the collected spruce needles in the vicinity of Zurich Airport for emissions caused by tire abrasion during aircraft landing. Current methods are only partially able to measure nanoscale plastic particles that could potentially be taken up by the plant through their leaf stomata. Another challenge is to differentiate the foreign particles from the rest of the plant, which also consists of carbon compounds. A recent method developed by Materic et al. (2020) may offer the possibility to chemically analyze spruce needles for microplastics, but more importantly for nanoplastics: thermal desorption–proton transfer reaction–mass spectrometry (TD-PTR-MS). The advantages of the method are a sensitivity 100 times better than conventional measuring instruments and the applicability also to organic samples (Materić et al., 2020). The question remains whether the method can also be applied to plant components. Together with aircraft tire samples, it would then be possible to search for a very specific "plastic fingerprint" in the biosphere that comes from the abrasive emissions of aircraft tires.

Finally, for a better understanding of the dispersion and dilution behavior of certain pollutants in the air and the relationship to meteorological conditions, statistical models or so-called back-trajectory analyses could be carried out. For this purpose, it would be necessary to improve measurement capabilities over a larger area, especially for the measurement of air pollutants. A great potential lies in the cooperation with OSTLUFT, which also motivates communities to monitor local air quality with low-cost technologies. In this way, the measurement network becomes more closely meshed and the dispersion and dilution of pollutants can be better understood in a spatial context. The disadvantage is that such stations are not always permanent, are more frequently affected by measurement interruptions and the temporal resolution would be lower. Long-term measuring stations with high temporal resolution are therefore particularly recommended, especially at such a busy and congested location as Zurich Airport.

5 Conclusion

The objective of this work was to quantify changes in atmospheric pollutants before and during Covid-19 pandemic lockdown in 2020 using trees as bio-indicators at Zurich Airport. The measures taken to combat the Covid-19 pandemic led to a massive traffic reduction throughout Switzerland. This unprecedented traffic-related emission reduction provided a unique opportunity to study air quality and its impact on the biosphere.

Radiocarbon results have shown a significant decrease in ^{14}C depletion in spruce needles in the year of the pandemic lockdown in 2020 of the sites closer to traffic-related emission sources compared to previous years. The 2020 spruce needle generation at the carparking site showed a mean decrease in -F^{14}C of 30%, which was very close to the reduction in local road traffic at that time. At the runway site, however, a higher mean decline of -F^{14}C of 52% was found, indicating that not only road traffic is responsible for the measured signal but also air traffic at this location.

Because no nitrogen isotope analysis was performed on soil samples from the sites, it was not possible to determine whether differences in site δ^{15}N ratio were due to distance from atmospheric N emission sources or to site-specific variations in soil properties. At all of the three sites, there was no significant change in the δ^{15}N of the 2020 spruce needle generation compared to previous years. Overall, a short-term reduction in NO_x was not reflected in the measured δ^{15}N ratio of spruce needles. Instead, the measured δ^{15}N signal in spruce needles could be influenced by several factors such as soil N availability and processes, internal circulations and redistribution of N, and dilution/distribution effects of airborne pollutants and distance of sites to such emission sources.

Furthermore, the ratio of stable isotopes could also be influenced by climatic conditions this is true for δ^{15}N, but especially for delta δ^{13}C. Increased δ^{13}C values at the carparking site, thus indicated either higher exposure to air pollutants or lower water availability. It was difficult to distinguish between pollution and climatic causes in both nitrogen isotope and tree-ring analyses, as one seems to always mask the other. Nevertheless, the analyses are useful for examining spatial patterns or trends related to air quality and climate change.

Weather conditions also play an important role in monitoring and interpreting air quality. For instance, the reduction in traffic in Zurich Airport area and the associated decrease in emissions due to the measures taken to combat the Covid-19 pandemic did not necessarily lead to an improvement in air quality. It is therefore important to always interpret changes in air quality in consideration of local and global meteorological conditions that influence the concentration and distribution of air pollutants.

In summary, spruce needles are useful bio-indicators that record past atmospheric pollutants, showing a reduction of ^{14}C free CO_2 from traffic-related emission sources at the time of pandemic lockdown in 2020. Moreover, the radiocarbon method is a sensitive tool in environmental monitoring research for quantifying anthropogenic CO_2 emissions with annual resolution in tree rings as well as in leaves. This thesis demonstrated that Norway spruce needles, based on radiocarbon measurements, can record anthropogenic emission changes during past times when humanity paused, and the Earth breathed through as "all things share the same breath" (Chief Seattle).

Bibliography

Aas, G. et al. (2017). "Die Fichte (Picea abies): Verwandtschaft, Morphologie und Ökologie". In: *LWF Wissen* 80, pp. 13–19.

Alessio, M, Anselmi, S, Conforto, L, Improta, S, Manes, F, and Manfra, L (2002). "Radiocarbon as a biomarker of urban pollution in leaves of evergreen species sampled in Rome and in rural areas (Lazio—Central Italy)". In: *Atmospheric Environment* 36 (34), pp. 5405–5416.

Allen, S., Allen, D., Phoenix, V. R., Le Roux, G., Jiménez, P. D., Simonneau, A., Binet, S., and Galop, D. (2019). "Atmospheric transport and deposition of microplastics in a remote mountain catchment". In: *Nature Geoscience* 12 (5), pp. 339–344.

Ammann, M., Siegwolf, R., Pichlmayer, F, Suter, M., Saurer, M., and Brunold, C. (1999). "Estimating the uptake of traffic-derived NO2 from 15N abundance in Norway spruce needles". In: *Oecologia* 118 (2), pp. 124–131.

Baensch-Baltruschat, B., Kocher, B., Stock, F., and Reifferscheid, G. (2020). "Tyre and road wear particles (TRWP)-A review of generation, properties, emissions, human health risk, ecotoxicity, and fate in the environment". In: *Science of the Total Environment* 733, p. 137823.

BAFU (2014). *Luftverschmutzung und Gesundheit*. Bundesamt für Umwelt (BAFU), Bern. Umwelt-Wissen. URL: https://www.bafu.admin.ch/bafu/de/home/themen/luft/fachinformationen/auswirkungen-der-luftverschmutzung/auswirkungen-der-luftverschmutzung-auf-die-gesundheit.html (visited on 01/17/2022).

— (2018). *Lärmbelastung der Schweiz. Ergebnisse des nationalen Lärmmonitorings sonBASE, Stand 2015*. Bundesamt für Umwelt (BAFU), Bern. Umwelt-Zustand. URL: https://www.bafu.admin.ch/bafu/de/home/themen/laerm/publikationen-studien/publikationen/laermbelastung-in-der-schweiz-sonbase.html (visited on 01/17/2022).

— (2020). *Faktenblatt: SAPALDIA - Swiss Cohort Study on Air Pollution and Lung and Heart Diseases in Adults*. Bundesamt für Umwelt (BAFU), Bern. Auswirkungen der Luftverschmutzung auf die Gesundheit. URL: https://www.bafu.admin.ch/bafu/de/home/themen/luft/fachinformationen/auswirkungen-der-luftverschmutzung/auswirkungen-der-luftverschmutzung-auf-die-gesundheit.html (visited on 01/21/2022).

— (2021a). *Emissionen von Treibhausgasen nach CO2-Gesetz und Kyoto-Protokoll, 2. Verpflichtungsperiode (2013-2020)*. Bundesamt für Umwelt (BAFU), Bern. CO2 statistics: Emissions from thermal and motor fuels. URL: https://www.bafu.admin.ch/bafu/en/home/topics/climate/state/data/co2-statistics.html (visited on 01/18/2022).

BAFU (2021b). *Kenngrössen zur Entwicklung der Treibhausgasemissionen in der Schweiz 1990–2019*. Bundesamt für Umwelt (BAFU), Bern. Switzerland's greenhouse gas inventory. URL: https://www.bafu.admin.ch/bafu/en/home/topics/climate/state/data/greenhouse-gas-inventory.html (visited on 01/17/2022).

— (2021c). *Luftqualität 2020: Messresultate des Nationalen Beobachtungsnetzes für Luftfremdstoffe (NABEL)*. Bundesamt für Umwelt (BAFU), Bern. Umwelt-Zustand. URL: https://www.bafu.admin.ch/bafu/de/home/themen/luft/fachinformationen/auswirkungen-der-luftverschmutzung/auswirkungen-der-luftverschmutzung-auf-die-gesundheit.html (visited on 01/18/2022).

BAG (Mar. 16, 2020a). *Coronavirus: Bundesrat erklärt die «ausserordentliche Lage» und verschärft die Massnahmen*. BAG - Bundesamt für Gesundheit: Medienmitteilungen. URL: https://www.admin.ch/gov/de/start/dokumentation/medienmitteilungen.msg-id-78454.html (visited on 01/17/2022).

— (Feb. 25, 2020b). *Neues Coronavirus COVID-19: Erster bestätigter Fall in der Schweiz*. BAG - Bundesamt für Gesundheit: Medienmitteilungen. URL: https://www.bag.admin.ch/bag/de/home/das-bag/aktuell/medienmitteilungen.msg-id-78233.html (visited on 01/17/2022).

Ballikaya, P., Marshall, J., and Cherubini, P. (2022). "Can tree-ring chemistry be used to monitor atmospheric nanoparticle contamination over time?" In: *Atmospheric Environment* 268, p. 118781. DOI: https://doi.org/10.1016/j.atmosenv.2021.118781.

Battipaglia, G., Marzaioli, F., Lubritto, C., Altieri, S., Strumia, S., Cherubini, P., and Cotrufo, M. F. (2010). "Traffic pollution affects tree-ring width and isotopic composition of Pinus pinea". In: *Science of the total Environment* 408 (3), pp. 586–593.

Bauer, J. (2008). *Flughafen Zürich, 1948-2008*. ger. Zürich: AS Verlag & Buchkonzept.

BAZL (2020). *CO2-Emissionen des Luftverkehrs - Grundsätzliches und Zahlen*. Bundesamt für Zivilluftfahrt BAZL. Luftfahrtentwicklung. URL: https://www.bafu.admin.ch/bafu/en/home/topics/climate/state/data/co2-statistics.html (visited on 01/12/2022).

Beloconi, A., Probst-Hensch, N. M., and Vounatsou, P. (2021). "Spatio-temporal modelling of changes in air pollution exposure associated to the COVID-19 lockdown measures across Europe". In: *Science of The Total Environment* 787, p. 147607. DOI: https://doi.org/10.1016/j.scitotenv.2021.147607.

Bennett, M., Christie, S. M., Graham, A., Thomas, B. S., Vishnyakov, V., Morris, K., Peters, D. M., Jones, R., and Ansell, C. (2011). "Composition of smoke generated by landing aircraft". In: *Environmental science & technology* 45 (8), pp. 3533–3538.

Bergmann, M., Mützel, S., Primpke, S., Tekman, M. B., Trachsel, J., and Gerdts, G. (2019). "White and wonderful? Microplastics prevail in snow from the Alps to the Arctic". In: *Science advances* 5 (8), eaax1157.

Berman, J. D. and Ebisu, K. (2020). "Changes in US air pollution during the COVID-19 pandemic". In: *Science of the total environment* 739, p. 139864.

BFS, and BAZL, (2021). *Schweizerische Zivilluftfahr, Flugbewegung und Passagierinnen & Passagiere*. BFS und BAZL Data. URL: https://www.bfs.admin.ch/bfs/de/home/statistiken/mobilitaet-verkehr/querschnittsthemen/zivilluftfahrt/linien-charterverkehr.html (visited on 01/12/2022).

BFS (2021). *Umweltauswirkungen*. Bundesamt für Statistik BFS. Mobilität und Verkehr. URL: https://www.bfs.admin.ch/bfs/de/home/statistiken/mobilitaet-verkehr/unfaelle-umweltauswirkungen/umweltauswirkungen.html (visited on 01/12/2022).

Binda, G., Di Iorio, A., and Monticelli, D. (2021). "The what, how, why, and when of dendrochemistry:(paleo) environmental information from the chemical analysis of tree rings". In: *Science of the Total Environment* 758, p. 143672.

Bronk Ramsey, C. (2008). "Radiocarbon dating: revolutions in understanding". In: *Archaeometry* 50 (2), pp. 249–275.

Brunner, I and Brodbeck, S (2001). "Response of mycorrhizal Norway spruce seedlings to various nitrogen loads and sources". In: *Environmental Pollution* 114 (2), pp. 223–233.

Buck, J. C. and Weinstein, S. B. (2020). "The ecological consequences of a pandemic". In: *Biology Letters* 16 (11), p. 20200641.

Bukata, A. R. and Kyser, T. K. (2007). "Carbon and nitrogen isotope variations in tree-rings as records of perturbations in regional carbon and nitrogen cycles". In: *Environmental science & technology* 41 (4), pp. 1331–1338.

Bunn, A. G. (2008). "A dendrochronology program library in R (dplR)". In: *Dendrochronologia* 26 (2), pp. 115–124.

Cipriani, G., Danti, S., Carlesi, C., and Borin, G. (2018). "Danger in the air: air pollution and cognitive dysfunction". In: *American Journal of Alzheimer's Disease & Other Dementias®* 33 (6), pp. 333–341.

Cocozza, C., Alterio, E., Bachmann, O., Guillong, M., Sitzia, T., and Cherubini, P. (2021). "Monitoring air pollution close to a cement plant and in a multi-source industrial area through tree-ring analysis". In: *Environmental Science and Pollution Research* 28 (38), pp. 54030–54040.

Cocozza, C., Perone, A., Giordano, C., Salvatici, M. C., Pignattelli, S., Raio, A., Schaub, M., Sever, K., Innes, J. L., Tognetti, R., et al. (2019). "Silver nanoparticles enter the tree stem faster through leaves than through roots". In: *Tree physiology* 39 (7), pp. 1251–1261.

Cooper, M. J., Martin, R. V., Hammer, M. S., Levelt, P. F., Veefkind, P., Lamsal, L. N., Krotkov, N. A., Brook, J. R., and McLinden, C. A. (2022). "Global fine-scale changes in ambient NO2 during COVID-19 lockdowns". In: *Nature* 601 (7893), pp. 380–387.

De Micco, V, Campelo, F, De Luis, M, Bräuning, A, Grabner, M, Battipaglia, G, and Cherubini, P (2016). "Intra-annual density fluctuations in tree rings: how, when, where, and why?" In: *IAWA Journal* 37 (2), pp. 232–259.

Douglass, A. E. (1941). "Crossdating in dendrochronology". In: *Journal of Forestry* 39 (10), pp. 825–831.

Ecoplan (2019). *Berechnung von DALY für die Schweiz*. Bundesamt für Umwelt (BAFU), Bern und Altdorf. Auswirkungen des Verkehrslärms auf die Gesundheit. URL: www.ecoplan.ch (visited on 03/14/2022).

Eichert, T., Kurtz, A., Steiner, U., and Goldbach, H. E. (2008). "Size exclusion limits and lateral heterogeneity of the stomatal foliar uptake pathway for aqueous solutes and water-suspended nanoparticles". In: *Physiologia plantarum* 134 (1), pp. 151–160.

Eisenman, T. S., Churkina, G., Jariwala, S. P., Kumar, P., Lovasi, G. S., Pataki, D. E., Weinberger, K. R., and Whitlow, T. H. (2019). "Urban trees, air quality, and asthma: An interdisciplinary review". In: *Landscape and urban planning* 187, pp. 47–59.

ESA (Apr. 16, 2020). *Air pollution remains low as Europeans stay at home*. ESA - European Space Agency. URL: https://www.esa.int/Applications/Observing_the_Earth/Copernicus/Sentinel-5P/Air_pollution_remains_low_as_Europeans_stay_at_home (visited on 01/17/2022).

Etheridge, D. M., Steele, L., Langenfelds, R. L., Francey, R. J., Barnola, J.-M., and Morgan, V. (1996). "Natural and anthropogenic changes in atmospheric CO2 over the last 1000 years from air in Antarctic ice and firn". In: *Journal of Geophysical Research: Atmospheres* 101 (D2), pp. 4115–4128.

Fleuti, E. (2020). "Effects of COVID-19-related air traffic restrictions on local air quality at Zurich airport". In: *Journal of Airport Management* 15 (1), pp. 59–70.

Fowler, D., Coyle, M., Skiba, U., Sutton, M. A., Cape, J. N., Reis, S., Sheppard, L. J., Jenkins, A., Grizzetti, B., Galloway, J. N., et al. (2013). "The global nitrogen cycle in the twenty-first century". In: *Philosophical Transactions of the Royal Society B: Biological Sciences* 368 (1621), p. 20130164.

Franssen, E., Van Wiechen, C., Nagelkerke, N., and Lebret, E (2004). "Aircraft noise around a large international airport and its impact on general health and medication use". In: *Occupational and environmental medicine* 61 (5), pp. 405–413.

Freer-Smith, P., Beckett, K., and Taylor, G. (2005). "Deposition velocities to Sorbus aria, Acer campestre, Populus deltoides× trichocarpa 'Beaupré', Pinus nigra and× Cupressocyparis leylandii for coarse, fine and ultra-fine particles in the urban environment". In: *Environmental pollution* 133 (1), pp. 157–167.

Freyer, H. (1991). "Seasonal variation of 15N/14N ratios in atmospheric nitrate species". In: *Tellus B* 43 (1), pp. 30–44.

Friedli, W. (1950). *Flughafen Zürich-Kloten*. ETH-Bibliothek Zürich, Bildarchiv/Stiftung Luftbild Schweiz. URL: http://doi.org/10.3932/ethz-a-000355194.

FZAG (2019). *Geschäftsbericht - Verantwortung*. Flughafen Zürich AG: Geschäftsberichte. URL: https://report.flughafen-zuerich.ch/2019/ar/de/ (visited on 01/06/2022).

— (2020a). *Geschäftsbericht - Verantwortung*. Flughafen Zürich AG: Geschäftsberichte. URL: https://report.flughafen-zuerich.ch/2020/ar/de/ (visited on 01/06/2022).

— (2020b). *Natur und Landschaft*. Flughafen Zürich AG. Umweltschutz. URL: https://www.flughafen-zuerich.ch/de/unternehmen/politik-und-verantwortung/umweltschutz/natur (visited on 01/06/2022).

— (2022). *Air pollution Data*. Private derived from FZAG and WWEA.

Galloway, J. N., Townsend, A. R., Erisman, J. W., Bekunda, M., Cai, Z., Freney, J. R., Martinelli, L. A., Seitzinger, S. P., and Sutton, M. A. (2008). "Transformation of the nitrogen cycle: recent trends, questions, and potential solutions". In: *Science* 320 (5878), pp. 889–892.

Gärtner, H. and Nievergelt, D. (2010). "The core-microtome: A new tool for surface preparation on cores and time series analysis of varying cell parameters". In: *Dendrochronologia* 28 (2), pp. 85–92. DOI: https://doi.org/10.1016/j.dendro.2009.09.002.

Gaudinski, J. B., Dawson, T. E., Quideau, S., Schuur, E. A., Roden, J. S., Trumbore, S. E., Sandquist, D. R., Oh, S.-W., and Wasylishen, R. E. (2005). "Comparative analysis of cellulose preparation techniques for use with 13C, 14C, and 18O isotopic measurements". In: *Analytical Chemistry* 77 (22), pp. 7212–7224.

Gebauer, G. and Dietrich, P. (1993). "Nitrogen isotope ratios in different compartments of a mixed stand of spruce, larch and beech trees and of understorey vegetation including fungi". In: *Isotopes in Environmental and Health Studies* 29 (1-2), pp. 35–44.

Geng, L., Alexander, B., Cole-Dai, J., Steig, E. J., Savarino, J., Sofen, E. D., and Schauer, A. J. (2014). "Nitrogen isotopes in ice core nitrate linked to anthropogenic atmospheric acidity change". In: *Proceedings of the National Academy of Sciences* 111 (16), pp. 5808–5812.

Grootes, P. M. and Plicht, H. van der (2021). "Hessel de Vries: radiocarbon pioneer from Groningen". In: *Radiocarbon*, pp. 1–15.

Grote, R., Samson, R., Alonso, R., Amorim, J. H., Cariñanos, P., Churkina, G., Fares, S., Thiec, D. L., Niinemets, Ü., Mikkelsen, T. N., et al. (2016). "Functional traits of urban trees: air pollution mitigation potential". In: *Frontiers in Ecology and the Environment* 14 (10), pp. 543–550.

Guerrieri, M. R., Siegwolf, R., Saurer, M, Jäggi, M, Cherubini, P, Ripullone, F., and Borghetti, M. (2009). "Impact of different nitrogen emission sources on tree physiology as assessed by a triple stable isotope approach". In: *Atmospheric Environment* 43 (2), pp. 410–418.

Güttler, N., Rhyner, N., and Stadler, M. (2018). *Flughafen Kloten : Anatomie eines komplizierten Ortes*. 1. Auflage. Æther 01. Zürich: intercom Verlag.

Hajdas, I., Ascough, P., Garnett, M. H., Fallon, S. J., Pearson, C. L., Quarta, G., Spalding, K. L., Yamaguchi, H., and Yoneda, M. (2021). "Radiocarbon dating". In: *Nature Reviews Methods Primers* 1 (1), pp. 1–26.

Han, C. and Hong, Y.-C. (2020). "Decrease in ambient fine particulate matter during COVID-19 crisis and corresponding health benefits in Seoul, Korea". In: *International journal of environmental research and public health* 17 (15), p. 5279.

Heaton, T. (1990). "15N/14N ratios of NOx from vehicle engines and coal-fired power stations". In: *Tellus B* 42 (3), pp. 304–307.

Hueglin, C, Gianini, M, and Gehrig, R (2012). *Chemische Zusammensetzung und Quellen von Feinstaub*. Untersuchungen an ausgewählten NABEL-Standorten. Projektbericht im Auftrag des Bundesamtes für Umwelt (BAFU).

Kalugina, O. V., Mikhailova, T. A., and Shergina, O. V. (2017). "Pinus sylvestris as a bioindicator of territory pollution from aluminum smelter emissions". In: *Environmental science and pollution research* 24 (11), pp. 10279–10291.

Karkour, S. and Itsubo, N. (2020). "Influence of the COVID-19 crisis on global PM2. 5 concentration and related health impacts". In: *Sustainability* 12 (13), p. 5297.

Keeling, C. (1991). "CO2 emissions—historical record". In: *Trends* 91, pp. 383–385.

Keeling, C. D., Piper, S. C., Bacastow, R. B., Wahlen, M., Whorf, T. P., Heimann, M., and Meijer, H. A. (2001). *Exchanges of atmospheric CO2 and 13CO2 with the terrestrial biosphere and oceans from 1978 to 2000. I. Global aspects*. 14C Data. URL: `https://scrippsco2.ucsd.edu/data/atmospheric_co2/mlo.html` (visited on 03/18/2022).

Kole, P. J., Löhr, A. J., Van Belleghem, F. G., and Ragas, A. M. (2017). "Wear and tear of tyres: a stealthy source of microplastics in the environment". In: *International journal of environmental research and public health* 14 (10), p. 1265.

Le Quéré, C., Jackson, R. B., Jones, M. W., Smith, A. J., Abernethy, S., Andrew, R. M., De-Gol, A. J., Willis, D. R., Shan, Y., Canadell, J. G., et al. (2020). "Temporary reduction in daily global CO 2 emissions during the COVID-19 forced confinement". In: *Nature climate change* 10 (7), pp. 647–653.

Leffler, A. J. and Evans, A. S. (1999). "Variation in carbon isotope composition among years in the riparian tree Populus fremontii". In: *Oecologia* 119 (3), pp. 311–319.

Leonelli, G., Battipaglia, G., Siegwolf, R. T., Saurer, M., Cella, U. M. di, Cherubini, P., and Pelfini, M. (2012). "Climatic isotope signals in tree rings masked by air pollution: A case study conducted along the Mont Blanc Tunnel access road (Western Alps, Italy)". In: *Atmospheric Environment* 61, pp. 169–179.

Lepp, N. (1975). "The potential of tree-ring analysis for monitoring heavy metal pollution patterns". In: *Environmental Pollution (1970)* 9 (1), pp. 49–61. DOI: `https://doi.org/10.1016/0013-9327(75)90055-5`.

Leung, D. Y., Tsui, J. K., Chen, F., Yip, W.-K., Vrijmoed, L. L., and Liu, C.-H. (2011). "Effects of urban vegetation on urban air quality". In: *Landscape Research* 36 (2), pp. 173–188.

Levin, I. and Hesshaimer, V. (2000). "Radiocarbon–a unique tracer of global carbon cycle dynamics". In: *Radiocarbon* 42 (1), pp. 69–80.

Levin, I. and Kromer, B. (2004). "The tropospheric 14CO2 level in mid-latitudes of the Northern Hemisphere (1959–2003)". In: *Radiocarbon* 46 (3), pp. 1261–1272.

Libby, W. F., Anderson, E. C., and Arnold, J. R. (1949). "Age determination by radiocarbon content: world-wide assay of natural radiocarbon". In: *science* 109 (2827), pp. 227–228.

Liu, Z., Ciais, P., Deng, Z., Lei, R., Davis, S. J., Feng, S., Zheng, B., Cui, D., Dou, X., Zhu, B., et al. (2020). "Near-real-time monitoring of global CO2 emissions reveals the effects of the COVID-19 pandemic". In: *Nature communications* 11 (1), pp. 1–12.

Luo, X., Bing, H., Luo, Z., Wang, Y., and Jin, L. (2019). "Impacts of atmospheric particulate matter pollution on environmental biogeochemistry of trace metals in soil-plant system: A review". In: *Environmental Pollution* 255, p. 113138.

Lv, J., Christie, P., and Zhang, S. (2019). "Uptake, translocation, and transformation of metal-based nanoparticles in plants: recent advances and methodological challenges". In: *Environmental Science: Nano* 6 (1), pp. 41–59.

Mariotti, A. (1983). "Atmospheric nitrogen is a reliable standard for natural 15N abundance measurements". In: *Nature* 303 (5919), pp. 685–687.

Materić, D., Kasper-Giebl, A., Kau, D., Anten, M., Greilinger, M., Ludewig, E., Sebille, E. van, Röckmann, T., and Holzinger, R. (2020). "Micro-and nanoplastics in alpine snow: a new method for chemical identification and (semi) quantification in the nanogram range". In: *Environmental science & technology* 54 (4), pp. 2353–2359.

Materić, D., Ludewig, E., Brunner, D., Röckmann, T., and Holzinger, R. (2021). "Nanoplastics transport to the remote, high-altitude Alps". In: *Environmental Pollution* 288, p. 117697. DOI: https://doi.org/10.1016/j.envpol.2021.117697.

MeteoSwiss, (2022). *Climate Data derived from IDAWEB.* MeteoSwiss Climate Data. URL: https://www.meteoschweiz.admin.ch/home/service-und-publikationen/beratung-und-service/datenportal-fuer-lehre-und-forschung.html.

Moser, P. (2020). *Mobilität im Lockdown - Eine Analsyse der Auswirkungen der COVID19-Krise auf das Mobilitätsverhalten*. Statistische Amt Kanton Zürich. URL: https://www.zh.ch/de/news-uebersicht/mitteilungen/2020/politik-staat/statistik/mobilitaet-im-lockdown---eine-erste-einschaetzung.html (visited on 01/17/2022).

Münzel, T., Sørensen, M., Gori, T., Schmidt, F. P., Rao, X., Brook, J., Chen, L. C., Brook, R. D., and Rajagopalan, S. (2017). "Environmental stressors and cardio-metabolic disease: part I–epidemiologic evidence supporting a role for noise and air pollution and effects of mitigation strategies". In: *European heart journal* 38 (8), pp. 550–556.

Münzel, T., Hahad, O., Daiber, A., and Lelieveld, J. (2021). "Air pollution and cardiovascular diseases." In: *Herz.* 46 (2).

Niemelä, P., Lumme, I., Mattson, W., and Arkhipov, V. (1997). "13C in tree rings along an air pollution gradient in the Karelian Isthmus, northwest Russia and southeast Finland". In: *Canadian journal of forest research* 27 (4), pp. 609–612.

Norby, R. J. (1998). "Nitrogen deposition: a component of global change analyses". In: *The New Phytologist* 139 (1), pp. 189–200.

Novak, K., De Luis, M., Gričar, J., Prislan, P., Merela, M., Smith, K. T., and Čufar, K. (2016). "Missing and dark rings associated with drought in Pinus halepensis". In: *Iawa Journal* 37 (2), pp. 260–274.

Nowak, D. J., Hirabayashi, S., Doyle, M., McGovern, M., and Pasher, J. (2018). "Air pollution removal by urban forests in Canada and its effect on air quality and human health". In: *Urban Forestry & Urban Greening* 29, pp. 40–48.

NZZ (Dec. 31, 2019). *Mysteriöse Lungenkrankheit in Zentralchina ausgebrochen - einige Stimmen befürchten einen erneuten Ausbruch der Lungenseuche Sars*. NZZ. URL: https://www.nzz.ch/panorama/mysterioese-lungenkrankheit-in-zentralchina-ausgebrochen-einige-befuerchten-einen-erneuten-ausbruch-der-lungenseuche-sars-ld.1531501 (visited on 01/17/2022).

Němec, M., Wacker, L., Hajdas, I., and Gäggeler, H. (2010). "Alternative Methods for Cellulose Preparation for AMS Measurement". In: *Radiocarbon an international journal of cosmogenic isotope research* 52 (3).

Ohlwein, S., Kappeler, R., Kutlar Joss, M., Künzli, N., and Hoffmann, B. (2019). "Health effects of ultrafine particles: a systematic literature review update of epidemiological evidence". In: *International journal of public health* 64 (4), pp. 547–559.

OSTLUFT (2021). *Ultrafeine Partikel in Kloten 2019 & 2020 - Belastungssituation und Einfluss des Flugverkehrs*. OSTLUFT–Die Luftqualitätsüberwachung, der Ostschweizer Kantone: Fachberichte. URL: https://www.ostluft.ch/index.php?id=80 (visited on 01/17/2022).

— (2022). *Stickstoffdioxid, Opfikon, Balsberg*. OSTLUFT Data. URL: https://www.ostluft.ch/index.php?id=datenabfragen (visited on 01/17/2022).

Panek, J. A. and Waring, R. H. (1997). "Stable carbon isotopes as indicators of limitations to forest growth imposed by climate stress". In: *Ecological Applications* 7 (3), pp. 854–863.

Pozzer, A., Dominici, F., Haines, A., Witt, C., Münzel, T., and Lelieveld, J. (2020). "Regional and global contributions of air pollution to risk of death from COVID-19". In: *Cardiovascular Research* 116 (14), pp. 2247–2253.

Rakowski, A. Z., Nakamura, T., and Pazdur, A. (2008). "Variations of anthropogenic CO2 in urban area deduced by radiocarbon concentration in modern tree rings". In: *Journal of Environmental Radioactivity* 99 (10). Natural Radiation, pp. 1558–1565. DOI: https://doi.org/10.1016/j.jenvrad.2007.12.007.

Reimer, P. J., Brown, T. A., and Reimer, R. W. (2004). "Discussion: reporting and calibration of post-bomb 14C data". In: *Radiocarbon* 46 (3), pp. 1299–1304.

Rennenberg, H. and Gessler, A. (1999). "Consequences of N deposition to forest ecosystems-recent results and future research needs". In: *Water, Air, and Soil Pollution* 116 (1), pp. 47–64.

Samson, R., Grote, R., Calfapietra, C., Cariñanos, P., Fares, S., Paoletti, E., and Tiwary, A. (2017). "Urban trees and their relation to air pollution". In: *The urban forest*. Springer, pp. 21–30.

Saurer, M, Cherubini, P, Ammann, M, De Cinti, B, and Siegwolf, R (2004). "First detection of nitrogen from NOx in tree rings: a 15N/14N study near a motorway". In: *Atmospheric Environment* 38 (18), pp. 2779–2787.

Savard, M. M. (2010). "Tree-ring stable isotopes and historical perspectives on pollution–An overview". In: *Environmental Pollution* 158 (6), pp. 2007–2013.

Savard, M. M., Bégin, C., Smirnoff, A., Marion, J., and Rioux-Paquette, E. (2009). "Tree-ring nitrogen isotopes reflect anthropogenic NO x emissions and climatic effects". In: *Environmental science & technology* 43 (3), pp. 604–609.

Savard, M. M., Martineau, C., Laganière, J., Bégin, C., Marion, J., Smirnoff, A., Stefani, F., Bergeron, J., Rheault, K., Paré, D., et al. (2021). "Nitrogen isotopes in the soil-to-tree continuum—Tree rings express the soil biogeochemistry of boreal forests exposed to moderate airborne emissions". In: *Science of The Total Environment* 780, p. 146581.

Schönwiese, C.-D. (2013). *Klimatologie*. utb GmbH.

Schwab, F., Zhai, G., Kern, M., Turner, A., Schnoor, J. L., and Wiesner, M. R. (2016). "Barriers, pathways and processes for uptake, translocation and accumulation of nanomaterials in plants–Critical review". In: *Nanotoxicology* 10 (3), pp. 257–278.

Schweingruber, F. H. (1993). *Trees and Wood in Dendrochronology : Morphological, Anatomical, and Tree-Ring Analytical Characteristics of Trees Frequently Used in Dendrochronology*. eng. 1st ed. 1993. Springer Series in Wood Science. Berlin, Heidelberg: Springer Berlin Heidelberg.

Schweingruber, F. H. (1980). *Dichteschwankungen in Jahrringen von Nadelhölzern in Beziehung zu klimatisch-ökologischen Faktoren, oder das Problem der falschen Jahrringe*. ger. Berichte / Eidgenössische Anstalt für das forstliche Versuchswesen Nr. 213. Birmensdorf: Eidgenössische Anstalt für das forstliche Versuchswesen.

— (1983). *Der Jahrring : Standort, Methodik, Zeit und Klima in der Dendrochronologie*. ger. Bern [etc: Haupt.

Schweingruber, F. H. (1988). *Tree rings : basics and applications of dendrochronology*. eng. 1st ed. 1988. Dordrecht, Netherlands ; Kluwer Academic Publishers.

Schweingruber, F. H. (2007). *Wood Structure and Environment*. eng. 1st ed. 2007. Springer Series in Wood Science. Berlin, Heidelberg: Springer Berlin Heidelberg.

Sensuła, B., Wilczyński, S., Monin, L., Allan, M., Pazdur, A., and Fagel, N. (2017). "Variations of tree ring width and chemical composition of wood of pine growing in the area nearby chemical factories". In: *Geochronometria* 44 (1), pp. 226–239.

Siegwolf, R. T., Matyssek, R., Saurer, M., Maurer, S., Günthardt-Goerg, M. S., Schmutz, P., and Bucher, J. B. (2001). "Stable isotope analysis reveals differential effects of soil nitrogen and nitrogen dioxide on the water use efficiency in hybrid poplar leaves". In: *New Phytologist* 149 (2), pp. 233–246.

Sintermann, J. (Apr. 14, 2020). *Auswirkungen der verringerten Aktivitäten durch die Sars-CoV-2 Pandemie auf die Luftqualität*. OSTLUFT–Die Luftqualitätsüberwachung, der Ostschweizer Kantone. URL: https://www.ostluft.ch/fileadmin/intern/LZ_Information/Publikationen/Fachberichte/Auswirkungen_Corona_Luftqualitaet.html#sars-

cov-2-pandemie-fÃijhrt-zu-einschrÃďnkungen-und-weniger-luftschadstoffemissionen%20 (visited on 01/17/2022).

Sookdeo, A., Kromer, B., Büntgen, U., Friedrich, M., Friedrich, R., Helle, G., Pauly, M., Nievergelt, D., Reinig, F., Treydte, K., Synal, H.-A., and Wacker, L. (2020-08). "Quality Dating: A Well-Defined Protocol Implemented at ETH for High-Precision 14C-Dates Tested on Late Glacial Wood". In: *Radiocarbon an international journal of cosmogenic isotope research* 62 (4).

Stenström, K., Skog, G., Georgiadou, E., Genberg, J., and Mellström, A. (2011). *A guide to radiocarbon units and calculations*. (LUNFD6(NFFR-3111)/1-17/(2011)). Lund University, Nuclear Physics. URL: https://lucris.lub.lu.se/ws/portalfiles/portal/5555659/2173661.pdf (visited on 02/16/2022).

Stuart K., G., Christoph, H., Lukas, E., and et, a. (Aug. 24, 2020). *Influence of COVID-19 lockdowns on Switzerland's air quality*. EMPA - Laboratory for Air Pollution/Environmental Technology. URL: https://empa-interim.github.io/empa.interim/swiss_air_quality_and_covid_19.html (visited on 01/17/2022).

Stuiver, M. (1961). "Variations in radiocarbon concentration and sunspot activity". In: *Journal of Geophysical Research* 66 (1), pp. 273–276.

Suess, H. E. (1955). "Radiocarbon concentration in modern wood". In: *Science* 122 (3166), pp. 415–417.

Sun, H., Lei, C., Xu, J., and Li, R. (2021). "Foliar uptake and leaf-to-root translocation of nanoplastics with different coating charge in maize plants". In: *Journal of Hazardous Materials* 416, p. 125854.

Swissair Photo AG, (1977). *Flughafen Zürich-Kloten*. ETH-Bibliothek Zürich, Bildarchiv/Stiftung Luftbild Schweiz. URL: http://doi.org/10.3932/ethz-a-000489940.

Synal, H.-A., Stocker, M., and Suter, M. (2007). "MICADAS: A new compact radiocarbon AMS system". In: *Nuclear Instruments and Methods in Physics Research Section B: Beam Interactions with Materials and Atoms* 259 (1). Accelerator Mass Spectrometry, pp. 7–13. DOI: https://doi.org/10.1016/j.nimb.2007.01.138.

Travaglio, M., Yu, Y., Popovic, R., Selley, L., Leal, N. S., and Martins, L. M. (2021). "Links between air pollution and COVID-19 in England". In: *Environmental Pollution* 268, p. 115859.

Vitousek, P. M., Porder, S., Houlton, B. Z., and Chadwick, O. A. (2010). "Terrestrial phosphorus limitation: mechanisms, implications, and nitrogen–phosphorus interactions". In: *Ecological applications* 20 (1), pp. 5–15.

Vogel, B, Corsmeier, U, Vogel, H, Fiedler, F, Kühlwein, J, Friedrich, R, Obermeier, A, Weppner, J, Kalthoff, N, Bäumer, D, et al. (2000). "Comparison of measured and calculated motorway emission data". In: *Atmospheric Environment* 34 (15), pp. 2437–2450.

Vos, P. E., Maiheu, B., Vankerkom, J., and Janssen, S. (2013). "Improving local air quality in cities: to tree or not to tree?" In: *Environmental pollution* 183, pp. 113–122.

Vries, H. de (1958). "Variation in concentration of radiocarbon with time and location on earth". In: *Proc. Koninkl. Nederl. Akad. Wetenschappen, B* 61, pp. 1–9.

Wacker, L, Bonani, G, Friedrich, M, Hajdas, I, Kromer, B, Němec, M, Ruff, M, Suter, M, Synal, H.-A., and Vockenhuber, C (2010a). "MICADAS: Routine and High-Precision Radiocarbon Dating". In: *Radiocarbon an international journal of cosmogenic isotope research* 52 (2).

Wacker, L., Němec, M., and Bourquin, J. (2010b). "A revolutionary graphitisation system: Fully automated, compact and simple". In: *Nuclear Instruments and Methods in Physics Research Section B: Beam Interactions with Materials and Atoms* 268 (7). Proceedings of the Eleventh International Conference on Accelerator Mass Spectrometry, pp. 931–934. DOI: https://doi.org/10.1016/j.nimb.2009.10.067. URL: https://www.sciencedirect.com/science/article/pii/S0168583X09011161.

Waldmann, N. (Jan. 25, 2022). *Nanoplastik in der Umwelt - In den Alpen schneit es Plastik*. EMPA - Laboratory for Air Pollution/Environmental Technology. URL: https://www.empa.ch/de/web/s604/nanoplastik-in-den-alpen (visited on 02/12/2022).

WHO (2016). *Ambient air pollution: A global assessment of exposure and burden of disease*. World Health Organization. URL: https://apps.who.int/iris/bitstream/handle/10665/250141/9789241511/9789241511353-eng.pdf?sequence=1 (visited on 03/19/2022).

— (2018). *Environmental Noise Guidelines for the European Region*. World Health Organization. Kopenhagen. URL: https://www.euro.who.int/en/publications/abstracts/environmental-noise-guidelines-for-the-european-region-2018 (visited on 03/19/2022).

WMO (2017). *WMO greenhouse gas bulletin. The state of greenhouse gases in the atmosphere based on global observations through 2015*. World Meteorological Organization, Geneva, Switzerland. URL: https://reliefweb.int/sites/reliefweb.int/files/resources/GHG_Bulletin_12_EN_web_JN161640.pdf (visited on 01/18/2022).

Wu, X., Nethery, R. C., Sabath, M. B., Braun, D., and Dominici, F. (2020). *Exposure to air pollution and COVID-19 mortality in the United States: A nationwide cross-sectional study*. Europe PMC.

Zhongming, Z., Linong, L., Wangqiang, Z., Wei, L., et al. (2012). *Particulate matter from natural sources and related reporting under the EU Air Quality Directive in 2008 and 2009*. European Environment Agency (EEA). Technical report. No. 10.

A Stable Isotopes

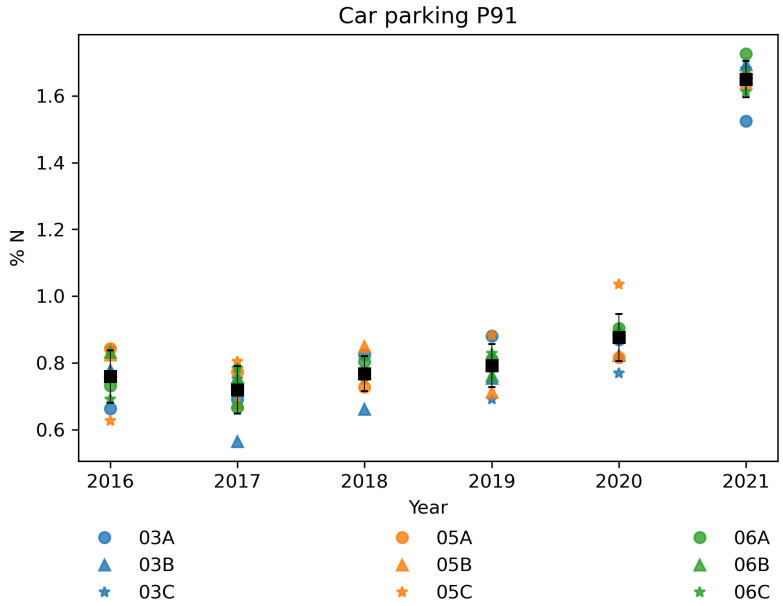

FIGURE A.1: Nitrogen concentration [%] with mean N-concentration and standard deviation (± SD) of Norway spruce needles from 2016-2021 at carparking site. Tree no. 3 (blue), tree no. 5 (orange), and tree no. 6 (green) with different branches (replication) A (circle), B (triangle), and C (star).

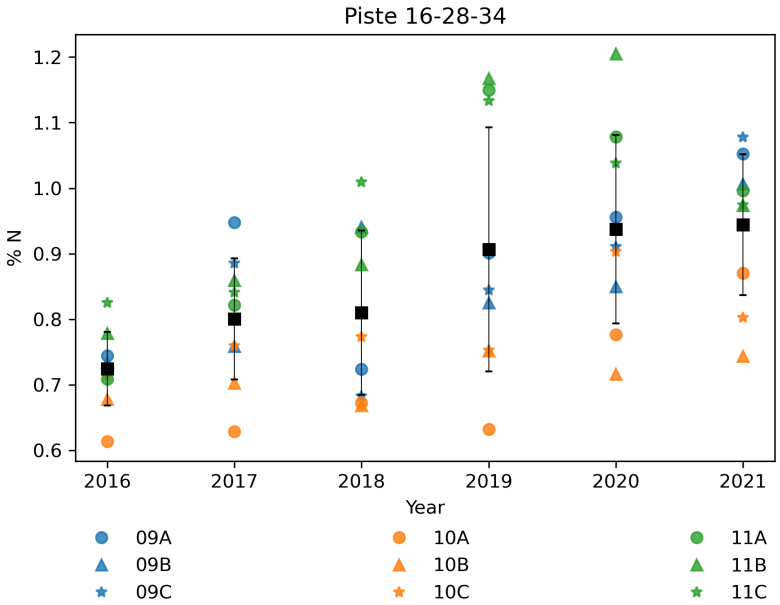

FIGURE A.2: Nitrogen concentration [%] with mean N-concentration and standard deviation (± SD) of Norway spruce needles from 2016-2021 at runway site. Tree no. 9 (blue), tree no. 10 (orange), and tree no. 11 (green) with different branches (replication) A (circle), B (triangle), and C (star).

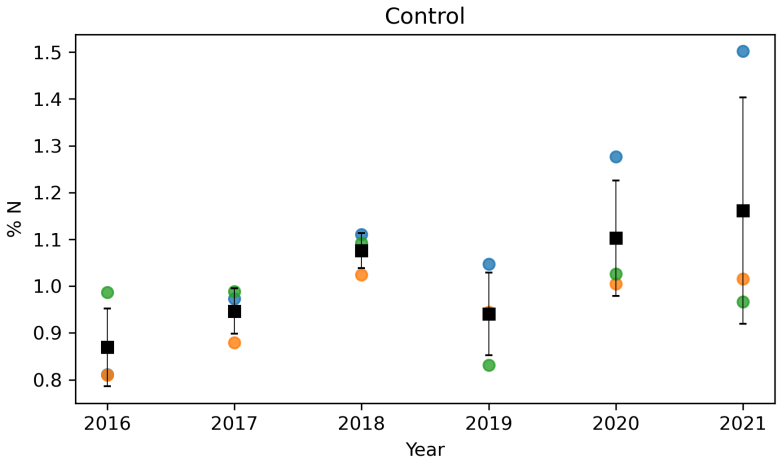

FIGURE A.3: Nitrogen concentration [%] with mean N-concentration and standard deviation (± SD) of Norway spruce needles from 2016-2021 at control site. Tree no. 24 (blue), tree no. 25 (orange), and tree no. 26 (green).

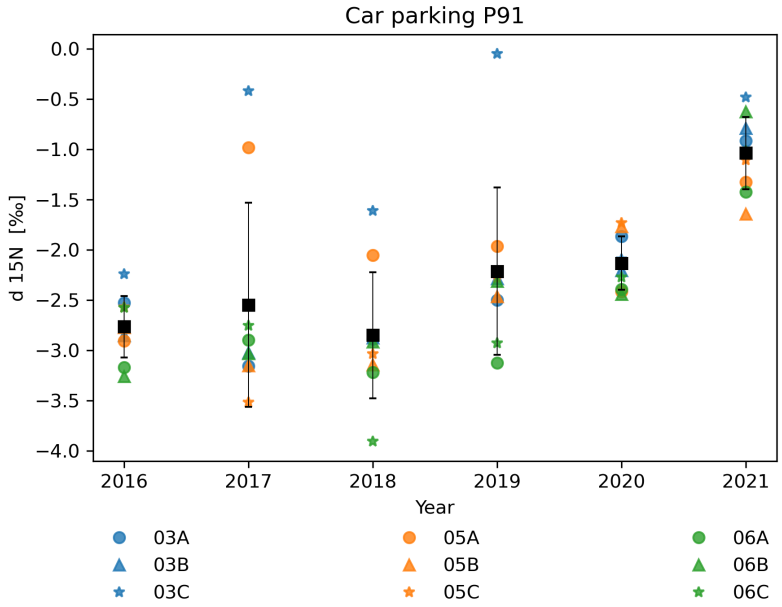

FIGURE A.4: δ^{15}N [‰] with mean δ^{15}N and standard deviation ($\pm$ SD) of Norway spruce needles from 2016-2021 at carparking site. Tree no. 3 (blue), tree no. 5 (orange), and tree no. 6 (green) with different branches (replication) A (circle), B (triangle), and C (star).

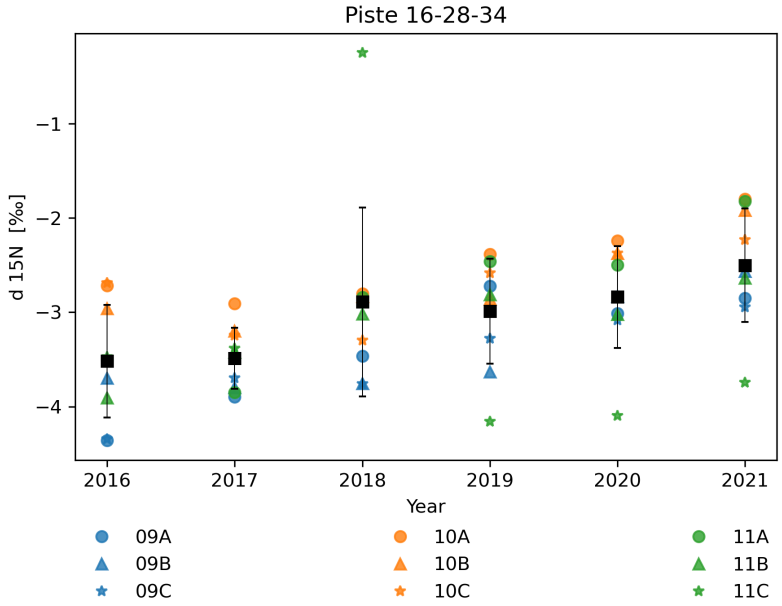

FIGURE A.5: δ^{15}N [‰] with mean δ^{15}N and standard deviation ($\pm$ SD) of Norway spruce needles from 2016-2021 at runway site. Tree no. 9 (blue), tree no. 10 (orange), and tree no. 11 (green) with different branches (repication) A (circle), B (triangle), and C (star).

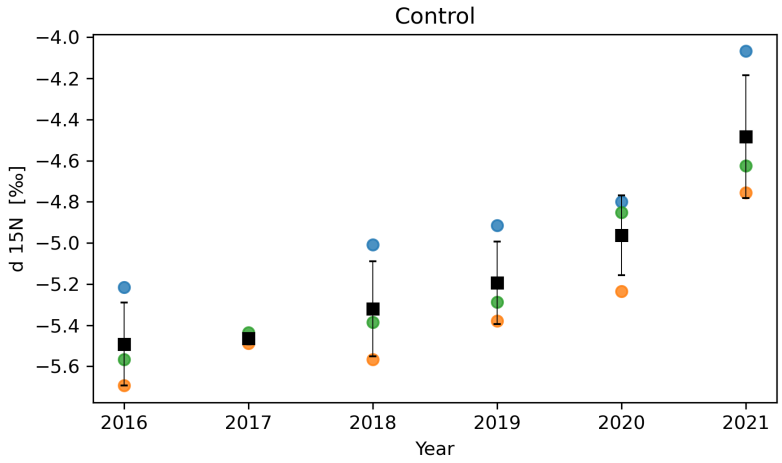

FIGURE A.6: δ^{15}N [‰] with mean δ^{15}N and standard deviation ($\pm$ SD) of Norway spruce needles from 2016-2021 at control site. Tree no. 24 (blue), tree no. 25 (orange), and tree no. 26 (green).

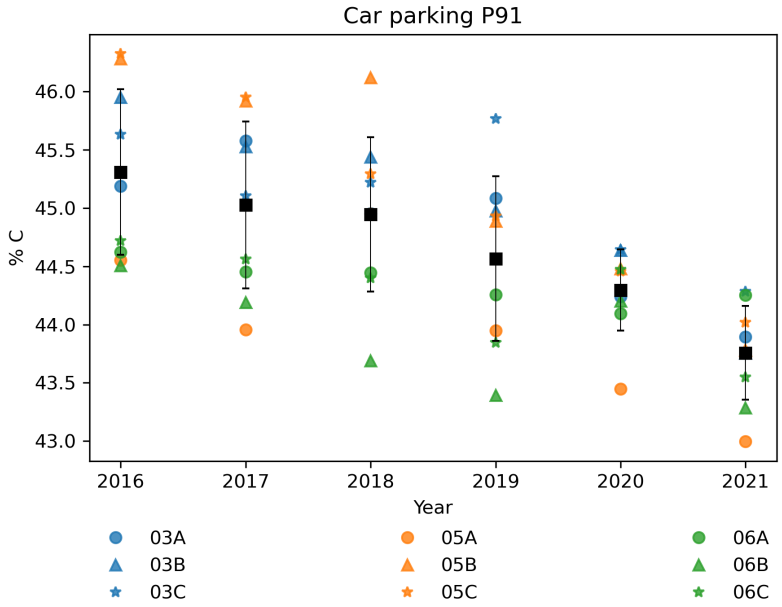

FIGURE A.7: Carbon concentration [%] with mean C-concentration and standard deviation ($\pm$ SD) of Norway spruce needles from 2016-2021 at carparking site. Tree no. 3 (blue), tree no. 5 (orange), and tree no. 6 (green) with different branches (replication) A (circle), B (triangle), and C (star).

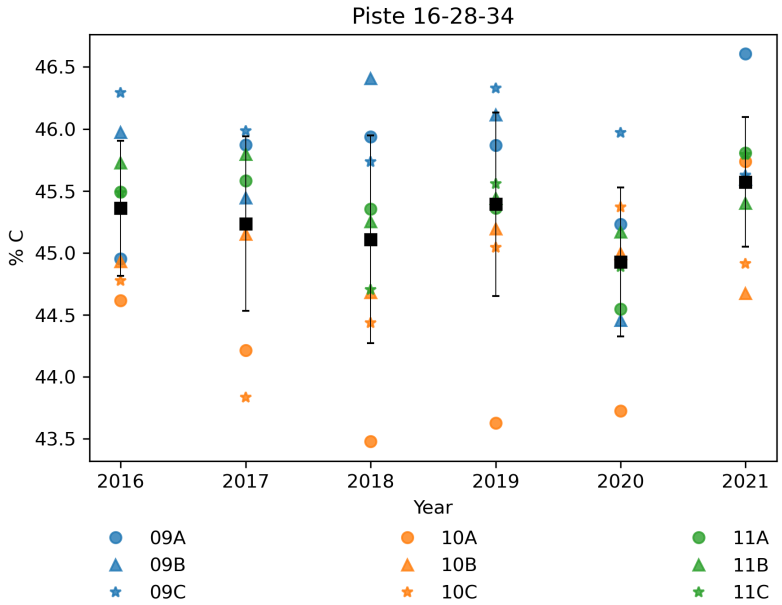

FIGURE A.8: Carbon concentration [%] with mean C-concentration and standard deviation (± SD) of Norway spruce needles from 2016-2021 at runway site. Tree no. 9 (blue), tree no. 10 (orange), and tree no. 11 (green) with different branches (replication) A (circle), B (triangle), and C (star).

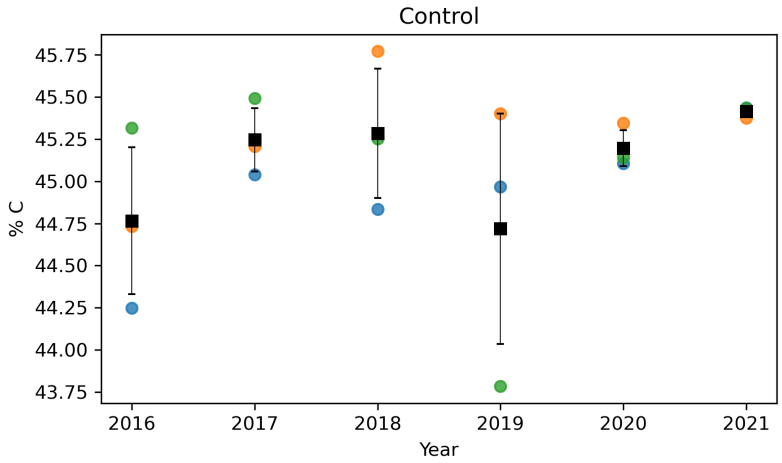

FIGURE A.9: Carbon concentration [%] with mean C-concentration and standard deviation (± SD) of Norway spruce needles from 2016-2021 at control site. Tree no. 24 (blue), tree no. 25 (orange), and tree no. 26 (green).

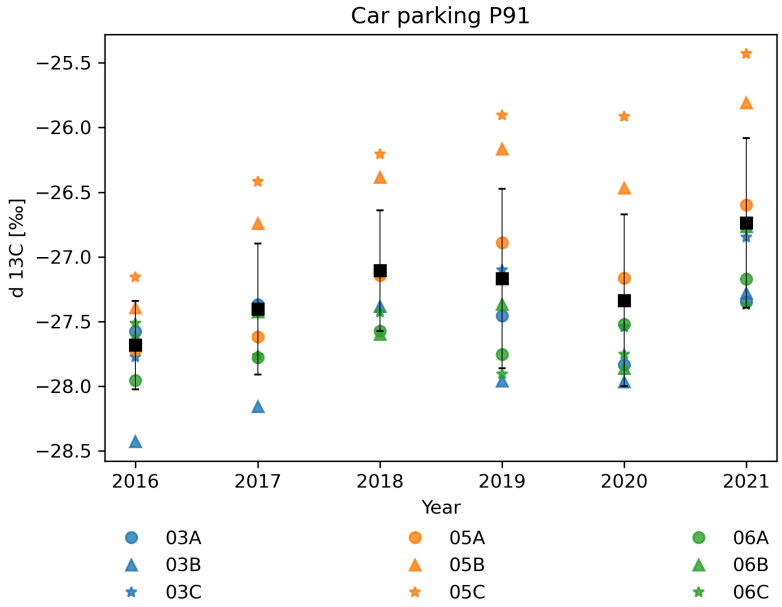

FIGURE A.10: δ^{13}C [‰] with mean δ^{13}C and standard deviation ($\pm$ SD) of Norway spruce needles from 2016-2021 at carparking site. Tree no. 3 (blue), tree no. 5 (orange), and tree no. 6 (green) with different branches (replication) A (circle), B (triangle), and C (star).

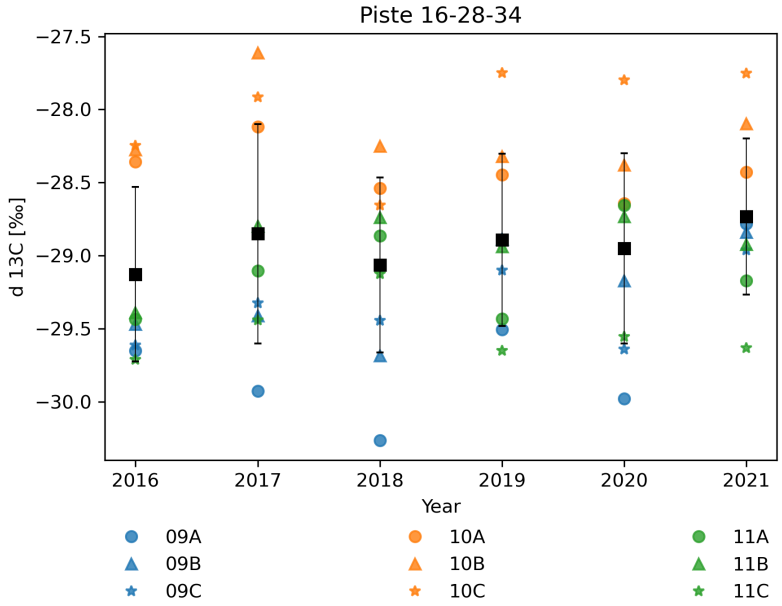

FIGURE A.11: δ^{13}C [‰] with mean δ^{13}C and standard deviation ($\pm$ SD) of Norway spruce needles from 2016-2021 at runway site. Tree no. 9 (blue), tree no. 10 (orange), and tree no. 11 (green) with different branches (replication) A (circle), B (triangle), and C (star).

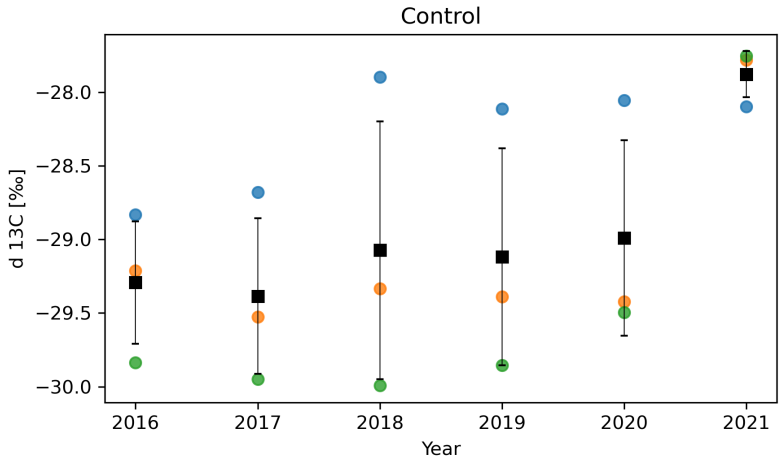

FIGURE A.12: δ^{13}C [‰] with mean δ^{13}C and standard deviation ($\pm$ SD) of Norway spruce needles from 2016-2021 at control site. Tree no. 24 (blue), tree no. 25 (orange), and tree no. 26 (green).

B Crossdating

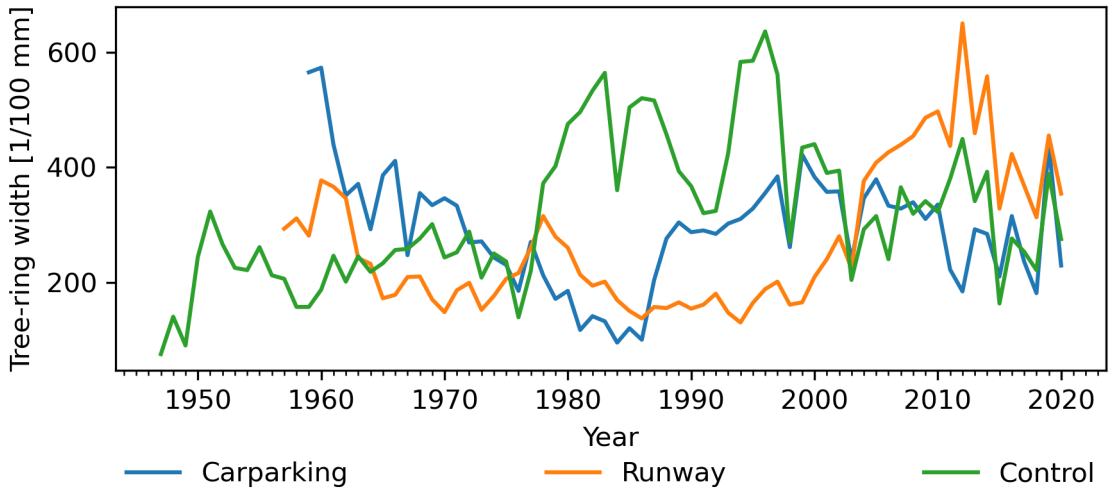

FIGURE B.1: Mean tree-ring widths [1/100 mm] by years of the sites: carparking (blue), runway (orange), and control (green).

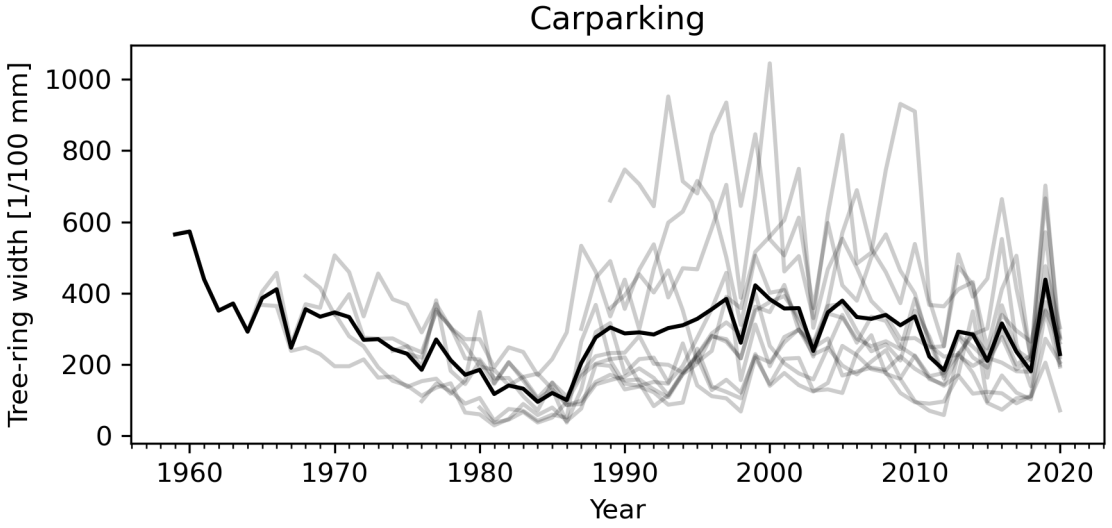

FIGURE B.2: Tree-ring width [1/100 mm] by years of mean tree-ring series of the different trees (light gray) and mean chronology (black) of the carparking site.

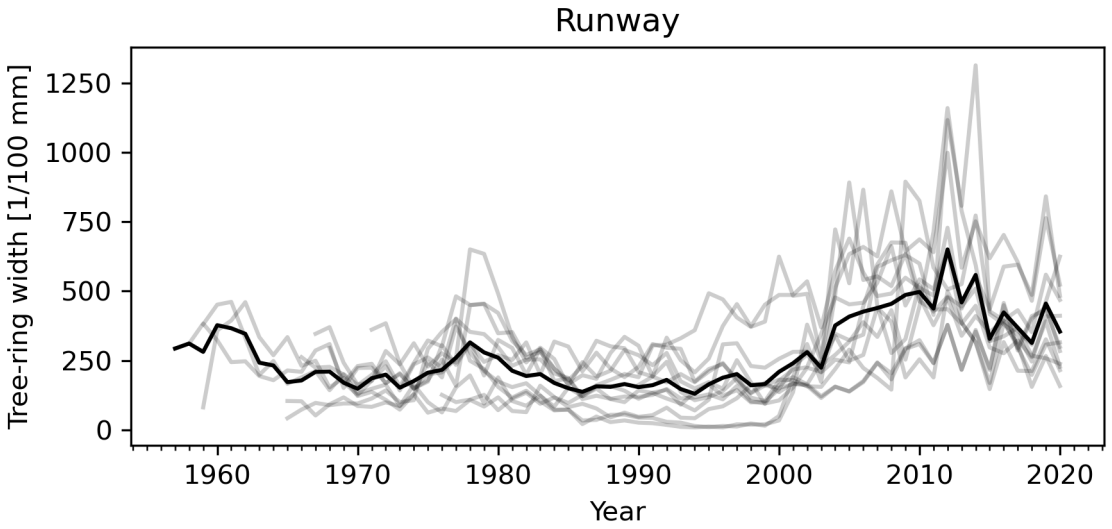

FIGURE B.3: Tree-ring width [1/100 mm] by years of mean tree-ring series of the different trees (light gray) and mean chronology (black) of the runway site.

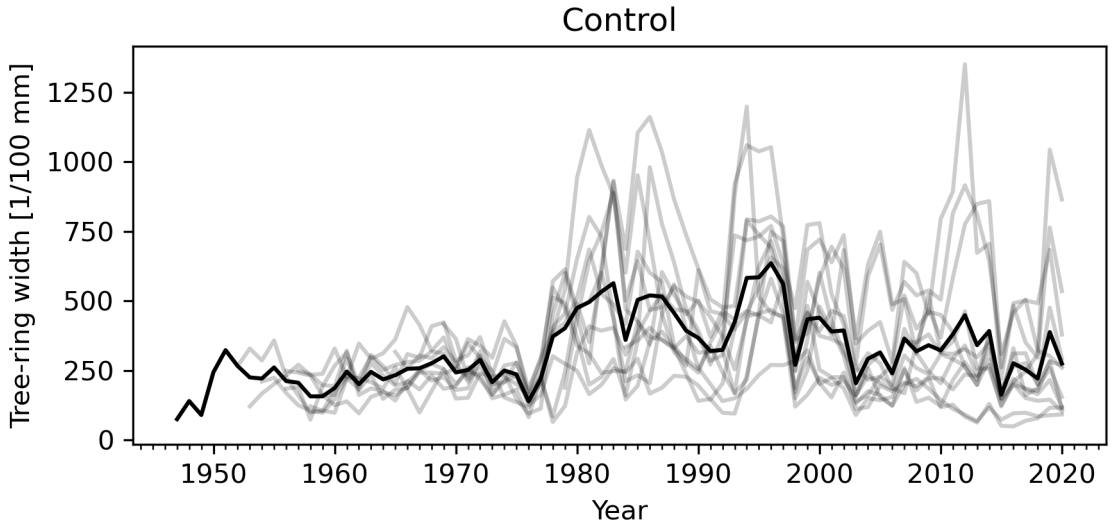

FIGURE B.4: Tree-ring width [1/100 mm] by years of mean tree-ring series of the different trees (light gray) and mean chronology (black) of the control site.

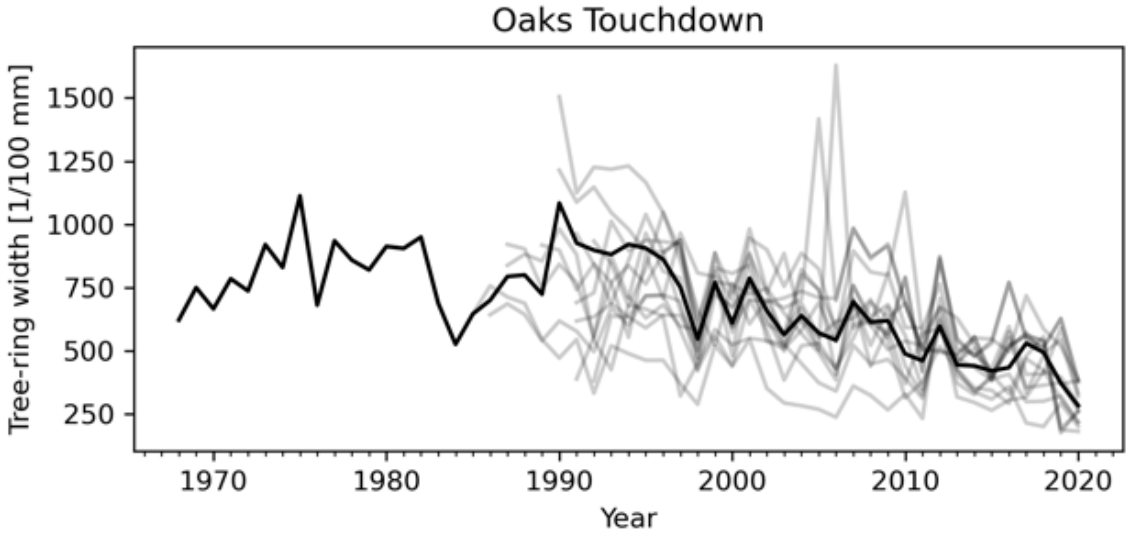

FIGURE B.5: Tree-ring width [1/100 mm] by years of mean tree-ring series of the different trees (light gray) and mean chronology (black) of the oaks touchdown site.

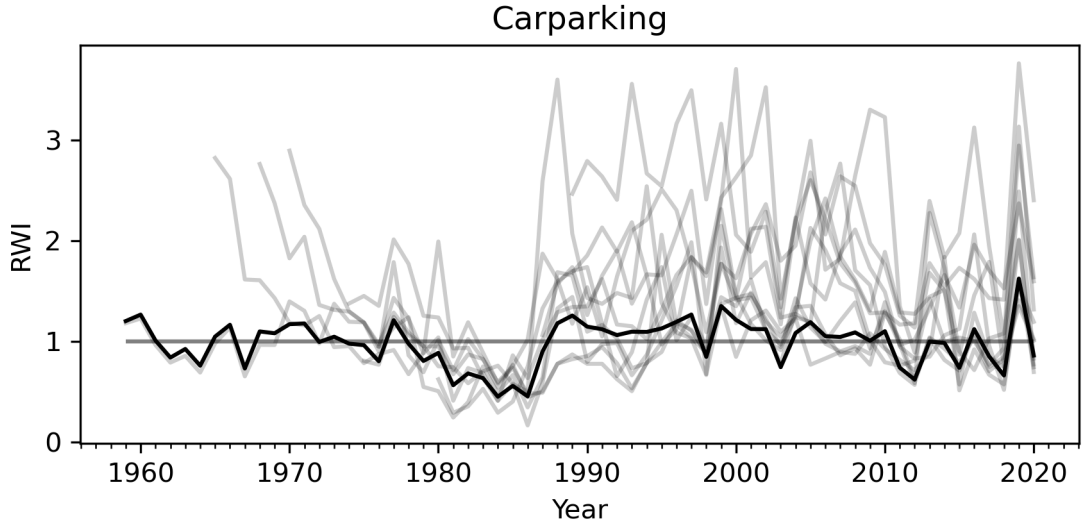

FIGURE B.6: Tree-ring width index (detrended) by years of mean tree-ring series of the different trees (light gray) and mean chronology (black) of the carparking site.

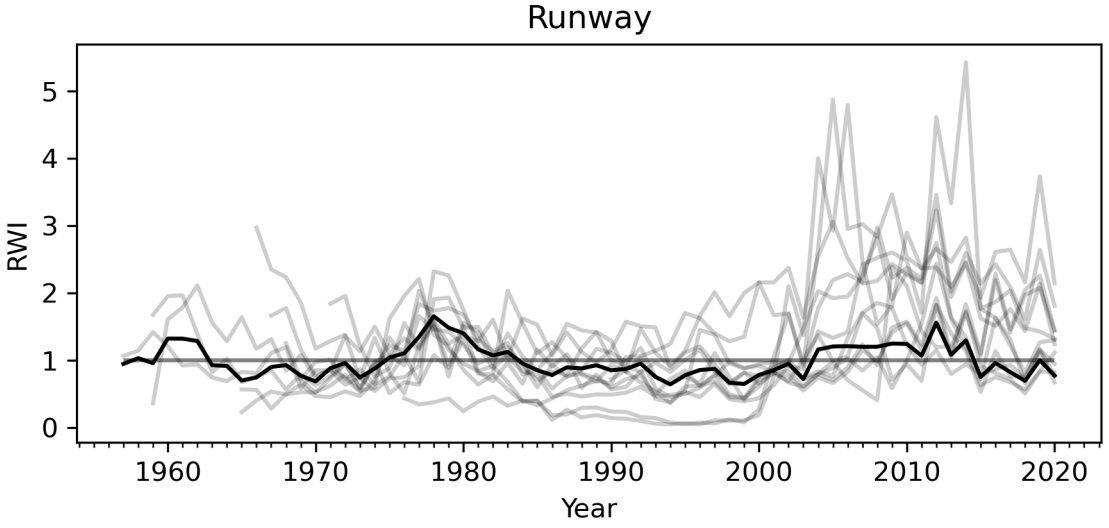

FIGURE B.7: Tree-ring width index (detrended) by years of mean tree-ring series of the different trees (light gray) and mean chronology (black) of the runway site.

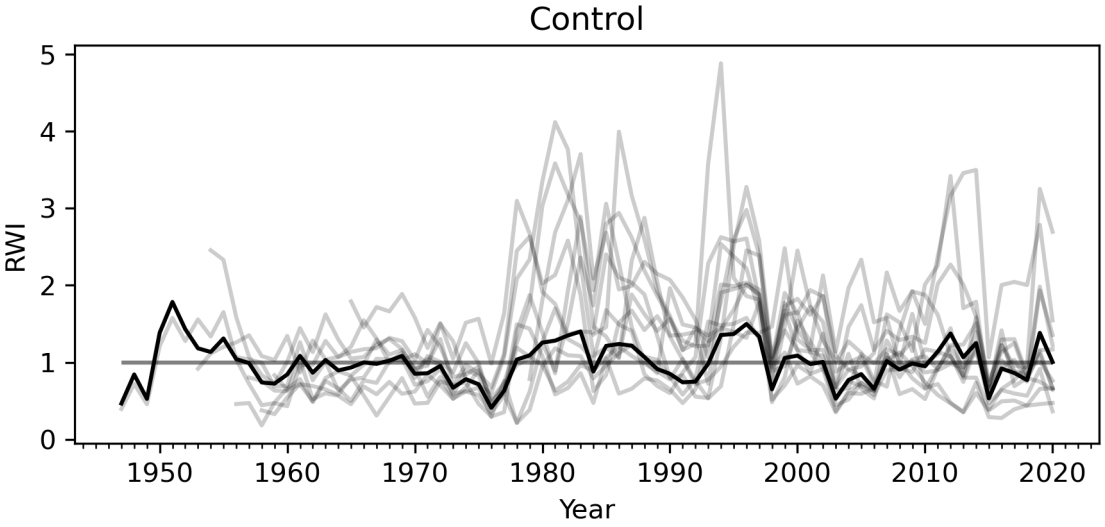

FIGURE B.8: Tree-ring width index (detrended) by years of mean tree-ring series of the different trees (light gray) and mean chronology (black) of the control site.

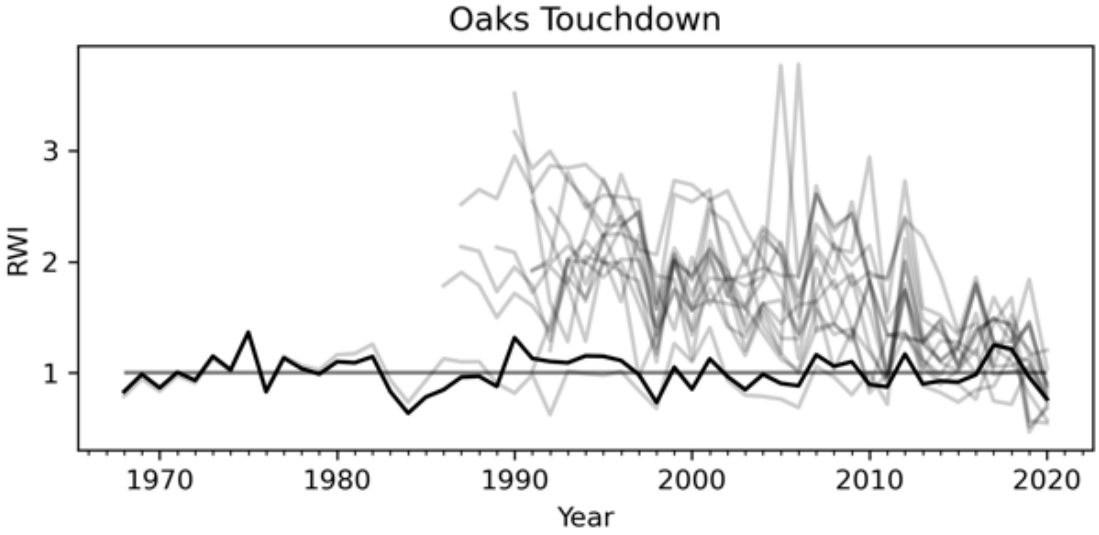

FIGURE B.9: Tree-ring width index (detrended) by years of mean tree-ring series of the different trees (light gray) and mean chronology (black) of the oaks touchdown site.

C Statistics

C.1 Pearson Correlation

Site	Correlation coefficient	Two-tailed p-value
	NO_2	
	Tree-ring width	
Carparking	0.25	0.29
Runway	-0.28	0.23
Control	0.05	0.83
	Detrended tree-ring width	
Carparking	0.25	0.29
Runway	0.12	0.61
Control	-0.33	0.16
	Temperature	
	Tree-ring width	
Carparking	-0.58	0.00076
Runway	0.25	0.19
Control	-0.66	7.5e-05
	Detrended tree-ring width	
Carparking	-0.58	0.00076
Runway	-0.048	0.8
Control	-0.47	0.0093
	Precipitation	
	Tree-ring width	
Carparking	0.53	0.0029
Runway	0.21	0.26
Control	0.28	0.13
	Detrended tree-ring width	
Carparking	0.53	0.0029
Runway	0.34	0.067
Control	0.28	0.13

C.2 Crosscorrelation

Site	Time Lag																			
	0	1	2	3	4	5	6	7	8	9	10	11	12	13	14	15	16	17	18	19
NO_2																				
Tree-ring width																				
Carparking	0.25	0.031	0.48	0.23	0.15	0.33	0.037	0.087	0.26	0.1	-0.16	-0.12	-0.2	-0.16	-0.17	-0.25	-0.12	0.071	-0.19	-0.14
Runway	-0.28	-0.24	-0.14	-0.13	-0.23	-0.1	-0.43	-0.28	-0.55	-0.12	-0.19	-0.064	-0.015	0.053	0.064	0.13	0.2	0.4	0.28	0.27
Control	0.05	0.039	0.29	0.092	0.18	0.23	-0.31	-0.17	-0.3	-0.11	0.0034	-0.026	-0.027	-0.06	0.18	0.012	0.074	0.17	-0.22	-0.16
Detrended tree-ring width																				
Carparking	0.25	0.031	0.48	0.23	0.15	0.33	0.037	0.087	0.26	0.1	-0.16	-0.12	-0.2	-0.16	-0.17	-0.25	-0.12	0.071	-0.19	-0.14
Runway	0.12	0.14	0.16	0.098	-0.017	0.064	-0.34	-0.22	-0.52	-0.14	-0.26	-0.18	-0.16	-0.11	-0.11	-0.065	0.021	0.27	0.12	0.15
Control	-0.33	-0.32	0.034	-0.079	0.013	0.13	-0.36	-0.2	-0.32	-0.081	0.057	0.068	0.084	0.071	0.28	0.15	0.2	0.28	-0.047	-0.022
Temperature																				
Tree-ring width																				
Carparking	-0.58	-0.089	-0.16	-0.2	0.005	-0.22	-0.15	0.002	-0.065	0.00096	0.2	0.022	0.12	0.12	0.086	0.0097	0.19	0.037	0.21	0.23
Runway	0.25	0.42	0.41	0.4	0.46	0.37	0.43	0.27	0.25	0.17	0.17	0.11	-0.0054	0.059	-0.0061	-0.13	-0.11	-0.18	-0.2	-0.2
Control	-0.66	-0.48	-0.47	-0.33	-0.053	-0.29	0.056	0.059	-0.04	0.057	0.016	-0.082	-0.099	-0.053	-0.12	-0.068	0.043	-0.031	0.13	0.14
Detrended tree-ring width																				
Carparking	-0.58	-0.089	-0.16	-0.2	0.005	-0.22	-0.15	0.002	-0.065	0.00096	0.2	0.022	0.12	0.12	0.086	0.0097	0.19	0.037	0.21	0.23
Runway	-0.048	0.24	0.26	0.24	0.28	0.22	0.41	0.27	0.26	0.16	0.21	0.22	0.087	0.13	0.092	-0.085	-0.048	-0.15	-0.16	-0.18
Control	-0.47	-0.25	-0.27	-0.16	0.18	-0.15	0.21	0.16	0.016	0.09	0.025	-0.11	-0.18	-0.086	-0.19	-0.15	-0.022	-0.11	0.053	0.068
Precipitation																				
Tree-ring width																				
Carparking	0.53	-0.089	0.32	0.16	0.019	0.25	0.34	0.064	0.14	0.013	-0.0097	0.18	-0.049	-0.035	-0.098	-0.014	-0.12	0.042	-0.2	-0.1
Runway	0.21	-0.084	-0.061	-0.13	-0.2	-0.19	-0.32	-0.3	-0.41	-0.29	-0.26	-0.2	-0.18	-0.24	-0.19	-0.079	-0.062	0.044	0.062	0.063
Control	0.28	-0.11	0.0023	-0.019	0.029	0.43	0.12	0.021	-0.015	-0.015	0.19	0.37	0.28	0.16	0.1	0.088	0.079	0.095	-0.11	-0.065
Detrended tree-ring width																				
Carparking	0.53	-0.089	0.32	0.16	0.019	0.25	0.34	0.064	0.14	0.013	-0.0097	0.18	-0.049	-0.035	-0.098	-0.014	-0.12	0.042	-0.2	-0.1
Runway	0.34	-0.028	0.066	0.0012	-0.068	-0.13	-0.31	-0.27	-0.36	-0.24	-0.2	-0.22	-0.22	-0.27	-0.17	-0.0093	-0.064	0.045	0.034	0.074
Control	0.28	-0.24	-0.095	-0.12	-0.12	0.37	-0.015	-0.11	-0.16	-0.12	0.11	0.33	0.26	0.094	0.052	0.054	0.067	0.12	-0.087	-0.046

D Declaration of originality

Personal declaration: I hereby declare that the submitted thesis is the result of my own, independent work. All external sources are explicitly acknowledged in the thesis.

Zurich, April 29th, 2022

Jana Gemperle